Secondary Organic Aerosol Formation and Gas/Aerosol Partitioning

Thesis by

Jay Russell Odum

In Partial Fulfillment of the Requirements

for the Degree of

Doctor of Philosophy

California Institute of Technology

Pasadena, California

(1998)

December 15th, 1997

ACKNOWLEDGMENTS

I would like to begin by first thanking my advisor John Seinfeld for always having enough faith in my scientific capabilities to allow me the complete freedom to envision, pursue, and conclude the work described herein. I cannot imagine having an advisor who would have been better suited to my style. Thanks for taking a chance on me, John.

I would also like to acknowledge the help and guidance that Rick Flagan imparted to me. His experimental advice and ideas were invaluable.

A great big round of thanks go out to all the people who sweatted the summers out with me in the roof lab—Thorsten, Frank, Tim, and Rob. Thanks guys for all the hours, talks, sweat, and laughs.

I would also like to give a bitter/sweet hug of appreciation to Heather Maynard. If not for her love, I would have never made it to California and hence would have never been returning to Atlanta in such grand style. I'll never regret a moment of it.

A special debt of gratitude is owed to my good friends and colleagues, Don and Jamie. Without Don's selfless help and patience, I may have never finished. Thanks for all the hours we spent together working and partying. The endless discussion that Jamie and I have been carrying on for the last 3.5 years has probably taught me more than any other experience at Caltech. We may not have solved any of the problems but it was sure fun talking about 'em.

Along those lines, I want to extend a big poke in the eye to all my friends here in Pasadena. Here's to the Rack Shack, the Colorado, the Idle Hour, and King of the Hill. I wish I could remember it all.

Finally I want to send the most special thanks to my mother. Without her love and support, I would be nothing. I'm just glad I could make you proud.

ABSTRACT

An intensive smog chamber study has revealed that secondary organic aerosol (SOA) formation follows Raoult's Law type gas/aerosol absorption thermodynamics. SOA formation was shown to occur via the gas/aerosol partitioning of semi-volatile, oxidation products rather than through the condensation of saturated, non-volatile products. The major consequence of this finding is that SOA yields are not constant, but rather are a function of the organic aerosol mass concentration. The theory has been used to successfully describe the aerosol formation potential of seventeen individual aromatic species, eight biogenic compounds, two different simple hydrocarbon precursor mixtures, and twelve different blends of whole gasoline vapor, in hundreds of smog chamber experiments. These results have been included in a 3-dimensional size- and chemically-resolved atmospheric chemical-transport model and used to simulate SOA formation in the South Coast Air Basin. The inherent dependence of SOA concentrations on primary organic aerosol (POA) concentrations, places strict constraints on organic and elemental carbon aerosol emissions inventories.

TABLE OF CONTENTS

LIST OF TABLES

CHAPTER 2

CHAPTER 3

CHAPTER 4

CHAPTER 5

LIST OF FIGURES

CHAPTER 2

CHAPTER 3

CHAPTER 4

CHAPTER 5

Chapter 1:

Introduction

Secondary organic aerosol (SOA) can significantly contribute to the particulate burden in urban atmospheres. As a result of this, and the mounting evidence that fine particulate matter (PM) represents a serious human health concern in our urban environments, it is important to establish methods which can be used to estimate the magnitude of this contribution. Along these lines there are two primary approaches than can be taken.

The first approach involves developing direct/indirect methods by which the amount of SOA present in ambient atmospheric samples can be quantified. Direct methods would involve identifying and quantifying all of the secondary organic reaction products present in ambient samples. While estimates made with direct measurements would offer the highest level of confidence, current knowledge of reaction mechanisms and products of all of the primary reactive organic species that contribute to SOA formation is too incomplete to allow for such direct measurements. As a result, a number of indirect methods have been developed to obtain estimates of SOA contributions.

Turpin and Huntzicker measured ambient aerosol organic carbon (OC) and elemental carbon (EC) contents and used empirical correlations between the two to estimate the magnitude of SOA contributions in the South Coast Air Basin (*1*). Another indirect method involves developing emission profiles for urban primary organic aerosol sources and combining these with ambient aerosol measurements and source/receptor

techniques to source apportion ambient organic aerosol carbon. If one has accurately determined all of the primary sources, then the portion of organic aerosol carbon remaining after apportionment can be assumed to be secondary in origin (*2*).

The second type of approach involves using ambient airshed models. Once again one can employ both direct and indirect methods to estimate SOA contributions. A direct approach involves including the complete chemistry of each of the hundreds of primary organic species that contribute to SOA formation along with the correct physics to emulate gas-to-particle conversion. However as mentioned previously, the complete chemistry of most of these organic precursors is unknown; and even if complete knowledge of all products was available, the associated properties which determine the SOA formation potentials (i.e. vapor pressures, activity coefficients, etc.) for these products are difficult to determine. Thus the current state of the science prohibits such *a priori* modeling.

To get around this problem, the concept of aerosol yields was introduced nearly twenty years ago to describe the aerosol formation potential of primary reactive organic gases. The aerosol yield (Y) is defined as the fraction of a reactive organic gas (ROG) that is converted to aerosol through atmospheric oxidation and subsequent gas-to-particle conversion,

$$Y = \frac{\Delta M_o}{\Delta \mathrm{ROG}} \qquad (1)$$

where ΔM_o is the organic aerosol mass concentration ($\mu g\ m^{-3}$) produced for a given amount of ROG reacted, ΔROG ($\mu g\ m^{-3}$). Aerosol yields are determined by performing

smog chamber experiments in which an individual ROG is placed in the chamber with an appropriate amount of nitrogen oxides and allowed to react photochemically to produce aerosol. The amount of ROG that reacts (ΔROG) and the amount of organic aerosol produced (ΔM_o) are measured and used to calculate the aerosol yield. These aerosol yields can then be used in ambient airshed models to predict SOA formation for an urban atmosphere.

Aerosol yields have been estimated from smog chamber data for a host of ROGs by various researchers over the last 20 years (*3-7*). The accepted theory of SOA formation assumed that an ROG reacted to produce a host of products, some of which would be non-volatile (i.e. have extremely low vapor pressures) and would condense to produce SOA. If SOA is formed only from non-volatile products, then theory suggests that each parent ROG should have a unique and constant aerosol yield. However literature aerosol yield values for a given ROG vary widely. For example, observed SOA yields for a-pinene range from less than 10% to greater than 50% (*8-9*). With theory predicting that aerosol yields should be constant and with experimental results unable to support this, use of aerosol yields to represent SOA formation in ambient models was done so with little confidence (*10-11*).

So before aerosol yield data can be used in ambient models to correctly predict SOA formation, this issue of disagreement between theory and experiment must be resolved. Such was the express purpose of this research project. The methodology that was used and the results that were obtained are discussed fully in the chapters that follow. Chapter 1 focuses on the development of a new theory of SOA formation which is

consistent not only with newly obtained Caltech smog chamber data but with smog chamber data from other research groups. Chapter 2 discusses the use of the new theory for describing the aerosol formation potential of complex hydrocarbon mixtures like whole gasoline vapor. In Chapter 4, ambient and smog chamber gas/particle partitioning data are compared to show that smog chamber aerosol yield data may be confidently extrapolated to the ambient atmosphere for use in predicting ambient SOA formation. And finally, Chapter 5 closes with a description of 3-D, grided, Eulerian modeling exercises of SOA formation in the Los Angeles Basin.

REFERENCES

(1) Turpin B. J. and Huntzicker J. J. (1995) *Atmos. Environ.*, 29B, 3527-3544.

(2) Schauer J. J., Rogge W. F., Hildermann L. M., Mazurek M. A., Simoneit B. R. and Cass G. R. (1996) *Atmos. Environ.*, 30, 3837-3855.

(3) Pandis S. N., Paulson S. E., Seinfeld J. H. and Flagan R. C. (1991) *Atmos. Environ.*, 25A, 997-1008.

(4) Wang S. C., Paulson S. E., Grosjean D., Flagan R. C. and Seinfeld J. H. (1992) *Atmos. Environ.*, 26A, 403-420.

(5) Izumi K. and Fukuyama T. (1990) *Atmos. Environ.*, 24A, 1433-1441.

(6) Stern J. E., Flagan R. C., Grosjean D. and Seinfeld J. H. (1987) *Environ. Sci. Technol.*, 21, 1224-1231.

(7) Grosjean D. (1977) In *Ozone and Other Photochemical Oxidants*, National Academy of Sciences: Washington, DC, Chapter 3, 45-125.

(8) Grosjean D. and Seinfeld J. H. (1989) *Atmos. Environ.*, 23, 1733-1747.

(9) Zhang S., Shaw M., Seinfeld J. H. and Flagan R. C. (1992) *J. Geophys. Res.*, 20, 717-729.

(10) Pandis S. N., Harley R. A., Cass G. R. and Seinfeld J. H. (1992) *Atmos. Environ.*, 26A, 2269-2282.

(11) Pandis S. N., Wexler A. S. and Seinfeld J. H. (1993) *Atmos. Environ.*, 27A, 2403-2416.

Chapter 2:
Gas/Particle Partitioning and Secondary Organic Aerosol Yields

Published in *Environ. Sci. Technol.*, **30**, 2580 (1996).

ABSTRACT

Secondary organic aerosol (SOA) formation is considered in the framework of the gas/particle partitioning absorption model outlined by Pankow (*1, 2*). Expressions for the fractional SOA yield (Y) are developed within this framework and shown to be a function of the organic aerosol mass concentration, M_o. These expressions are applied to over 30 individual reactive organic gas (ROG) photooxidation smog chamber experiments. Analysis of the data from these experiments clearly shows that Y is a strong function of M_o and that secondary organic aerosol formation is best described by a gas/particle partitioning absorption model. In addition to the 30 individual ROG experiments, three experiments were performed with ROG mixtures. The expressions developed for Y in terms of M_o, used in conjunction with the overall yield data from the individual ROG experiments, are able to account for the M_o generated in the ROG mixture experiments. This observation not only suggests that SOA yields for individual ROGs are additive but that smog chamber SOA yield data may be confidently extrapolated to the atmosphere in order to determine the important ambient sources of SOA in the environment.

INTRODUCTION

It is now well recognized that secondary organic matter can significantly contribute to the particulate burden in urban atmospheres. However because of the enormous complexity of the chemical matrix of organic aerosol and the lack of direct chemical analysis methods for a majority of the compounds comprising the organic aerosol fraction, estimates of secondary organic aerosol (SOA) contributions in the urban environment have been restricted to indirect methods of determination. For example, Turpin and Huntzicker used correlations between measured organic carbon (OC) and elemental carbon (EC) to estimate SOA contributions in Los Angeles during the summer Southern California Air Quality Study (SCAQS) in 1987 (*3*). The study showed that as much as 70% of the organic aerosol can be of secondary origin under peak photochemical conditions. Other estimates, based on chemical mass balance methods, suggest that on a yearly average, 20-30% of the fine organic particulate matter in the South Coast Air Basin is secondary (*4*).

Efforts to represent SOA formation in ambient models have primarily been based on using experimentally determined fractional aerosol yields (*5-7*). The fractional aerosol yield (Y), defined as the fraction of a reactive organic gas (ROG) that is converted to aerosol, is calculated by

$$Y = \frac{\Delta M_o}{\Delta ROG} \qquad (1)$$

where ΔM_o is the organic aerosol mass concentration ($\mu g\ m^{-3}$) produced for a given amount of ROG reacted, ΔROG ($\mu g\ m^{-3}$). Aerosol yields have been estimated from smog chamber data for a variety of ROG's by various researchers over the last 20 years (*8-15*). In general, measured yields for a single compound have shown a wide degree of variation both between and within laboratories. For example, observed SOA yields for α-pinene

range from less than 10% to greater than 50% (*5, 16*). Several factors likely contribute to this dramatic variability, but the major factor may be the way that SOA formation has been represented.

Secondary aerosols are formed by reaction of an ROG to produce both semi-volatile and non-volatile products. Previously, it has been assumed that the vapor-phase products begin to condense onto existing seed particles (or to homogeneously nucleate) only after a product exceeds its saturation concentration, and that the amount of a product that condenses is the quantity in excess of its saturation concentration. For the initial condensation process, and certainly for the initial nucleation process, this may be the case. However, Pankow has suggested that, once organics have begun to condense and an organic layer has formed on the particles, even products whose gas-phase concentrations are below their saturation concentrations will partition a portion of their mass into this condensed organic phase (*2*). For each compound that partitions into the absorbing organic material (*om*) phase, Pankow has defined an absorption equilibrium constant ($K_{p,i}$) as

$$K_{p,i} = \frac{F_{i,om}}{A_i TSP} = \frac{760RT f_{om}}{MW_{om} 10^6 \zeta_i p^o_{L,i}} \qquad (2)$$

where A_i is the gas phase concentration (ng m^{-3}) of compound i, $F_{i,om}$ is the concentration of compound i (ng m^{-3}) in the absorbing *om* phase, *TSP* is the total suspended particulate concentration (μg m^{-3}), R is the ideal gas constant (8.206x10^{-5} m^3atm mol^{-1} K^{-1}), T is temperature (K), f_{om} is the mass fraction of the *TSP* that is the absorbing *om* phase, MW_{om} is the mean molecular weight of the absorbing *om* (g mol^{-1}), ζ_i is the activity coefficient of compound i in the *om* phase, and $p^o_{L,i}$ is the vapor pressure (torr) of the absorbing compound as a liquid (sub-cooled, if necessary).

Considering only the mass of the *om* phase, one can similarly define a partitioning coefficient for species *i* ($K_{om,i}$) in terms of the organic mass concentration

$$K_{om,i} = \frac{F_{i,om}}{A_i M_o} = K_{p,i} / f_{om} \quad (3)$$

where like K_p, K_{om} has units of (m^3 μg^{-1}), and M_o is the absorbing organic mass concentration (μg m^{-3}). This equilibrium partitioning coefficient suggests that, for $K_{om,i}$ to be constant for a given compound, the fraction of a compound's total mass residing in the particulate phase will increase with increasing organic mass concentrations. This behavior for the semi-volatile products involved in SOA formation would lead to the high variability found for published values of SOA yields for a given ROG, since the fractional aerosol yields will be dependent on the organic mass concentration.

Pandis et al. state that two of the three major uncertainties in predictions of ambient SOA are the discrepancies in experimentally determined SOA yields and in the partitioning of the condensable vapors between the gas and aerosol phases (*6*). In this paper both of these factors will be addressed. We shall use the partitioning theory of Pankow (*1, 2*) to develop expressions for the fractional secondary aerosol yield (*Y*) in terms of organic mass concentration. These expressions are then applied to over 30 SOA smog chamber experiments conducted in the summer of 1995. This analysis is used to show how SOA smog chamber data can be used to identify the important sources of SOA in the urban environment.

EXPERIMENTAL DESCRIPTION

Experiments were performed in a 60 m^3 sealed collapsible Teflon bag that has been described in detail previously (*8, 9*). Most of these experiments were conducted in a dual-chamber mode, in which the bag was divided in the center with a clamped PVC pipe, so that two different experiments could be conducted under identical environmental (i.e. sunlight intensity, temperature, etc.) conditions. The two resulting chambers had volumes of approximately 20 m^3. The gas-phase instrumentation and aerosol data acquisition system are housed in a laboratory adjacent to the chamber. All aerosol sampling equipment was housed in a cart adjacent to the chamber that was maintained at a constant temperature of 25°C. Prior to every experiment the chamber was continuously flushed with purified laboratory compressed air for at least 38 hours and baked in sunlight for at least one day. The compressed air was processed through three consecutive packed-bed scrubbers containing, in order, Purafil, Drierite and 13x molecular sieves, and activated charcoal. After purification, the air was rehumidified to a relative humidity of approximately 10% with distilled/dionized water before entering the chamber. The resulting air contained no detectable reactive hydrocarbons, no particles, and less than 5 ppb NO_x.

Hydrocarbon measurements were made using a Hewlett Packard (Palo Alto, CA) 5890 gas chromatograph (GC) that was equipped with a DB-5 column (J&W Scientific, Davis, CA) and a flame ionization detector (FID). The GC temperature program was: -60 °C for 1 min, -60 to 100 °C at 40 °C min^{-1}, hold at 100 °C for 1 min. Hydrocarbon calibrations were performed prior to each experiment either using certified gas mixtures or by vaporizing microliter volumes of a calibration solution of the pure hydrocarbon in CH_2Cl_2 into a 60L Teflon bag filled with a measured volume of Ultra Zero (Air Liquid America Corp., Houston, TX) compressed air.

The calibrations were generally followed by injection of $(NH_4)_2SO_4$ seed particles to obtain particle concentrations of 5,000-10,000 particles cm^{-3} with a number mean diameter of approximately 100 nm. The particles were generated by atomizing an aqueous solution of $(NH_4)_2SO_4$ using a stainless steel, constant rate atomizer. The aerosol was passed through heated copper tubing into a diffusional dryer, followed by a ^{85}Kr charge neutralizer before entering the chamber.

After obtaining the desired initial seed particle concentration, propene, hydrocarbons, NO_x, and hexafluorobenzene (C_6F_6) were injected (approximately 1 hour prior to the start of the experiment) through Teflon lines into the chamber, which was completely shrouded from sunlight with an black polyethylene tarpaulin. Propene, NO, and NO_2 were injected using certified cylinders containing approximately 500 ppm of the gas in nitrogen. Hydrocarbons and C_6F_6 were introduced into the chamber by injecting microliter quantities of the pure liquid compound into a glass bulb that was gently heated while being diluted with purified compressed lab air that went directly to the chamber. Propene was used at mixing ratios of 250-350 ppb to generate OH radicals in sufficient concentrations for the inception of the experiment. The C_6F_6 was used as an internal standard for hydrocarbon gas chromatographic (GC) samples in order to normalize for injection variations of the 6-port stainless steel injection valve (Valco, Houston, TX), equipped with a heated (100 °C) 2 ml Teflon sampling loop. The half-life of C_6F_6 in the chamber was of the order of several days (k_{OH} = 1.72x10-13 cm^3 $molecule^{-1}$ s^{-1}), and so its concentrations were stable for times much longer than the typical experiment, allowing it to serve as an excellent internal standard. The use of the internal standard yielded estimated uncertainties in the hydrocarbon measurements of less than ±2% for most experiments.

After injection of the gases and seed aerosol, but before uncovering the chamber, initial measurements of hydrocarbons, NO_x, O_3, and aerosol concentrations and size

distributions were made to obtain initial values and to ensure that the contents were well mixed. Generally three to five initial hydrocarbon measurements, using the HP 5890 GC described above, were made for each side of the bag. A Thermo Environmental Instruments (Franklin, MA) Model 42 chemiluminescence NO_x monitor was used to measure NO, NO_2, and NO_x. Prior to start of each experiment, a zero/span calibration was performed on the NO_x monitor using certified cylinders of NO and NO_2. In addition, a complete calibration of the NO_x monitor was performed on approximately a weekly basis. A Dasibi Environmental Corp. (Glendale, CA) Model 1008-PC O_3 analyzer was used to monitor O_3 concentrations. The NO_x and O_3 measurements were made at 10 min. intervals between alternating sides of the chamber. The estimated uncertainties in the NO and NO_2 measurements are approximately ±4% and ±7%, respectively. The ozone instrument has an estimated uncertainty of ±4% in its initial calibration and was seen to drift only a few percent over the period of several months.

Complete number and size distribution measurements were recorded for both sides of the chamber with a one-minute frequency throughout an experiment. The aerosol instrumentation consisted of one radial scanning electrical mobility spectrometer (*17*) and one TSI Model 3071 cylindrical scanning electrical mobility spectrometer for each side of the divided chamber. All four scanning electrical mobility spectrometers (SEMS) were equipped with either a model 3760 or model 3025 TSI condensation nuclei counter (CNC) to count transmitted particles. SEMS voltages were scanned from 40-8500V with a one minute ramp. The radial SEMS were operated with sheath and excess flows of 15 L min^{-1} and inlet and classified aerosol flows of 1.5 L min^{-1} to allow for measurement of particle size distributions over the range of 5-80 nm. The cylindrical SEMS were operated with sheath and excess flows of 2.5 L min^{-1} and inlet and classified aerosol flows of 0.25 L min^{-1} to allow for measurement of particle size distributions in the range of 30-850 nm. A more complete description of the SEMS scanning cycle and operation

have been published previously (*9*). Particle losses in the SEMS, SEMS response functions, particle charging efficiencies, CNC counting efficiency, and particle deposition in the chamber have been taken into account in the analysis of the aerosol data (*9*). The estimated uncertainty in the SEMS size and concentration measurements are approximately ±10%.

After making initial measurements prior to the start of the experiment, the black tarpaulin (chamber cover) was removed to begin the photooxidation experiment. Hydrocarbon measurements were made for both sides of the chamber every 8-10 min throughout the experiment. NO, NO_2, NO_x, and O_3, were continuously monitored during 10 min intervals alternating between the two sides of the chamber. Temperature, total solar radiation, and UV were continuously monitored over the course of the experiment.

EXPRESSIONS FOR SOA YIELDS

In the presence of absorption partitioning of secondary organic aerosol species, fractional aerosol yields should be dependent on the total organic aerosol mass concentration. In order to derive the functional form of this dependence, let us begin by assuming that the concentrations of the dozens of individual products that result from the photooxidation of an ROG are simply proportional to the amount of ROG that reacts (ΔROG) such that

$$1000\alpha_i \Delta ROG = C_i \qquad (4)$$

where α_i is the proportionality constant relating the concentration of ROG that reacts to the total concentration of product i (C_i) that is formed. The total concentration of a product that is formed is simply the concentration of the product that is in the gas phase

(A_i) plus the concentration of the product that is in the aerosol phase (F_i). The factor of 1000 in equation (4) is needed because the units of ΔROG are $\mu g\ m^{-3}$ and the units of C_i are $ng\ m^{-3}$. Since the parent ROG and the products have different molecular weights, α_i is actually the product of the stoichiometric factor for the reaction forming product *i* and the ratio of the molecular weight of product *i* to the molecular weight of the parent ROG.

The desired property of the aerosol yield (Y) is that it possess a value that, when multiplied by the total mass of an ROG that reacts, gives the total mass of products that end up in the aerosol phase,

$$Y(1000V_c\Delta ROG) = \sum_i (F_i V_c) \tag{5}$$

where V_c is the volume in which the reaction takes place, and once again a factor of 1000 is needed due to the difference in units for ΔROG and F_i. Combining equations (3),(4), and (5) and using the mass balance constraint (i.e. $C_i = A_i + F_i$) gives the following expression for the yield of an individual product (Y_i):

$$Y_i = M_o\left(\frac{\alpha_i K_{om,i}}{1 + K_{om,i} M_o}\right) \tag{6}$$

Similarly, the expression for the overall SOA yield (Y) is given by:

$$Y = \sum_i Y_i = M_o \sum_i \left(\frac{\alpha_i K_{om,i}}{1 + K_{om,i} M_o}\right) \tag{7}$$

Equations (6) and (7) have several interesting features. First, they suggest that for low organic mass concentrations and for products that have relatively small partitioning coefficients, the SOA yield will be directly proportional to the total aerosol organic mass concentration, M_o. Secondly, for very nonvolatile products and/or for large organic mass

concentrations, the individual product yields will be independent of the organic mass concentration and will be equal to α_i. Finally, they suggest that the individual yields for the more volatile products will be sensitive to temperature since $K_{om,i}$ is inversely proportional to the vapor pressure of the species (see equations 2 and 3). If the semi-volatile products involved in SOA formation exhibit the type of partitioning behavior indicated in equations (6) and (7), then it is highly unlikely that a particular ROG will have a unique fractional aerosol yield. Instead, it will exhibit a range of yields over a range of organic mass concentrations.

EXPERIMENTALLY DETERMINED SOA YIELDS

A list of the SOA experiments that are discussed in this paper are summarized in Table 1. Over 30 experiments were performed with *m*-xylene, 1,2,4-trimethylbenzene, and α-pinene. Table 1 lists the date on which the experiment was performed, the initial ROG concentrations (ROG_o), the total amount of ROG consumed in each experiment (ΔROG), the total organic aerosol mass that was produced (M_o), the initial NO_x concentration, the initial propene concentration (C_3H_6), the ratio of consumed hydrocarbon to initial NO_x ($\Delta HC/NO_x$), and the overall SOA yield (Y). Total organic aerosol mass concentration was calculated from the observed total organic aerosol volume, assuming a density of 1 g cm^{-3}.

SOA YIELDS OF AROMATICS

The functional form of equation (7) suggests that fractional aerosol yields should be a function of organic aerosol mass concentrations. For example, fractional aerosol yields (Y) versus organic aerosol mass concentrations (M_o) for *m*-xylene and 1,2,4-trimethylbenzene are shown in Figures 1 and 2. As is evident from the figures, Y is a strong function of the value of M_o. It can be seen that for small M_o, the yield increases rapidly with increasing M_o and becomes a weaker function of M_o at higher concentrations, in accord with the behavior predicted by equation (7). The lines through the data in Figures 1 and 2 have been generated from equation (7) assuming that there are two products that partition to the absorbing *om* phase to a measurable degree for each ROG. Values for α_1, α_2, $K_{om,1}$, and $K_{om,2}$ are chosen to fit the data for each ROG by minimizing the square of the residuals. Two products are the minimum number needed to fit the behavior of the system. A one-product model is insufficient to represent the shape of the curve, and three or more products are superfluous. Since it is known that there are dozens of products in the particle phase from the reactions of these two aromatics, the four constants that were chosen to fit the data for each ROG have no actual physical meaning, other than perhaps as an average of all the α's and K_{om}'s. However, the degree of fit to the data does suggest that the functional form of equation (7) captures the dependence of Y on M_o and that fractional aerosol yields do indeed depend on organic aerosol mass concentrations. This dependence also offers an explanation for observed increasing yields for increasing amounts of ROG reacted (*8, 16*); as more ROG reacts, more condensed organic mass is produced leading to a higher observed yield.

The data points in Figure 1 come from data obtained from 12 experiments that cover a range of initial hydrocarbon concentrations from 399 to 4194 $\mu g\ m^{-3}$ (96 to 1008 ppb) and a range of $\Delta HC/NO_x$ ratios from 1.3 to 20.2 ppbC/ppb (Table 1). The model

line through the data was chosen to fit the data points that were obtained from the experiments with $\Delta HC/NO_x$ ratios less than 15. As can be seen in the figure, the two points with a $\Delta HC/NO_x$ ratio greater than 15 have yields that are slightly higher than those with ratios less than 15. So it appears that the fractional aerosol yield for *m*-xylene is slightly dependent upon $\Delta HC/NO_x$. This is not surprising considering that the photooxidation product distributions will depend on $\Delta HC/NO_x$. However, the data suggests that the effect on the yield is minimal.

The yields in Figure 1 and 2 were calculated using equation (1), where ΔM_o is the total organic aerosol mass concentration that was produced and ΔROG is the total amount of ROG that reacted over the course of an experiment. Most of the data in Figures 1 and 2 are from the experiments that were conducted in our laboratory in the summer and fall of 1995 (Table 1). However, two of the data in Figure 1 and one datum in Figure 2 are those of Izumi and Fukuyama (*11*). The points from the data of Izumi and Fukuyama agree quite well with the Caltech measurements and further demonstrate the generality of the dependence of Y on M_o.

The temperature dependence of Y is illustrated in Figure 3. The line in the figure is the two-product model line used to fit the data in Figure 1 which corresponds to experiments that were conducted in the temperature range of 35-40 °C. The data points in Figure 3 correspond to yield data that was obtained from an experiment (10/17A) that was conducted at 26.6±1 °C. As equations (2) and (7) suggest, Y seems to be a strong function of temperature. Since K_{om} is inversely proportional to the pure component vapor pressure, the yield is higher at lower temperatures for a given M_o. The yield values from Izumi and Fukuyama (*11*) agree better with the higher temperature yields from this group even though they were generated at a temperature closer to the lower temperature run from this group. The most likely cause for this discrepancy is that Izumi and Fukuyama (*11*) did not take aerosol deposition losses into account in estimating their yields and,

therefore, probably slightly underestimated the yield values for the temperature at which they were obtained. However it is still remarkable that the values obtained by Izumi and Fukuyama agree so well with the Caltech data when viewed in terms of organic aerosol mass concentrations.

The SOA yields for 1,2,4-trimethylbenzene that are shown in Figure 2 are from experiments that were conducted at temperatures from 22-26 °C. The yield values are very similar to those for both the lower and higher temperature *m*-xylene data at organic mass concentrations below 60 μg m^{-3}. At organic mass concentrations above 60 μg m^{-3}, the yields for 1,2,4-trimethylbenzene are higher than those for the higher temperature *m*-xylene data and lower than those for the lower temperature *m*-xylene data. Thus, for most atmospherically relevant M_o values (i.e. 60 μg m^{-3} or less), 1,2,4-trimethylbenzene has a similar yield to *m*-xylene for a given organic mass concentration. This is not all that surprising considering that the types of products that are formed from the oxidation of these two aromatic species are quite similar.

SOA YIELDS OF α-PINENE

SOA smog chamber experiments were also conducted with α-pinene. The overall yields (Y) for α-pinene versus M_o are shown in Figure 4. As for *m*-xylene and trimethylbenzene, the line through the data is generated using a two product model, where α_1, α_2, $K_{om,1}$, and $K_{om,2}$ were chosen to fit the data by minimizing the square of the residuals. Yields for α-pinene follow the same trend with M_o as do those for the aromatics but are considerably higher for a given M_o. For example, the yield for α-pinene at an M_o of 50 μg m^{-3} is 8.85 % while that for *m*-xylene is 3.3 %. As with the majority of the experiments for *m*-xylene, the experiments for α-pinene were conducted at 35-40 °C.

The yields are expected to be even higher for lower temperatures. Also the yield experiments for α-pinene were conducted over a range of $\Delta HC/NO_x$ ratios of 6.9-15.1. There was little observed dependence of the yield on the ratio.

SOA YIELDS FOR ROG MIXTURES

In addition to the individual ROG experiments, three multiple ROG experiments were also conducted. Two experiments were performed with a mixture of *m*-xylene and α-pinene, and one experiment was conducted with a mixture of *m*-xylene and 1,2,4-trimethylbenzene. These experiments were used to further test the hypothesis that Y is a function of organic aerosol mass concentrations. In both cases selected concentrations of the two ROG's were placed in the chamber together with NO_x and irradiated with sunlight. The initial ROG concentrations, $\Delta HC/NO_x$ ratios, and the final M_o values are listed in Table 1. The two experiments with *m*-xylene and α-pinene were conducted at temperatures between 35-40 °C.

In experiment 09/15A, a maximum organic aerosol mass concentration of 80.3 μg m^{-3} was generated by the end of the experiment. Using the model generated lines in Figures 1 and 4, an M_o of 80.3 μg m^{-3} corresponds to a yield of 4.4 % for *m*-xylene and a yield of 11.5 % for α-pinene. Multiplying the value for *m*-xylene by the amount of *m*-xylene that reacted (1207 μg m^{-3}) gives an M_o of 53.1 μg m^{-3}. Multiplying the value for α-pinene by its amount reacted (278 μg m^{-3}) gives an M_o of 32.0 μg m^{-3}. The sum of these two values is 85.1 μg m^{-3}, which is extremely close to the overall observed organic aerosol mass concentration of 80.3 μg m^{-3} that was generated from the mixture of the two ROGs. This observation lends strong support to the idea that equation (7) correctly describes the dependence of SOA yields on organic aerosol mass concentrations.

A second multiple ROG experiment (09/19A) was conducted with *m*-xylene and α-pinene, and the final M_o that was generated from the combined oxidation of these two ROGs was 82.2 μg m^{-3}. If one goes through the same procedure as above, using Figures 1 and 4 to obtain the appropriate yield values that correspond to an M_o of 82.2 μg m^{-3}, the combined single M_o values add up to 81.2 μg m^{-3}. Once again the yields for the individual hydrocarbons, when used in conjunction with equation (7), are capable of accounting for the total organic aerosol mass concentrations that are produced from the oxidation of the ROG mixture.

A multiple ROG experiment with *m*-xylene and 1,2,4-trimethylbenzene was also conducted. The experiment was performed at a temperature of 25.5±2 °C and the final organic aerosol mass concentration was 195 μg m^{-3}. Since the experiment was conducted at 25.5±2 °C, the two product model line for *m*-xylene in Figure 1 that applies at 35-40 °C cannot be used. However the data points for experiment 10/17A in Figure 3 were obtained at 26.6±1 °C. Using these points to generate a two product model line, gives a yield of 9.94 % for *m*-xylene at an M_o of 195 μg m^{-3} and a temperature of 26.6 °C. Using the model line for 1,2,4-trimethylbenzene in Figure 2, the yield is 7.61 % at an M_o of 195 μg m^{-3}. Multiplying these yields for each of the ROG's by the amount that each ROG reacted gives M_o values of 97.3 μg m^{-3} for *m*-xylene and 97.6 μg m^{-3} for 1,2,4-trimethylbenzene. The sum of these is 194.9 μg m^{-3}, which is virtually identical to the M_o of 195 μg m^{-3} that was generated from the mixture. That the single ROG yields used in conjunction with equation (7) account for the organic aerosol mass concentrations generated in the multiple ROG experiments clearly shows that an absorption model correctly represents SOA formation.

AMBIENT SOA YIELDS

Ambient SOA yields cannot be represented by a unique value for a given ROG, because they are dependent on organic aerosol mass concentration and temperature. Examination of equations (2), (3), and (7), suggests that the only differences between the yields obtained from smog chamber studies and those in the ambient environment, for a given M_o and temperature, will be due to differences in the mean molecular weight of the absorbing *om* phase and in the activity coefficients of the absorbing products in the *om* phase. In smog chamber studies, the *om* phase is generated from the products of oxidation of a single ROG; in the ambient environment, the *om* phase is comprised of a mixture of condensed primary and secondary species. Even though there will be differences in the mean molecular weight of the *om* phase and in the activity coefficients between smog chamber SOA and ambient atmospheric aerosol, it seems unlikely that these differences will be large.

The mean molecular weight of the *om* phase is most likely in the range 150-250 g mol^{-1} both in smog chamber studies and in the ambient environment. On days when SOA formation in the atmosphere is important and oxidation products comprise a significant fraction of the *om* phase, activity coefficients for SOA products in the ambient *om* phase will likely be similar to those for SOA products in smog chamber generated secondary organic aerosol . This hypothesis is supported by the fact that the individual ROG yield data was able to so accurately account for the organic aerosol mass that was generated in the ROG mixture experiments. For example, if the products of α-pinene and *m*-xylene oxidation had terribly different polarities, then the activity coefficients of the products from *m*-xylene oxidation would be different if those products were partitioned into an organic aerosol layer comprised entirely of *m*-xylene oxidation products as opposed to an organic aerosol layer that was comprised of the oxidation products of both

m-xylene and α-pinene. This would mean that the yield for *m*-xylene would be different, for a given organic aerosol mass concentration, depending on whether it was measured from an experiment in which only *m*-xylene was used or whether a mixture of *m*-xylene and some other ROG was used. If this were the case, then the organic aerosol mass concentrations in the ROG mixture experiments would not be so accurately accounted for by the individual yield data. This is rather significant because it suggests that SOA yield data obtained from smog chamber studies will most likely account for the yield of individual ROG's when applied to the ambient atmosphere and could thus be used in conjunction with ambient models to determine the important sources of secondary organic aerosol in an urban airshed.

ACKNOWLEDGMENT

This work was supported by U.S. Environmental Protection Agency Exploratory Environmental Research Center on Airborne Organics (R-819714-01-0), National Science Foundation grant ATM-9307603, the Coordinating Research Council (A-5-1), and the Chevron Corporation.

REFERENCES

(1) Pankow, J. F. *Atmos. Environ.* **1994**, 28A, 185-188.

(2) Pankow J. F. *Atmos. Environ.* **1994**, 28A, 189-193.

(3) Turpin, B. J.; Huntzicker, J. J. *Atmos. Environ.* **1995**, 29B, 3527-3544.

(4) Schauer, J. J.; Rogge, W. F.; Hildemann, L. M.; Mazurek, M. A.; Simoneit, B. R.;

Cass, G. R. *Atmos. Environ.* **1996**, accepted for publication.

(5) Grosjean, D.; Seinfeld, J. H. *Atmos. Environ.* **1989**, 23, 1733-1747.

(6) Pandis, S. N.; Harley, R. A.; Cass, G. R.; Seinfeld, J. H. *Atmos. Environ.* **1992**, 26A, 2269-2282.

(7) Pandis, S. N.; Wexler, A. S.; Seinfeld, J. H. *Atmos. Environ.* **1993**, 27A, 2403-2416.

(8) Pandis, S. N.; Paulson, S. E.; Seinfeld, J. H.; Flagan, R. C. *Atmos. Environ.* **1991**, 25A, 997-1008.

(9) Wang, S. C.; Paulson, S. E.; Grosjean, D.; Flagan, R. C.; Seinfeld, J. H. *Atmos. Environ.* **1992**, 26A, 403-420.

(10) Hatakeyama, S.; Izumi, K.; Fukuyama, T.; Akimoto, H.; Washida, N. *J. Geophys. Res.* **1991**, 96, 947-958.

(11) Izumi, K; Fukuyama, T. *Atmos. Environ.* **1990**, 24A, 1433-1441.

(12) Stern, J. E.; Flagan, R. C.; Grosjean, D.; Seinfeld, J. H. *Envir. Sci. Technol.* **1987**, 21, 1224-1231.

(13) Gery, M. W.; Fox, D. L; Jeffries, H. E. *Int. J. Chem. Kinet.* **1985**, 17, 931-955.

(14) Leone, J. A.; Flagan, R. C.; Grosjean, D.; Seinfeld, J. H. *Int. J. Chem. Kinet.* **1985**, 17, 177-216.

(15) Grosjean D. In *Ozone and Other Photochemical Oxidants. Chapter 3: Aerosols*; National Academy of Sciences: Washington D. C., 1977; 45-125 pp.

(16) Zhang, S.; Shaw, M.; Seinfeld, J. H.; Flagan, R. C. *J. Geophys. Res.* **1992**, 97, 20.717-20.729.

(17) Zhang, S.; Akutsu, Y.; Russell, L. M.; Flagan, R. C.; Seinfeld, J. H. *Aerosol Sci. Technol.* **1995**, 23, 357-372.

(18) Atkinson, R. *J. Phys. Chem. Ref. Data.* **1989**, Monograph 1, 1.

(19) Atkinson, R.; Aschmann, S. M.; Arey, J. *Int. J. Chem. Kinet.* **1991**, 23, 77-97.

(20) Grosjean, D. *Sci. Total Environ.* **1991**, 100, 367-414.

Table 1. Outdoor Smog Chamber Experiment Summary.

	DATE	ROG_0 ($\mu g\ m^{-3}$)	ΔROG ($\mu g\ m^{-3}$)	M_0 ($\mu g\ m^{-3}$)	NO_x (ppb)	C_3H_6 (ppb)	$\Delta HC/NO_x$ (ppbC/ppb)	Y (%)
m-xylene	07/27A	2264	2114	101	629	300	7.8	4.78
"	07/27B	399	362	1.7	342	300	4.6	0.47
"	07/31A	1423	1219	20.1	521	235	6.0	1.64
"	07/31B	1494	1290	38.1	528	245	6.1	2.95
"	08/04A	4194	3953	396	1697	300	4.9	10.0
"	08/04B	2160	2018	106	933	300	4.9	5.25
"	08/09B	1049	795	18.8	1077	325	2.4	2.36
"	08/11A	1136	728	26.5	130	265	16.9	3.64
"	08/11B	1203	945	23.0	235	263	11.1	2.43
"	09/11A	1215	861	32.0	146	421	20.2	3.72
"	09/11B	1248	1032	35.5	279	421	11.8	3.44
"	09/13A	1211	1028	21.4	231	294	12.4	2.08
"	09/13B	1252	774	1.5	1609	294	1.3	0.19
m-xylene + α-pinene	09/15A	1394 + 278	1207 + 278	80.3	503	300	7.4	
m-xylene + α-pinene	09/19A	1132 + 342	936 + 342	82.2	409	300	8.1	
m-xylene	10/17A	2331	1945	188	998	300	4.5	9.67
1,2,4-Tmb	10/17B	2391	1996	113	975	300	4.7	5.66
"	11/02A	3367	2282	155	1178	300	4.3	6.79
"	11/02B	1607	1198	43.0	490	300	6.3	3.59
"	11/07A	1932	1533	78.0	590	300	6.3	5.09
"	11/07B	1237	1020	26.5	359	300	7.7	2.60
"	11/09B	1745	1309	53.0	528	300	6.2	4.05
1,2,4-Tmb + *m*-xylene	11/09A	1633 + 1538	1270 + 979	195	1048	300	4.8	
α-pinene	08/14A	726	726	87.0	240	300	9.8	12.0
"	08/14B	769	769	96.0	240	300	10.2	12.5
"	08/17A	384	384	22.7	203	300	8.0	5.91
"	08/17B	104	104	1.3	113	300	9.7	1.25
"	09/15B	283	283	8.0	206	300	6.9	2.83
"	09/22A	505	505	33.0	135	300	13.7	6.53
"	09/22B	467	467	38.2	125	300	14.5	8.18
"	09/25A	510	510	39.3	124	300	14.9	7.71
"	09/25B	505	505	34.2	122	300	15.1	6.77

LIST OF FIGURES

Figure 1. SOA Yields for *m*-Xylene

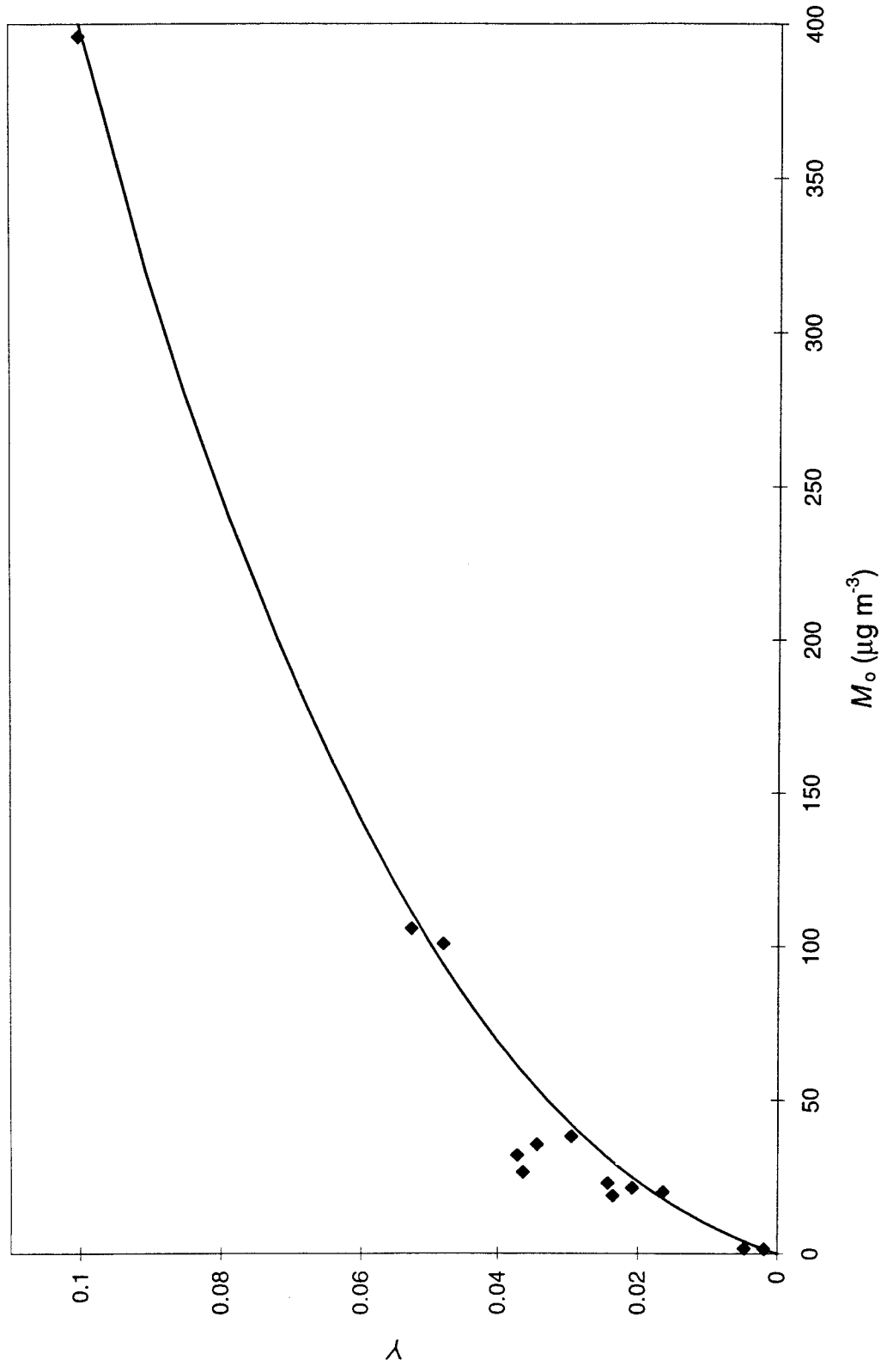

Figure 2. SOA Yields for 1,2,4-Trimethylbenzene

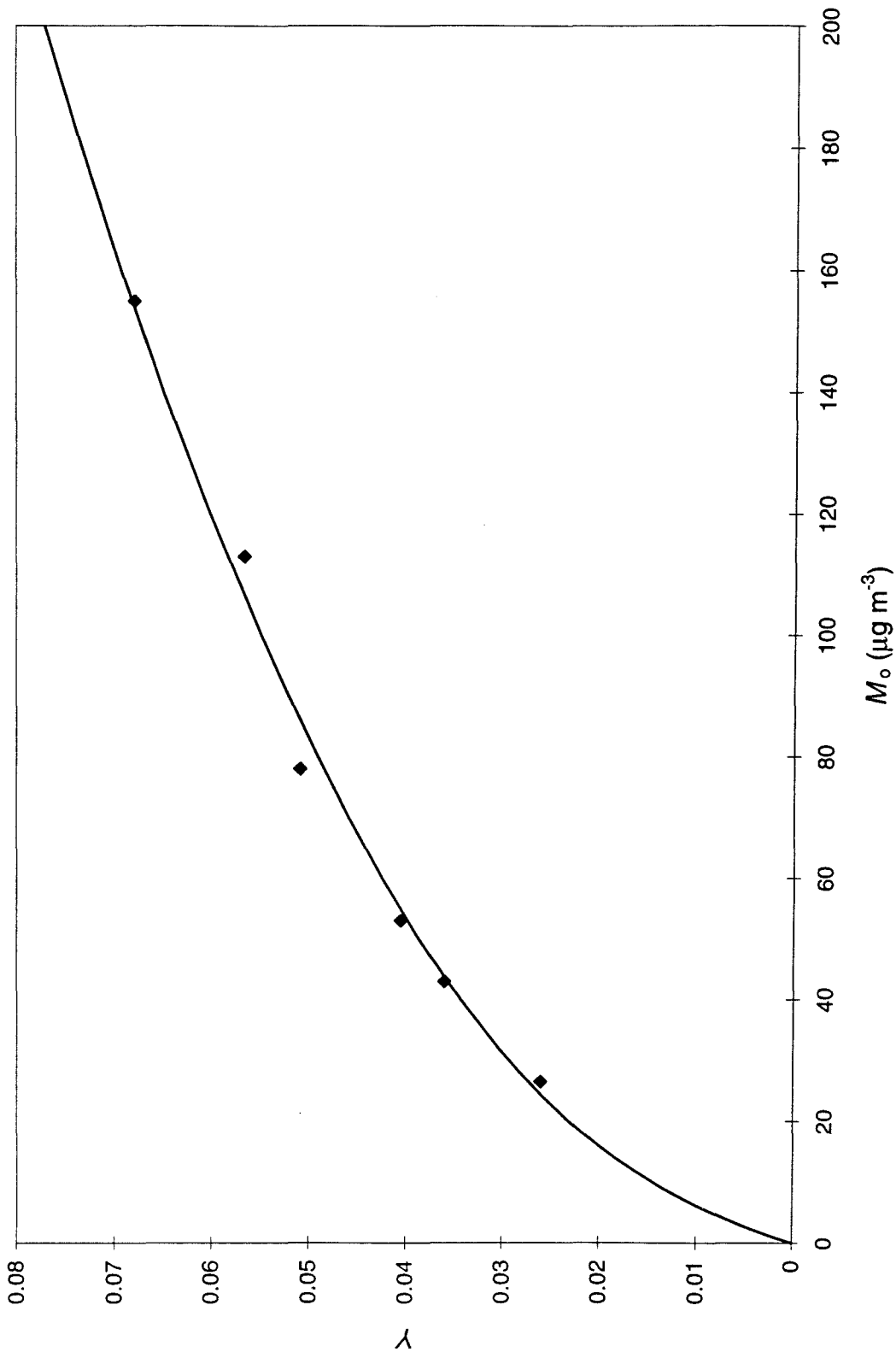

Figure 3. Temperature Dependence of m-Xylene Yields

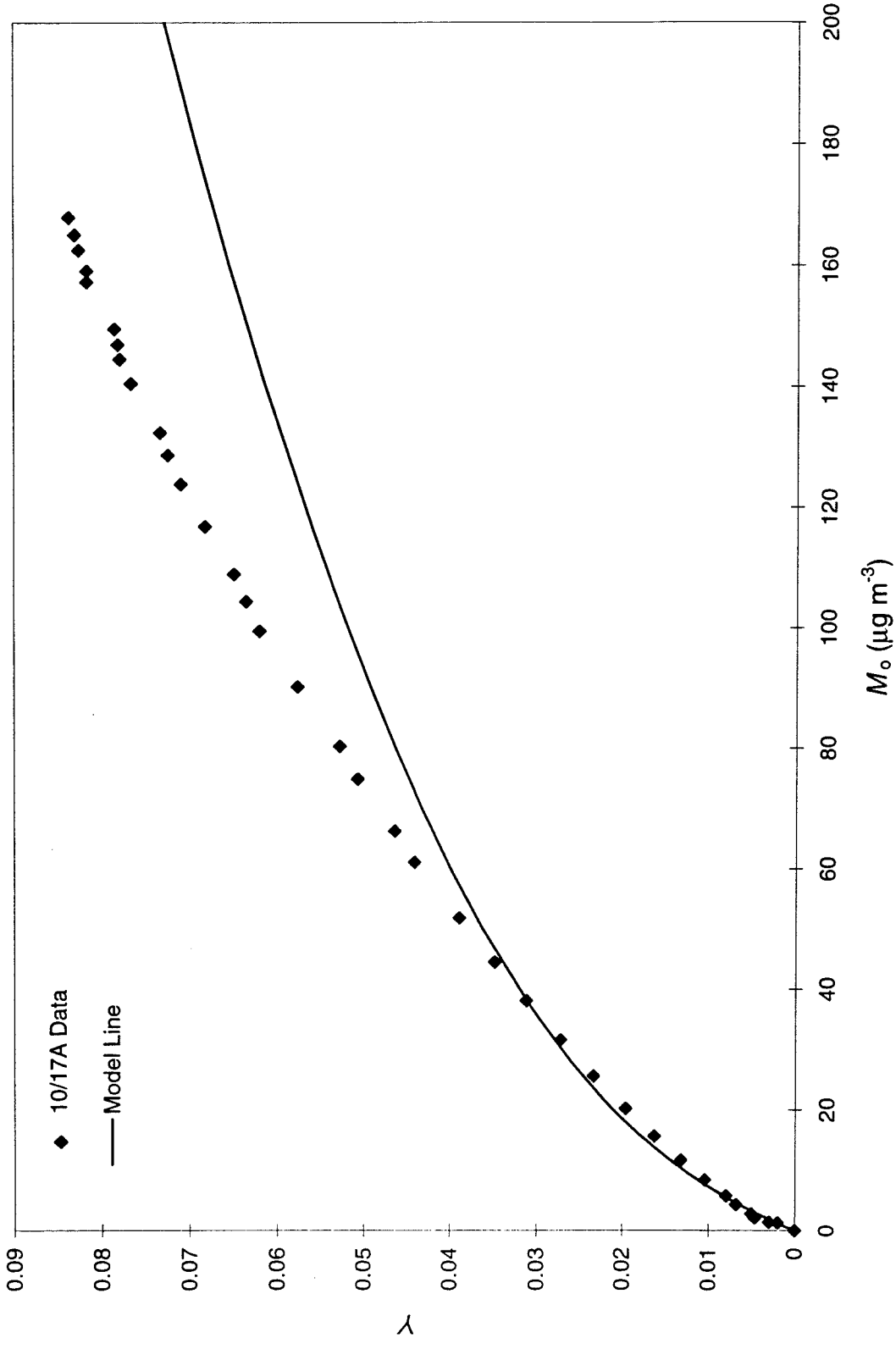

Figure 4. SOA Yields for α-Pinene

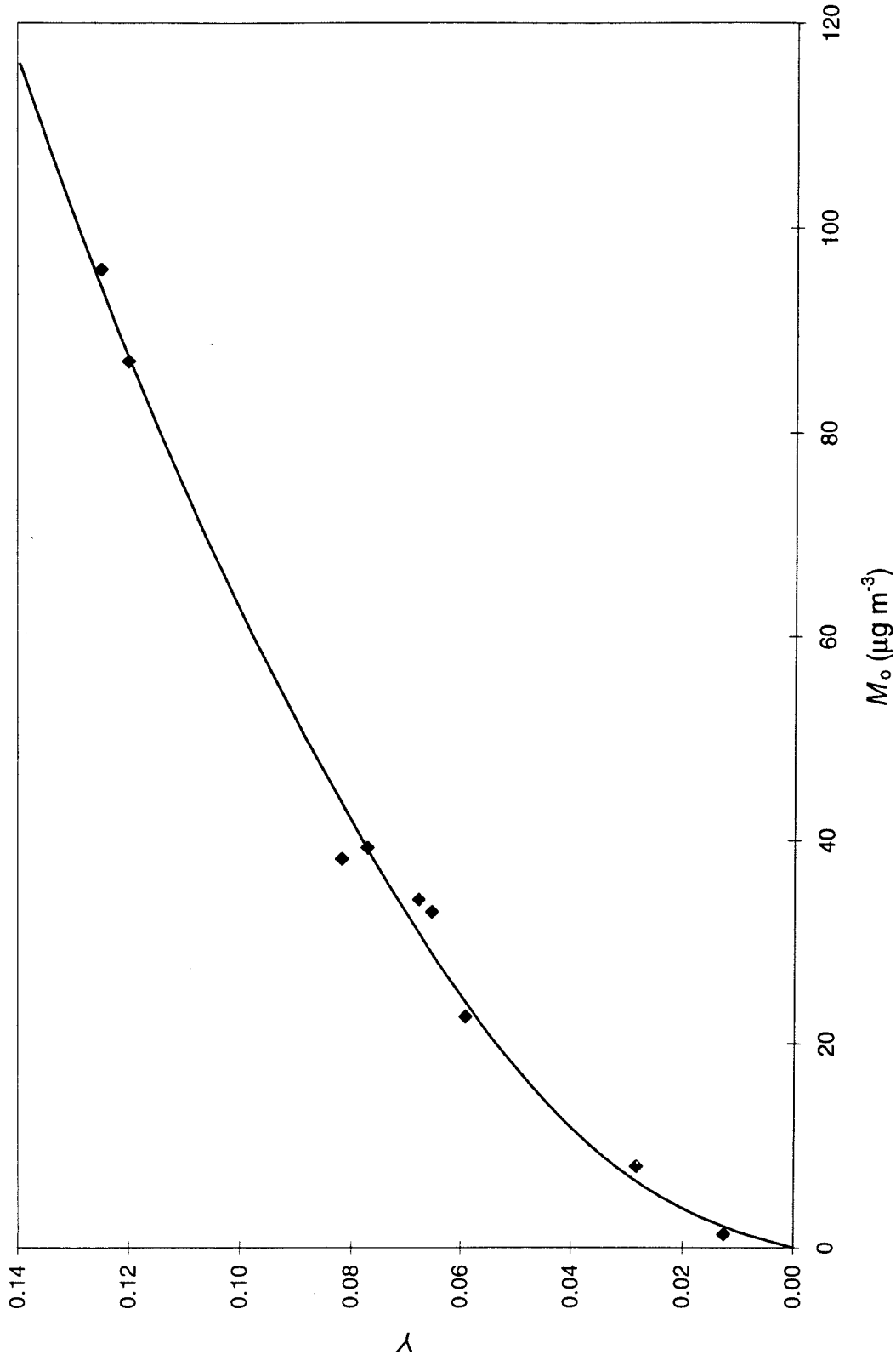

Chapter 3:
Aromatics, Reformulated Gasoline, and Atmospheric Organic Aerosol Formation

Published in *Environ. Sci. Technol.*, **31**, 1890 (1997) and *Science*, **276**, 96 (1997).

ABSTRACT

Secondary organic aerosol (SOA) yield curves have been obtained for 17 individual aromatic species from an extensive series of sunlight-irradiated smog chamber experiments. These yield curves, interpreted within the framework of a gas/aerosol absorption model, are used to quantitatively account for the SOA that is formed in a series of smog chamber experiments performed with the whole vapor of 12 different reformulated gasolines. The total amount of secondary organic aerosol produced from the atmospheric oxidation of whole gasoline vapor can be represented as the sum of the contributions of the individual aromatic molecular constituents of the fuel.

INTRODUCTION

Urban fine particulate matter is comprised of a complex mixture of both primary and secondary organic and inorganic compounds and emanates from a wide variety of sources. An important source that can significantly contribute to the fine particulate burden, especially during severe urban smog episodes, is secondary organic aerosol (SOA), (*1-5*). Much like ozone, secondary organic aerosol results from the atmospheric oxidation of reactive organic gases (ROGs). Whereas the oxidation of most ROGs results in ozone formation, SOA is generally formed only from the oxidation of ROGs comprised of seven or more carbon atoms, because oxidation products must have vapor pressures that are sufficiently low to enable them to partition into the aerosol phase (*1, 2*).

The chemical reaction pathways of large ROG molecules are complex, and resulting oxidation products are both numerous and difficult to quantify analytically. As a result, it is currently not possible, ab-initio, to determine the aerosol formation potential of individual ROGs and their contribution to the secondary organic urban particulate burden. However, a number of indirect methods have been employed to estimate the fraction of urban particulate carbon that is of secondary origin. Turpin and Huntzicker (*3*), using measured ratios of elemental carbon to organic carbon, estimated that as much as 70% of the organic carbon in Claremont, CA during a 1987 smog episode was secondary. Friedlander and coworkers (*4, 5*), using chemical element mass balance methods, suggested that SOA represented more than 75% of the total organic aerosol in Pasadena, CA in 1973. More recent estimates using chemical mass balance methods

suggest that, on a yearly average, 20-30% of the fine organic particulate matter in the South Coast Air Basin may be SOA (*6*).

Another approach that has been used to estimate the importance of SOA involves the use of experimentally measured secondary organic aerosol yields (Y). An SOA yield is a measure of the amount of aerosol that is produced from the atmospheric oxidation of an ROG and is defined as

$$Y = \frac{\Delta M_o}{\Delta \mathrm{ROG}} \qquad (1)$$

where ΔM_o is the amount of aerosol produced ($\mu g\ m^{-3}$) for a given reacted amount of an ROG, ΔROG ($\mu g\ m^{-3}$). Traditionally yields have been measured in smog chamber studies where an individual ROG is placed in the chamber with an appropriate amount of nitrogen oxides and is photooxidized until the reaction is complete. The amount of aerosol produced for the amount of reacted ROG is used to calculate the aerosol yield.

Yields have been measured for dozens of individual ROGs by a host of researchers over the last 20 years (*7-14*). While it was believed that each ROG must possess a constant yield value, measured yields for an individual ROG have exhibited a wide degree of variation both between and within laboratories. Odum *et al.* offered a possible explanation for this variation by proposing a new framework within which to interpret SOA yield data (*15*). Rather than considering the aerosol formation process as a product supersaturation/condensation phenomena, Odum *et al.* suggested that secondary organic aerosol formation is best described by a gas/aerosol absorptive partitioning model (*15-17*). Within that framework, oxidation products, produced from the atmospheric

oxidation of an ROG, are considered to be semi-volatile and can partition themselves into an absorbing organic aerosol (*om*) phase at concentrations below their saturation concentrations. The partitioning of each semi-volatile oxidation product is described by a partitioning coefficient ($K_{om,i}$) as

$$K_{om,i} = \frac{A_{om,i}}{G_i M_o} = \frac{760RT}{10^6 MW_{om} \zeta_i p^o_{L,i}} \quad (2)$$

where $A_{om,i}$ is the concentration of product *i* in the absorbing aerosol *om* phase (ng m^{-3}), G_i is the gas phase concentration of product *i* (ng m^{-3}), M_o is the absorbing organic aerosol mass concentration (μg m^{-3}), *R* is the ideal gas constant (8.206×10^{-5} m^3 atm mol^{-1} K^{-1}), *T* is the temperature (K), MW_{om} is the mean molecular weight of the *om* phase, ζ_i is the activity coefficient of product *i* in the *om* phase, and $p^o_{L,i}$ is the vapor pressure of product *i* as a pure liquid (sub-cooled, if necessary).

Using the gas/aerosol absorption model to interpret yield data, Odum *et al.* showed that SOA yields for an individual ROG are not uniquely valued, but rather are a function of the available absorbing organic aerosol concentration (*15*),

$$Y = M_o \sum_i \left(\frac{\alpha_i K_{om,i}}{1 + K_{om,i} M_o} \right) \quad (3)$$

where α_i is the mass-based stoichiometric coefficient for the reaction generating product *i* (i.e. $1000\alpha_i \Delta ROG = C_i$, where $C_i = A_{om,i} + G_i$). Assuming that there are two hypothetical products for each ROG, Odum *et al.* were successfully able to fit over 30 experimentally determined aerosol yields for three different ROGs (*m*-xylene, 1,2,4-trimethylbenzene,

and α-pinene) (*15*). Hoffmann *et al.* were also able to use this partitioning theory to describe aerosol yields for 8 different biogenic ROGs (*18*).

Nearly all of the smog chamber studies of secondary aerosol formation in the past have been conducted using only one ROG per experiment. However with the advent of an appropriate theory for SOA formation, the opportunity exists to study the aerosol formation potentials of complex ROG mixtures, in an attempt to more accurately mimic atmospheric SOA formation. In this paper, we discuss a series of 35 smog chamber experiments that were conducted on 17 individual alkylated aromatic species in order to determine the appropriate yield curves for these compounds. We also present data from a series of 20 smog chamber experiments that were conducted using the whole vapor of 12 different reformulated gasoline blends to determine those fuel parameters that control the aerosol formation potential of whole gasoline vapor. We then show that gas/aerosol absorption partitioning theory can be successfully applied to the SOA formation resulting from the atmospheric photooxidation of a complex mixture like whole gasoline vapor.

EXPERIMENTAL DESCRIPTION

Experiments were performed in a 60 m^3 sealed, collapsible Teflon bag that has been described in detail previously (*7, 8, 15*). Most of these experiments were conducted in a dual-chamber mode, in which the bag was divided in the center, so that two different experiments could be conducted under identical environmental (i.e. sunlight intensity,

temperature, etc.) conditions. Prior to each experiment the chamber was continuously flushed with purified laboratory compressed air for at least 38 hours (4-5 bag volumes) and baked in sunlight for at least one day, as described in Odum *et al.* (*15*).

Hydrocarbon measurements were made using a Hewlett Packard (Palo Alto, CA) 5890 gas chromatograph (GC) that was equipped with an HP-1 capillary column (20 m x 0.1 mm x 0.1 μm film thickness, Hewlett Packard) and a flame ionization detector (FID). The GC temperature program was: -60 °C for 1 min, -60 to 50 °C at 40 °C min^{-1}, 50 to 70 °C at 5 °C min^{-1}, 70 to 225 °C at 40 °C min^{-1}. Hydrocarbon calibrations were performed prior to each experiment by vaporizing microliter volumes of a calibration solution into a 60 L Teflon bag filled with a measured volume of Ultra Zero (Air Liquid America Corp., Houston, TX) compressed air. For each of the gasoline runs a calibration solution containing methyl-tertiary-butyl-ether, 2-methylpentane, 3-methylpentane, 2,2,4-trimethylpentane, toluene, ethylbenzene, *o*-xylene, and 1,2,4-trimethylbenzene was used.

The calibrations were followed by injection of $(NH_4)_2SO_4$ seed particles into the smog chamber to attain particle concentrations of 5,000-10,000 particles cm^{-3} with a number mean diameter of approximately 100 nm. The particles were generated by atomizing an aqueous solution of $(NH_4)_2SO_4$ using a stainless steel, constant rate atomizer. The aerosol was passed through heated copper tubing into a diffusional dryer, followed by a ^{85}Kr charge neutralizer before entering the chamber.

After obtaining the desired initial seed particle concentration, propene, hydrocarbons, NO_x, and hexafluorobenzene (C_6F_6) were injected (approximately 1 hour prior to the start of the experiment) through Teflon lines into the chamber, which was

completely shrouded from sunlight with a black polyethylene tarpaulin. Propene, NO, and NO_2 were injected using certified cylinders containing approximately 500 ppm of the gas in nitrogen. Hydrocarbons and C_6F_6 were introduced into the chamber by injecting microliter quantities of the pure liquid into a glass bulb that was gently heated while being diluted with purified compressed lab air that went directly to the chamber. Propene was used at mixing ratios of 250-350 ppb to facilitate the production of hydroxyl (OH) radicals in sufficient concentrations for the inception of the experiment. The C_6F_6 was used as an internal standard for hydrocarbon gas chromatographic (GC) samples in order to normalize for injection variations of the 6-port stainless steel injection valve (Valco, Houston, TX), equipped with a heated (100 °C) 2 ml Teflon sampling loop. The use of the internal standard yielded estimated uncertainties in the hydrocarbon measurements of less than ±2% for most experiments.

After injection of the gases and seed aerosol, but before uncovering the chamber, initial measurements of hydrocarbons, NO_x, O_3, and aerosol concentrations and size distributions were made to obtain initial values and to ensure that the contents were well mixed. Generally three to five initial hydrocarbon measurements, using the HP 5890 GC described above, were made for each side of the bag. A Thermo Environmental Instruments (Franklin, MA) Model 42 chemiluminescence NO_x monitor was used to measure NO, NO_2, and NO_x. Complete NO_x monitor calibrations were performed daily. A Dasibi Environmental Corp. (Glendale, CA) Model 1008-PC O_3 analyzer was used to monitor O_3 concentrations. NO_x and O_3 measurements were made at 10 min. intervals between alternating sides of the chamber. Estimated uncertainties in the NO and NO_2 measurements are approximately ±4% and ±7%, respectively. The ozone instrument has

an estimated uncertainty of ±4% in its initial calibration and was seen to drift only a few percent over the period of several months.

Complete number and size distribution measurements were recorded for both sides of the chamber with a one-minute frequency throughout an experiment. The aerosol instrumentation consisted of one TSI Model 3071 cylindrical scanning electrical mobility spectrometer for each side of the divided chamber. Each electrical mobility spectrometer (SEMS) was equipped with a TSI model 3760 condensation nuclei counter (CNC) to count transmitted particles. SEMS voltages were scanned from 40-8500V with a one minute ramp. The cylindrical SEMS were operated with sheath and excess flows of 2.5 L min^{-1} and inlet and classified aerosol flows of 0.25 L min^{-1} to allow for measurement of particle size distributions in the range of 30-850 nm. A more complete description of the SEMS scanning cycle and operation have been published previously (*8*). Particle losses in the SEMS, SEMS response functions, particle charging efficiencies, CNC counting efficiency, and particle deposition in the chamber have been taken into account in the analysis of the aerosol data (*8*). Estimated uncertainties in the SEMS size and concentration measurements are approximately ±10%.

After making initial measurements prior to the start of the experiment, the black tarpaulin (chamber cover) was removed to expose the chamber contents to sunlight. Hydrocarbon measurements were made for both sides of the chamber every 8-10 min throughout the experiment. NO, NO_2, NO_x, and O_3, were continuously monitored during 10 min intervals alternating between the two sides of the chamber. Temperature, total solar radiation, and UV were continuously monitored over the course of the experiment.

All gasoline blends used in this study were produced during the Auto/Oil Air Quality Improvement Program (AQIRP). The Auto/Oil industry AQIRP was a study conducted by 14 petroleum companies and the three domestic automakers, the prime objective of which was to examine the potential improvements in vehicle emissions, and ultimately air quality, from reformulated gasoline (*19, 20*). The AQIRP produced over 80 different fuel blends in which specific fuel properties were controlled. Detailed chemical speciation/quantitation was performed on all of the AQIRP fuels during that program (*21, 22*). For the individual aromatic smog chamber experiments, the concentration-time profile of the hydrocarbon was explicitly determined from GC/FID peak areas and calibration data. For the gasoline experiments, only the 8 calibration species mentioned above were explicitly tracked using the GC/FID. Initial concentrations of the 8 calibration species for the gasolines were measured for each experiment. Knowing the mass percent of every compound in a fuel (obtained from AQIRP speciation data) allowed the initial concentration of all species to be calculated from the initial concentrations of the 8 calibration species. Then by measuring the concentration-time profiles of the 8 calibration species and knowing their reaction rate constants with hydroxyl radical, a concentration-time profile for OH was calculated for each experiment. Typical calculated OH concentrations ranged from $1x10^6$ to $5x10^6$ molec cm^{-3}. This, along with the measured ozone (O_3) concentrations, and OH and O_3 rate constants, was used to calculate the concentration-time profile for each speciated compound in a fuel.

Hydroxyl radical and ozone reaction rate constants for the speciated compounds were obtained either from the literature (*23*) and NIST chemical kinetic database (*24*), or when experimentally not known, were estimated using structure reactivity relationships

(*25*). Whereas the structure reactivity relationships (SAR) expressions for alkanes and alkenes were used unchanged, those for the aromatic species were modified. The Hammet substituent constant σ_m^+ used in the SAR expression had to be optimized for alkyl substituted aromatics, since the values in the range of $\sigma_m^+ \sim -0.06$ derived originally for different alkyl substituents by Brown and Okamoto (*26*) lead to spurious results for those aromatics with a substitution pattern of alkyl groups in the *meta*-position. Experimentally known OH overall reaction rate constants (*23*) for 15 alkyl substituted aromatics were used to derive ring addition rate constants k^{add}. The contribution of side chain reactivity to the experimental values was accounted for by subtracting the SAR estimates of OH abstraction rate constants. Predicted addition rate constants obtained by the Hammet expression were fit to the experimental k^{add} rates by minimizing the sum of square error varying the value of σ_m^+, taken to be uniform for the various alkyl substituents. The optimized expression for OH addition rate constant $\log_{10}k^{add}$ (cm^3 molecule^{-1} s^{-1}) = $-11.89 - 1.82\sum\sigma^+$ was obtained with $\sigma_m^+ = -0.190$ for alkyl substituents and $\sigma_{o,p}^+$ as used in (*25*). The quality of the fit for the overall OH radical rate constant estimates for the aromatics was improved to 30% maximum error compared to 110% using the parameters in (*25*).

AROMATIC AEROSOL YIELDS

A series of 35 smog chamber experiments were performed with 17 individual aromatic species to determine the SOA yields for these individual compounds. Table 1

lists the experimental conditions and results for each smog chamber run. The total organic aerosol mass concentration produced (ΔM_o) and the total concentration of aromatic consumed (ΔROG) in each experiment were measured and used to calculate the SOA yield ($Y = \Delta M_o/\Delta$ROG) for each experiment. These individual aromatic aerosol yields are shown as a function of ΔM_o in Figure 1. In general, the data falls into two distinct classes, which we have labeled low-yield and high-yield aromatics. The high yield aromatic species are those species containing one of fewer methyl substituent and one or fewer ethyl substituent (i.e. toluene; ethylbenzene; and ethyltoluenes) as well as *n*-propylbenzene. The low yield aromatics are those aromatics that contain 2 or more methyl substituents (i.e. xylenes; trimethylbenzenes, dimethyl-ethylbenzenes, tetramethylbenzenes). Eighteen of the low-yield aromatic points are from experiments conducted in the Caltech smog chamber in the summer of 1995, the experimental conditions of which have been previously published (*15*). The curves through the data in Figure 1 have been generated using equation (3) assuming a hypothetical two-product model. That is, a set of α_1, α_2, $K_{om,1}$, $K_{om,2}$ are chosen for each curve and these values are adjusted to minimize the square of the residuals. Whereas the organic aerosol phase produced from the atmospheric oxidation of an individual aromatic is comprised of dozens of oxidation products (27), the yield data can be fit assuming that there are only two hypothetical products (i.e. four parameters). The use of only one model product (i.e. two parameters) is insufficient to capture the behavior of the data over the complete range of organic aerosol mass concentrations. While using three or more model products (i.e. 6 or more parameters) is superfluous.

Since the parent aromatics species corresponding to each of the curves in Figure 1 are similar in structure, it is highly likely that they generate similar atmospheric oxidation products. Indeed, Forstner et al. found that many individual aromatic species generate similar (and in some cases identical) atmospheric oxidation products (*27*). Therefore it does not seem surprising that much of the data in Figure 1 fall on only two yield curves. At present, we are not able to determine why compounds corresponding to curve 1 have higher yields than those corresponding to curve 2. One might speculate that the single substituted aromatics (i.e. those on curve 1) might generate a higher ratio of ring-retaining to ring-cleavage products than the multiply substituted aromatics (i.e. those on curve 2). Ring-retaining products may have lower vapor pressures than the smaller ring-cleavage products, resulting in higher yields for the single-substituted aromatics. However, in the absence of complete product information, it is difficult to definitively determine the correct explanation for this observation.

Another fairly comprehensive aromatic aerosol yield data set is that of Izumi and Fukuyama (*10*). Figure 2 shows this data set analyzed within the framework of the absorptive partitioning model outlined above. The yield curves shown in the figure are curves 1 and 2 from Figure 1. Although the fit is not perfect, the agreement between the data set of Izumi and Fukuyama and the curves generated from the Caltech data is quite striking. Thus it would seem that much of the variability seen in aerosol yield data sets can be accounted for if yields are interpreted within the gas/aerosol absorption model.

To predict the amount of SOA that is formed from the atmospheric oxidation of an ROG based on first principles would require complete knowledge of all the oxidation products, their stoichiometric reaction coefficients, their vapor pressures, and their

activity coefficients in the om-phase (i.e. see equations 2 and 3). Whereas from a fundamental standpoint this would be the most satisfying approach, it is rather impractical given the current state of knowledge. Complete product information is not available for any aromatic parent species, and even if it were, estimating all the associated parameters would prove to be a formidable task. However, therein lies the power of yield curves like those shown in Figure 1. Using these curves, one can predict the amount of aerosol formed from the atmospheric oxidation of a mixture of these compounds, despite the lack of knowledge concerning oxidation products.

AEROSOL FORMATION POTENTIAL OF WHOLE GASOLINE VAPOR

A series of 20 smog chamber experiments using 12 different reformulated gasolines obtained from the Auto/Oil Air Quality Improvement Research Program (AQIRP) were performed to determine those fuel properties (e.g. % aromatics, % olefins, T_{90} distillation temperature, etc.) that are important for predicting the atmospheric aerosol formation potential of the whole fuel vapor. The 12 fuels used in this study and some of their controlled properties are listed in Table 2.

Experimental conditions and results for the gasoline smog chamber runs are listed in Tables 3 and 4. In Figure 3a, the organic aerosol concentration (ΔM_o) produced from the atmospheric oxidation of whole gasoline vapor is shown as a function of the total reacted organic gas concentration (ΔROG). The most striking feature of this figure is that

the data points fall into two distinct classes. The high aromatic content fuels (32% ≤ % aromatic < 48%) produce significantly more aerosol for the same amount of total reacted organic gas than the low aromatic content fuels (20% ≤ % aromatic < 25.5%). This suggests that aromatic content is an important parameter influencing the amount of organic aerosol that is produced from the atmospheric oxidation of whole gasoline vapor. Indeed, if ΔM_o is instead plotted against the total amount of aromatics that reacted during the oxidation of a fuel ($\Delta Aromatic$), as is shown in Figure 3b, the data collapse onto a single curve.

A second interesting feature to note in Figures 3a and 3b is that the curves through the data are nonlinear. This results from the fact that SOA yields increase as a function of ΔM_o as shown by equation (3) and Figure 1. In other words, as more hydrocarbon reacts, producing more organic aerosol, a larger mass fraction of each semi-volatile oxidation product will partition to the aerosol phase. This effect is clearly demonstrated in Figure 4 where $\Delta M_o / \Delta Aromatic$ is shown as a function of ΔM_o. Curves 1 and 2 from Figure 1 have been included as well. The ratio $\Delta M_o / \Delta Aromatic$ is a measure of the SOA yield from the aromatic fraction of the fuel. Indeed, for the individual aromatic curves $\Delta M_o / \Delta Aromatic = Y$. As equation (3) predicts, the value of the "yield" increases as a function of ΔM_o. More importantly however, data points for all fuels, other than fuel RF-L, fall within the range defined by curves 1 and 2. This strongly re-enforces the point that aromatics are the class of compounds that are responsible for producing the majority of the SOA formed during the atmospheric oxidation of whole gasoline vapor. If significant amounts of SOA were being produced by other classes of compounds (i.e. olefins,

alkanes, and oxygenates) present in the fuels, then most points would lie above the envelope defined by curves 1 and 2.

For most of the fuels, between 92-99 % of the mass of each fuel was speciated in AQIRP. However only 83 % of the mass of fuel RF-L, which was the only high T_{90} fuel from Phase I of AQIRP used in this study, was speciated in AQIRP. The ninety percent distallation temperature, T_{90}, of a fuel relates to the fuel's heavy-end volatilty. Fuels with large T_{90} values contain a larger fraction of heavier species. Many of these heavier species are C_{10}-C_{12} aromatics that were not speciated in Phase I of AQIRP. Thus, much of the remaining 17 % of the mass that was not speciated for fuel RF-L is most likely heavy aromatic species that contribute to the SOA formed from the oxidation of this fuel. Since this 17 % was not speciated, its contribution to $\Delta Aromatic$ could not be estimated. Thus $\Delta Aromatic$ is most likely underestimated and is the reason that this fuel does not fall within the envelope as all other fuels in Figure 4.

Determining that aromatics clearly control the aerosol formation potential of whole gasoline vapor presents the opportunity to quantitatively predict the SOA formed during its atmospheric oxidation using the procedure that was applied to the five aromatic mixture experiment. Even though yield curves are not available for every aromatic species present in the fuels, using the curves for the 17 species in Figure 1, along with the observation that all isomers of a given compound seem to be described by the same yield curve, yield curves are available for 19 of the 26 aromatics that were speciated in Phase I of AQIRP. These 19 species represented, on average, 96 % of $\Delta Aromatic$ for all fuels other than RF-A and RF-L. Of the 57 aromatic compounds that were speciated for the

AQIRP Phase II fuels, yield curves are available for 28 species representing, on average, 95 % of $\Delta Aromatic$. Obtaining yield values for each aromatic, corresponding to the amount of SOA formed (ΔM_o) in an individual experiment and multiplying these values by the reacted amount of the respective aromatic, yields an estimate of the amount of SOA that is attributable to each of the aromatic species. Summing these values for all aromatics in a given fuel for a given experiment gives a quantitative estimate of the amount of SOA that was produced by the aromatic fraction of each fuel in a given experiment. Table 4 lists the observed total SOA concentration produced from the atmospheric oxidation of the whole gasoline vapor as well as the total SOA predicted to be formed solely from the aromatic fraction of the fuel. This method accounts for 70-130 % of the SOA that was produced for all fuels other than fuel RF-L. The average for all fuels, excluding RF-L, is 100 ± 16 % (1σ). Thus by simply accounting for the aerosol formation potential of a fuel's aromatic content, one can quantitatively account for the SOA formed from the atmospheric oxidation of whole gasoline vapor.

Besides RF-L, of the 12 fuels listed in Table 4, Industry Average (RF-A) is accounted for with the lowest level of accuracy. The SOA predicted to be formed from Industry Average is consistently under-predicted. This most likely results from the fact that RF-A contains a significant fraction of heavy aromatics for which no yield curves are available. These aromatics include naphthalene, methyl-naphthalenes, indan, and methyl-indans. These compounds most certainly have substantial aerosol forming potentials and thus would significantly contribute to the SOA formed from this fuel. However at present, aerosol yield curves are not available for these compounds and thus their

contribution to the SOA formed could not be included in the calculations. Despite this problem however, this amounts to an average under-prediction of only 20% (n = 3) for this fuel, which is certainly adequate for atmospheric modeling purposes. Considering that whole gasoline vapor is comprised of over 300 chemical species, it is striking that the aerosol formed from its atmospheric oxidation can be accounted for using the methods described above with such accuracy. These results certainly suggest that it is highly likely that SOA formation in an urban airshed can be modeled using yield data like that presented in this paper.

CALIFORNIA PHASE II AND INDUSTRY AVERAGE

Two experiments were performed in which California Phase II (C2) and Industry Average (RF-A) gasoline were placed in opposing sides of the chamber so that the aerosol forming potential of the two fuels could be examined simultaneously under identical environmental conditions. The most interesting of this series is the experiment performed on 7/29/96. The initial concentration of RF-A on side A of the chamber was 6926 $\mu g\ m^{-3}$ and C2 on side B of the chamber was 8595 $\mu g\ m^{-3}$. Despite the much larger initial concentration of C2, the total amount of ROG that reacted (ΔROG) was identical for the two fuels (see Table 4). The lower olefin and aromatic content of C2 make it a considerably less reactive fuel than RF-A. For identical reacted amounts of carbon, the two fuels produced virtually the same amount of ozone. This was the case for most fuels.

The ratio of Max O_3 to ΔROG for all fuels, other than RF-L and RF-F, was 0.50 ± 0.06 ppb ug^{-1} m^3 (see Table IV). Despite having reacted the same amount of carbon and having produced the same amount of ozone, Industry Average gasoline produced twice as much secondary organic aerosol as did California Phase II. This is because, despite the fact that ΔROG is identical for the two fuels, a much larger fraction of ΔROG for RF-A is aromatic, and as was shown before, it is that aromatic content of the fuel that is responsible for forming SOA.

ATMOSPHERIC AEROSOL FORMATION

The data in Figure 4, excluding RF-L, can be fit rather well with the following power-law relationship

$$\Delta M_o / \Delta Aromatic = 0.0042(\Delta M_o)^{0.6023} \quad (4)$$

with an $r^2 = 0.997$. This suggests that if a mixture of mono-cyclic aromatic species is sufficiently complex, then the aerosol formed from the oxidation of that mixture can be predicted using equation (4) simply by knowing the total reacted aromatic concentration, rather than accounting for the aerosol formation potential of each aromatic species individually. Since the urban atmospheric, anthropogenic, volatile hydrocarbon (UAVHC) profile is well approximated by whole gasoline vapor, it would seem that equation (4) would be applicable for predicting SOA formation from atmospheric oxidation of UAVHC with ambient models.

ACKNOWLEDGMENT

We would like to acknowledge support by the U. S. Environmental Protection Agency Center on Airborne Organics, the National Science Foundation, the Coordinating Research Council, and the Chevron Corporation. T.P.W Junkamp would also like to acknowledge a Forschungsstipendium by the Deutsche Forschungsgemeinschaft.

REFERENCES

(1) Grosjean, D. *Atmos. Environ.* **1992**, 26A, 953-963.

(2) Grosjean, D.; Seinfeld, J. H. *Atmos. Environ.* **1989**, 23, 1733-1747.

(3) Turpin, B. J.; Huntzicker, J. J. *Atmos. Environ.* **1995**, 29B, 3527-3544.

(4) Gartrell, G. Jr.; Friedlander, S. K. *Atmos. Environ.* **1975**, 9, 279-299.

(5) Grosjean, D.; Friedlander, S. K. *J. Air Pollut. Control Ass.* **1975**, 25, 1038-1044.

(6) Schauer, J. J.; Rogge, W. F.; Hildemann, L. M.; Mazurek, M. A.; Simoneit, B. R.; Cass, G. R. *Atmos. Environ.* **1996**, 30, 3837-3855.

(7) Pandis, S. N.; Paulson, S. E.; Seinfeld, J. H.; Flagan, R. C. *Atmos. Environ.* **1991**, 25A, 997-1008.

(8) Wang, S. C.; Paulson, S. E.; Grosjean, D.; Flagan, R. C.; Seinfeld, J. H. *Atmos. Environ.* **1992**, 26A, 403-420.

(9) Hatakeyama, S.; Izumi, K.; Fukuyama, T.; Akimoto, H.; Washida, N. *J. Geophys. Res.* **1991**, 96, 947-958.

(10) Izumi, K.; Fukuyama, T. *Atmos. Environ.* **1990**, 24A, 1433-1441.

(11) Stern, J. E.; Flagan, R. C.; Grosjean, D.; Seinfeld, J. H. *Environ. Sci. Technol.* **1987**, 21, 1224-1231.

(12) Gery, M. W.; Fox, D. L.; Jeffries, H. E. *Int. J. Chem. Kinet.* **1985**, 17, 931-955.

(13) Leone, J. A.; Flagan, R. C.; Grosjean, D.; Seinfeld, J. H. *Int. J. Chem. Kinet.* **1985**, 17, 177-216.

(14) Grosjean. D. Aerosols. *In Ozone and Other Photochemical Oxidants; National Academy of Sciences*: Washington, DC, **1977**; Chapter 3, pp 45-125.

(15) Odum, J. R.; Hoffmann, T.; Bowman, F.; Collins, D.; Flagan, R. C.; Seinfeld, J. H. *Environ. Sci. Technol.* **1996**, 30, 2580-2585.

(16) Pankow, J. F. *Atmos. Environ.* **1994**, 28A, 185-188.

(17) Pankow, J. F. *Atmos Environ.* **1994**, 28A, 189-193.

(18) Hoffmann, T.; Odum, J. R.; Bowman, F.; Collins, D.; Klockow, D.; Flagan, R. C.; Seinfeld, J. H. *J. Atmos. Chem.* **1997**, in press.

(19) Burns, V. R.; Benson, J. D.; Hochhauser, A. M.; Koehl, W. J.; Kreucher, W. M.; Reuter, R. M. *SAE technical paper no. 912320*, Society of Automotive Engineers, Warren, PA, **1991**.

(20) Hochhauser, A. M.; Benson, J. D.; Burns, V. R.; Gorse, R. A.; Koehl, W. J.; Painter, L. J.; Rippon, B. H.; Reuter, R. M. *SAE technical paper no. 912322*, Society of Automotive Engineers, Warren, PA, **1991**.

(21) Paul, R. H.; Mc Nally, M. J. *SAE technical paper no. 902098*, Society of Automotive Engineers, Warren, PA, **1991**.

(22) Kopp, V. R.; Bones, C. J.; Doerr, D. G.; Ho, S.; Schubert, A. J. *SAE technical paper no. 930143*, Society of Automotive Engineers, Warren, PA, **1993**.

(23) Atkinson, R. *J. Phys, Chem. Ref. Data*, Monograph (2), **1994**.

(24) Mallard, W. G.; Westley, F.; Herron, J. T.; Hampson, R. F. *NIST Chemical Kinetics Database-Version 6.01*, NIST Standard Ref. Data, Gaitherburg, MD, **1994**.

(25) Kwok, E. S. C.; Atkinson, R. *Atmos. Environ.* **1995**, 29, 1685-1695.

(26) Brown, H. C.; Okamoto, Y. *J. Am. Chem. Soc.* **1958**, 80, 4979.

(27) Forstner, H. J. L.; Flagan, R. C.; Seinfeld, J. H. *Environ. Sci. Technol.* **1997**, 31, 1345.

(28) Harley, R. A.; Hannigan, M. P.; Cass, G. R. *Atmos. Environ.* **1992**, 26, 2395.

(29) Odum, J. R.; Jungkamp, T. P. W.; Griffin, R. J., Flagan, R. C.; Seinfeld, J.H. *Science* **1997**, 276, 96.

Table 1. Results from Individual Aromatic Experiments.

Date	Compound	ΔROG ($\mu g\ m^{-3}$)	ΔM_o ($\mu g\ m^{-3}$)	Y
06/06/96a	*m*-ethyltoluene	1927	208	0.108
06/06/96b	*m*-xylene	1891	106	0.056
06/12/96a	1,3,5-trimethylbenzene	1029	31	0.031
06/12/96b	*m*-ethyltoluene	971	30	0.068
06/17/96a	ethylbenzene	434	13	0.030
06/17/96b	*m*-ethyltoluene	334	13	0.039
06/19/96a	*m*-xylene	1571	46	0.029
06/19/96b	*m*-xylene	1528	48	0.031
06/21/96a	ethylbenzene	3176	394	0.124
06/21/96b	*p*-Diethylbenzene	314	17	0.055
06/24/96a	ethylbenzene	1872	185	0.099
06/24/96b	*p*-Diethylbenzene	742	61	0.082
06/28/96a	toluene	1413	133	0.094
06/28/96b	*p*-Xylene	823	16	0.019
07/01/96a	toluene	1268	111	0.088
07/01/96b	*p*-xylene	1063	32	0.030
07/05/96a	toluene	1710	171	0.100
07/05/96b	*n*-propylbenzene	1314	103	0.078
07/08/96a	*p*-ethyltoluene	708	38	0.054
07/08/96b	*m*-ethyltoluene	789	49	0.062
07/10/96a	ethylbenzene	1169	104	0.089
07/10/96b	toluene	923	68	0.074
07/12/96a	1-methyl-3-*n*-propylbenzene	1220	72	0.059
07/12/96b	1,2-dimethyl-4-ethylbenzene	1426	49	0.034
07/15/96a	1,2-dimethyl-4-ethylbenzene	1602	72	0.045
07/15/96b	1-methyl-3-*n*-propylbenzene	1041	54	0.052
07/17/96a	*n*-propylbenzene	657	39	0.059
07/17/96b	1,2,4,5-tetramethylbenzene	1394	40	0.029
07/19/96a	*n*-propylbenzene	1790	190	0.106
07/19/96b	1,2,4,5-tetramethylbenzene	2339	70	0.030
07/22/96	1,4-dimethyl-2-ethylbenzene	1251	50	0.040
09/09/96	*o*-xylene	1117	35	0.031
09/11/96	*o*-xylene	1082	23	0.021
09/16/96a	1,2,3,5-tetramethylbenzene	2142	65	0.030
09/16/96b	1,2,3,5-tetramethylbenzene	1071	25	0.023
07/24/96	Aromatic Mixture	802	28	NA

Table 2. Properties of AQIRP Reformulated Gasolines

Fuel Code/ AQIRP Phase	Fuel ID	Aromatics Volume %	MTBE Volume %	Olefins Volume %	T_{90} (°F)
A/I	Industry Avg	32.0	0.0	9.2	330
F/I	amot	20.0	0.0	3.2	279
G/I	AmOt	44.3	0.0	17.4	286
K/I	Amot	45.7	0. 0	4.9	294
L/I	AmOT	47.8	0.0	17.7	357
O/I	AMOt	46.7	14.6	19.3	283
P/I	amOt	20.3	0.0	18.3	284
C2/II	Cal Phs II	25.4	11.2	4.1	293
1B/II	Matrix B Base	25.3	11.2	15.0	267
2B/II	Base+RMH	35.1	10.4	11.2	314
3B/II	Base+AH	22.1	10.4	13.3	299
4B/II	Base+AH+RMH	32.2	10.2	10.7	334

A/a = High/Low Aromatics
M/m = High/Low MTBE
O/o = High/Low Olefins
T/t = High/Low T_{90} (90 percent distillation temperature)
RMH = Medium and Heavy Reformate Cut (predominantly C_9 and C_{10} aromatics)
AH = Heavy Alkylate Cut (heavy paraffins)

Table 3. Conditions For Gasoline Experiments.

Experiment	Fuel	$[ROG]_o$ ($\mu g\ m^{-3}$)	$[NO]_o$ (ppb)	$NO_2]_o$ (ppb)	Chamber T_{avg} (K)
07/26/96a	C2	7179	950	476	315
07/26/96b	RF-A	6603	926	480	315
07/29/96a	RF-A	6926	1038	529	315
07/29/96b	C2	8595	953	490	315
08/19/96a	RF-L	3421	845	424	310
08/21/96a	RF-A	3756	469	256	313
08/21/96b	RF-F	5457	930	460	313
08/23/96b	RF-L	2733	456	250	313
08/26/96a	RF-F	6217	1011	498	311
08/26/96b	RF-G	6042	987	511	311
08/28/96a	RF-1B	5855	957	517	315
08/28/96b	RF-3B	5371	955	516	315
08/30/96a	RF-2B	6377	1046	570	314
08/30/96b	RF-4B	5019	903	456	314
09/02/96a	RF-G	5991	940	495	309
09/02/96b	RF-O	6326	989	533	309
09/04/96a	RF-P	6759	1068	550	308
09/04/96b	RF-F	5999	878	453	308
09/06/96a	RF-K	6528	1007	500	310
09/06/96b	C2	6561	916	468	310

Table 4. Results for Gasoline Experiments.

Date	Fuel	ΔROG ($\mu g\ m^{-3}$)	Δ*Aromatic* ($\mu g\ m^{-3}$)	Max O_3 (ppb)	Actual ΔM_o ($\mu g\ m^{-3}$)	Predicted ΔM_o ($\mu g\ m^{-3}$)	Pred/ Actual
7/26/96	RF-A	3642	1742	1668	160	113	0.71
7/29/96	RF-A	3554	1725	1733	110	94	0.85
8/21/96	RF-A	2601	1178	1248	64	53	0.83
7/26/96	C2	3203	1200	1536	36	47	1.31
7/29/96	C2	3551	1421	1687	54	63	1.17
9/06/96	C2	2072	814	1012	18	21	1.17
8/19/96	RF-L	1876	907	1156	130	60	0.46
8/23/96	RF-L	1784	846	1269	95	52	0.55
8/21/96	RF-F	2326	823	1084	22	26	1.18
8/26/96	RF-F	1826	627	540	18	17	0.97
9/04/96	RF-F	1648	551	469	15	13	0.87
8/26/96	RF-G	3088	1407	1476	110	98	0.89
9/02/96	RF-G	3134	1459	1484	108	102	0.94
9/06/96	RF-K	2638	1409	1328	84	90	1.07
9/02/96	RF-O	3348	1549	1479	118	115	0.97
9/04/96	RF-P	2918	777	1371	35	29	0.83
8/28/96	RF-1B	2663	788	1513	28	28	1.00
8/30/96	RF-2B	3273	1556	1595	64	76	1.19
8/28/96	RF-3B	2243	678	1482	17	18	1.06
8/30/96	RF-4B	2534	1270	1564	56	58	1.04
						Avg =	1.00±0.16

LIST OF FIGURES

Figure 1. Aromatic SOA Yields

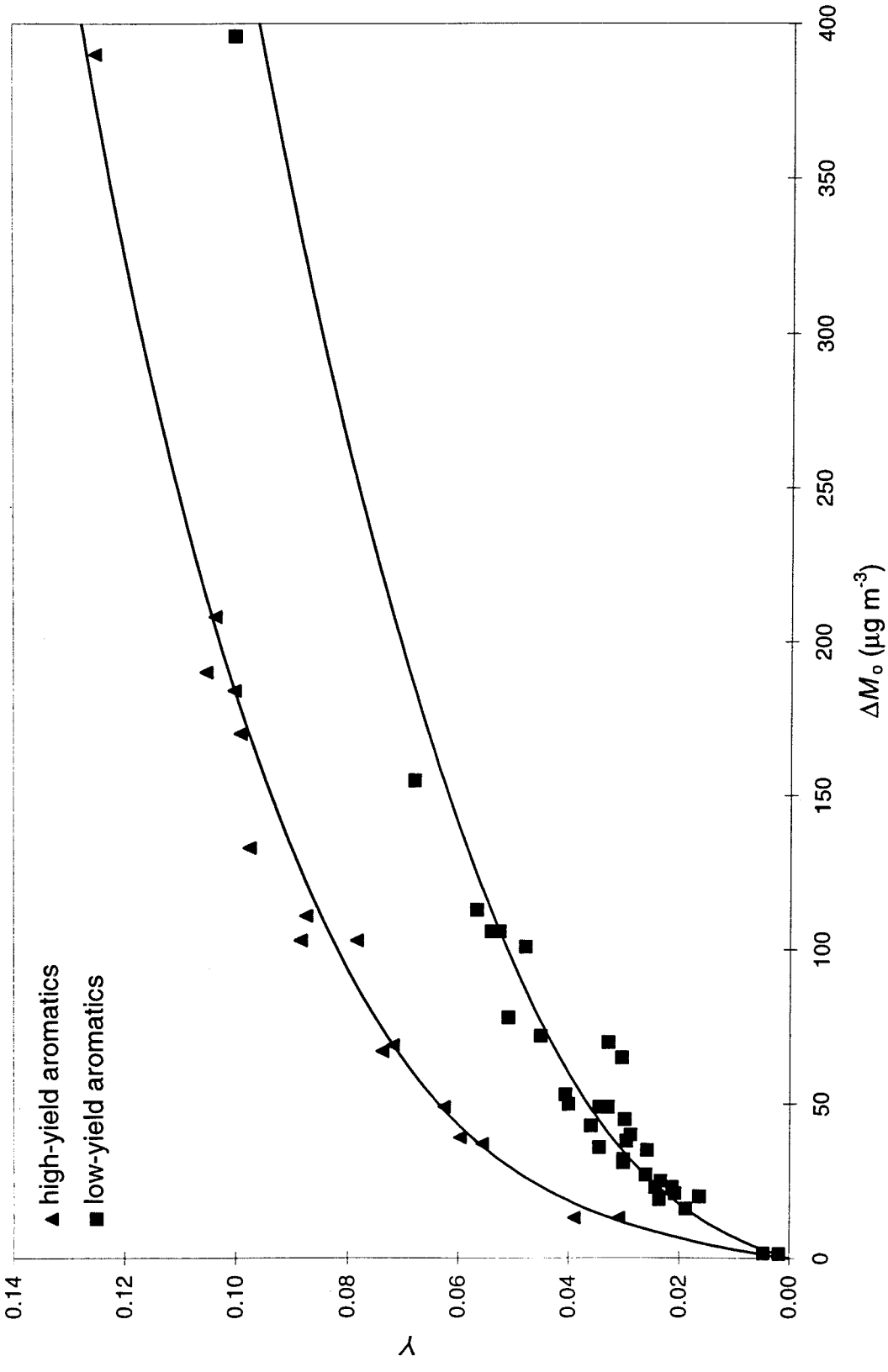

Figure 2. Aromatic Yields of Izumi and Fukuyama

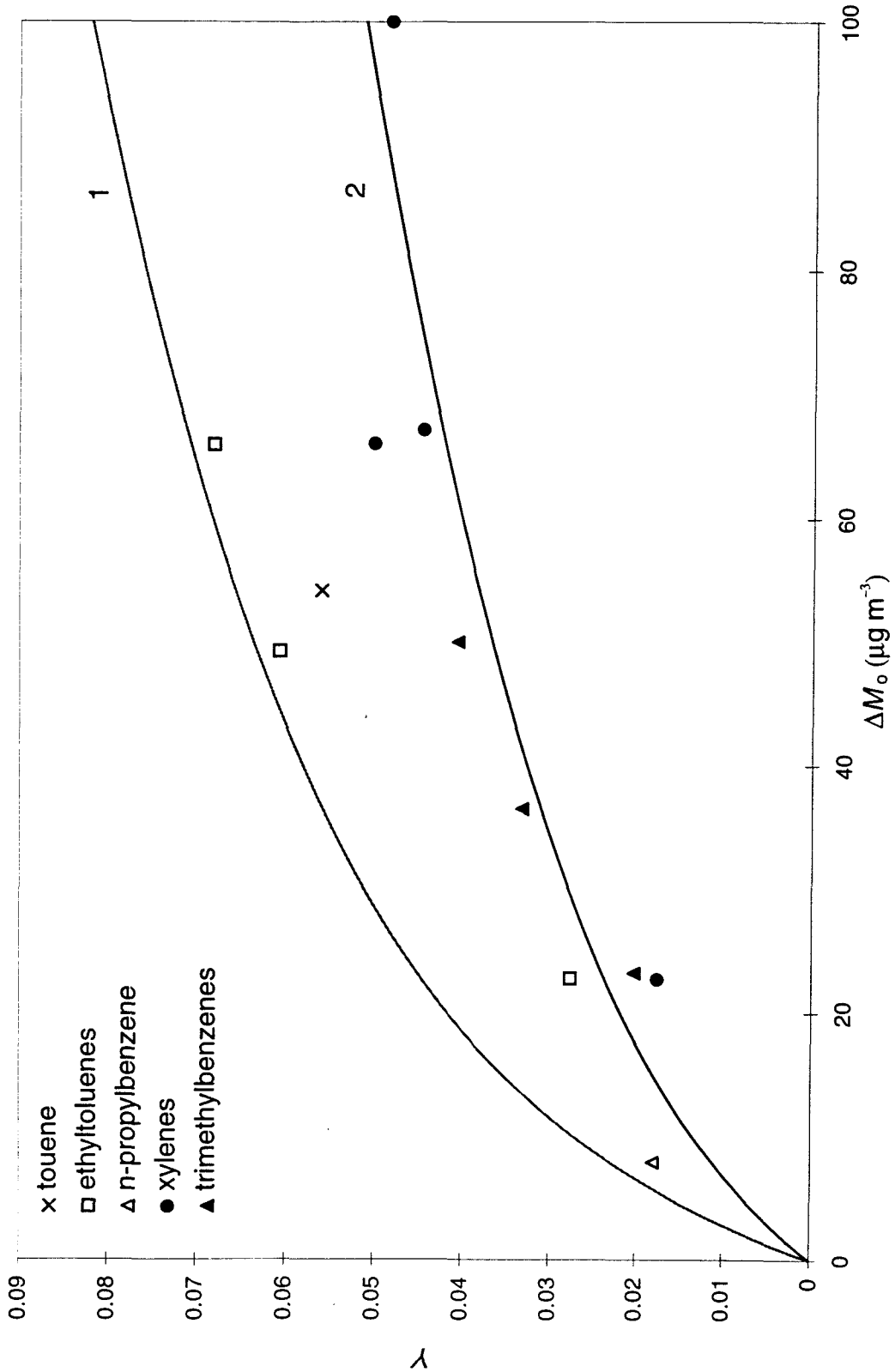

Figure 3a. ΔM_o as a Function of ΔROG for Gasolines

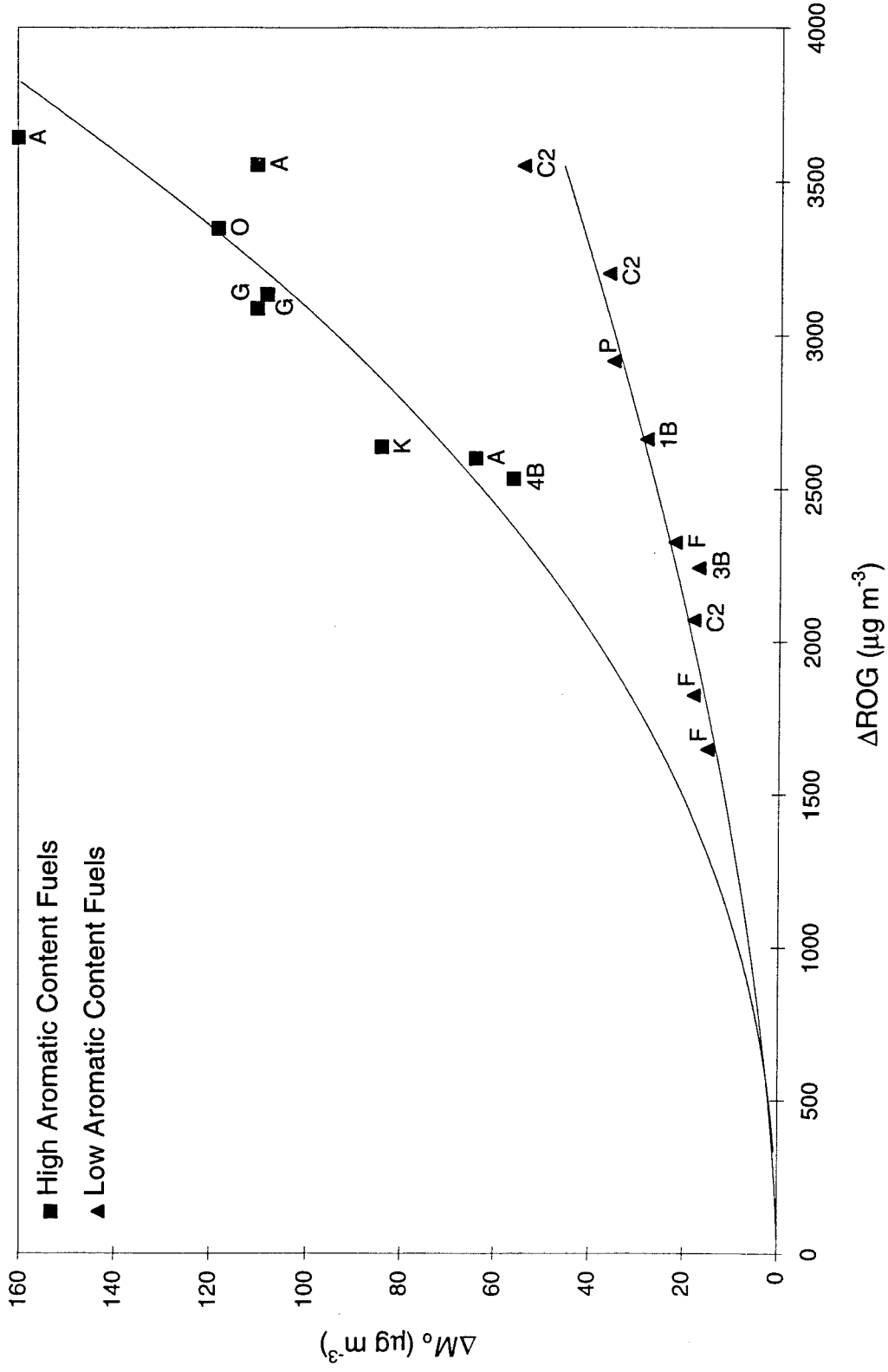

Figure 3b. ΔM_o as a Function Δ *Aromatic* for Gasolines

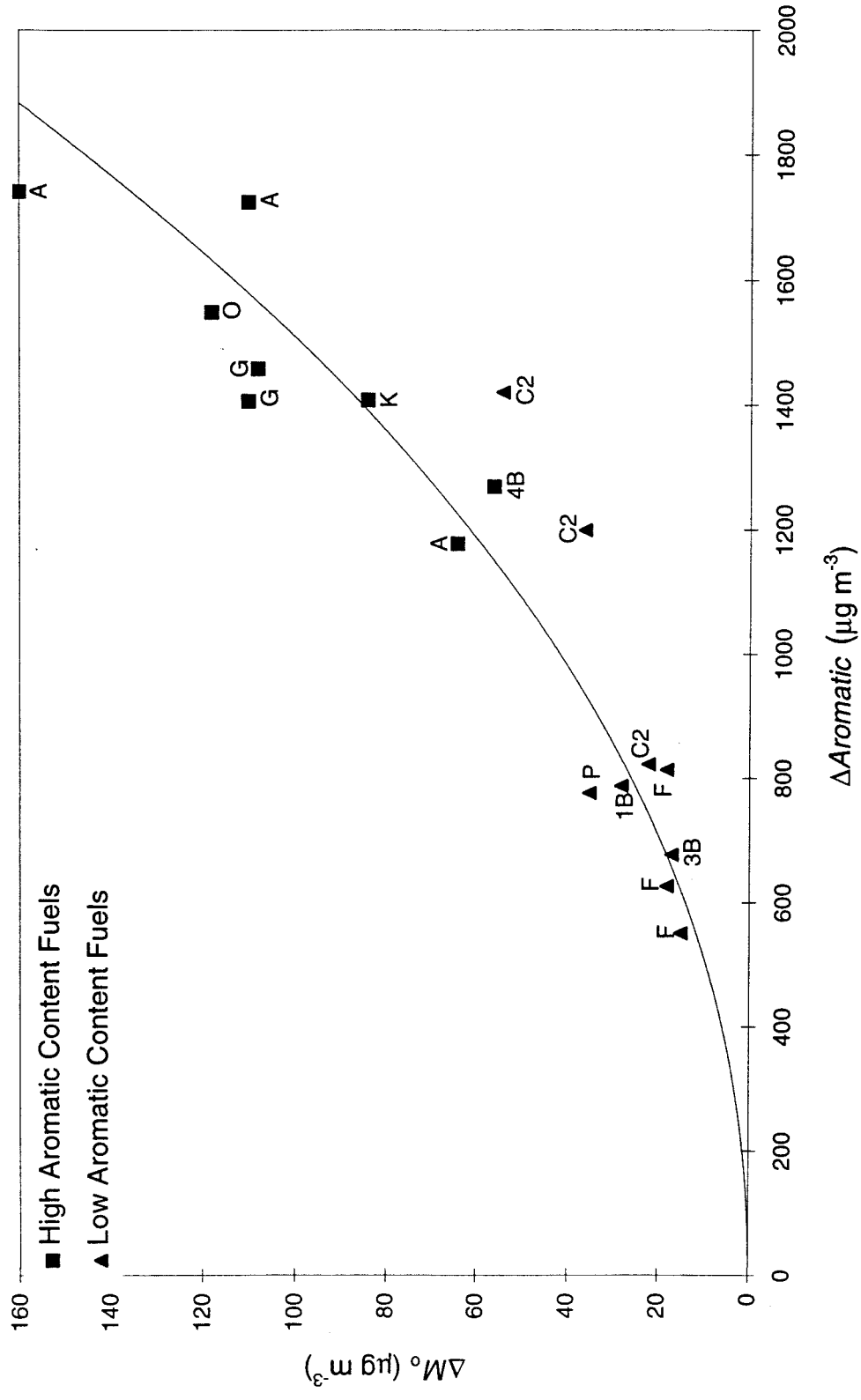

Figure 4. Aromatic Envelope for Gasoline Yields

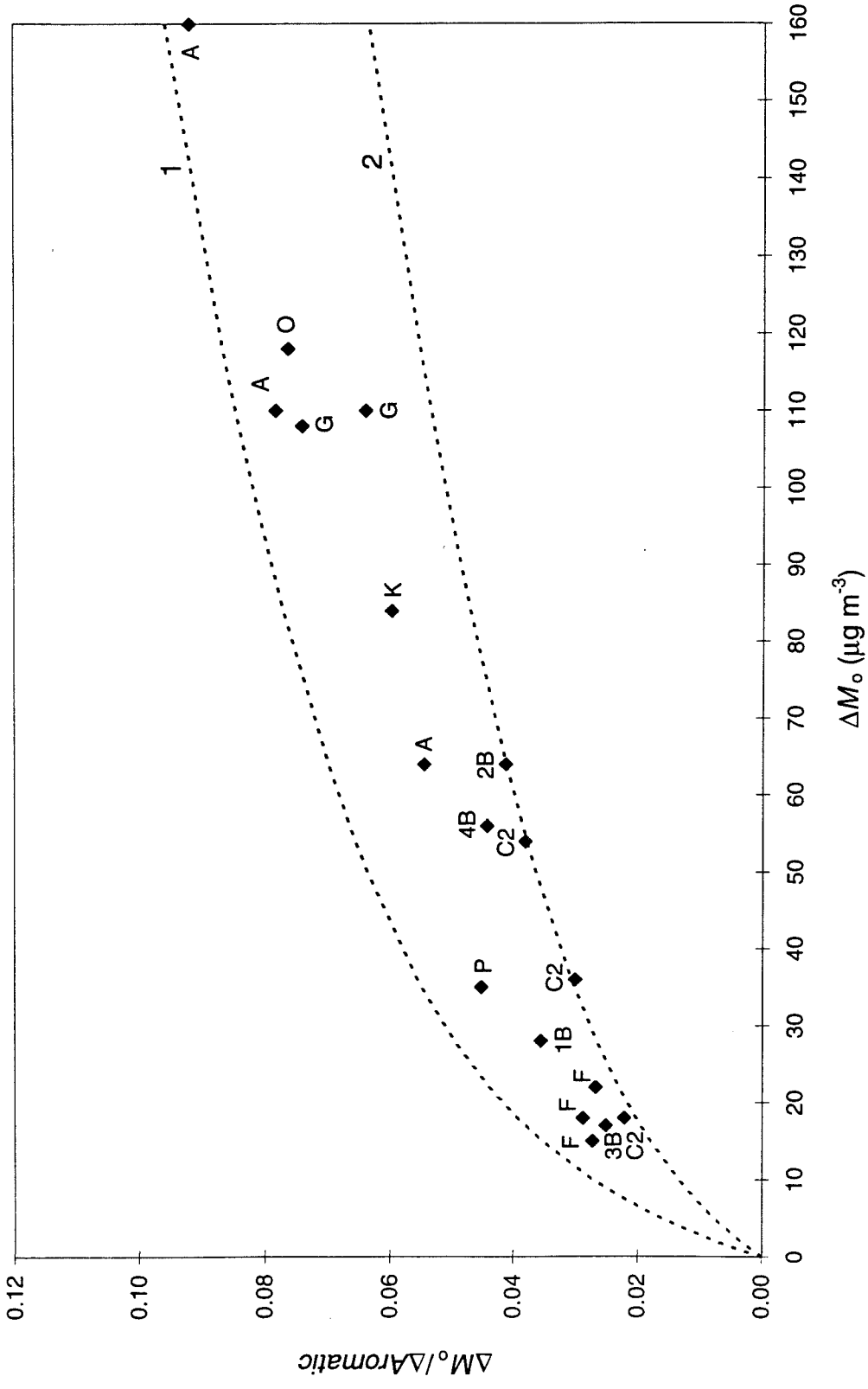

Chapter 4:

Gas/Particle Partitioning of Semi-Volatile Organic Compounds to Model Inorganic, Model Organic, and Ambient Smog Aerosols

Published in *Environ. Sci. Technol.*, **31**, 3086 (1997).

ABSTRACT

Gas/particle (G/P) partitioning coefficients (K_p) were measured in an outdoor smog chamber for a group of polycyclic aromatic hydrocarbons (PAHs) and *n*-alkanes sorbing to three types of model aerosol materials: solid ammonium sulfate, liquid dioctyl-phthalate, and amorphous secondary organic aerosol (SOA) generated from the photooxidation of whole gasoline vapor. Gas/particle partitioning coefficients were also measured for ambient *n*-alkanes sorbing to urban particulate material collected during summertime smog episodes in Pasadena, CA. Based on K_p values obtained for the aerosols studied here, we conclude that G/P partitioning of semi-volatile organic compounds (SOCs) to urban particulate matter during summer smog episodes is dominated by absorption into the organic fraction of urban aerosol. Comparisons of partitioning of SOCs to three different types of aerosols demonstrate that: 1) dioctyl-phthalate aerosol might be a good surrogate for ambient aerosol that consists mainly of organic compounds from primary emissions; 2) environmental tobacco smoke particles may be a good surrogate for SOA; and 3) sorption properties of the ambient smog aerosol and the chamber-generated SOA are nearly identical. Similarities observed between ambient smog aerosol and chamber generated SOA support the use of SOA yield data from smog chamber studies to predict SOA formation during summer midday smog episodes.

INTRODUCTION

Gas/particle (G/P) partitioning is an important process that affects the deposition, chemical reactions, long-range transport, and impact on human health of atmospheric semi-volatile organic compounds (SOCs). Much of the thinking about the G/P partitioning of SOCs has involved the assumption that the partitioning process involves simple physical adsorption (*1-3*). Whereas this sorption mechanism seems appropriate when atmospheric particulate material is comprised solely of solid inorganic materials, urban particulate material (UPM) generally contains a significant amount of amorphous, organic carbon (*4*, *5*). Thus, it seems likely that absorptive partitioning must play a role in atmospheres affected by urban sources.

An equation that has been used successfully to parameterize G/P partitioning is (*2*, *6*, *7*)

$$K_p = \frac{F / TSP}{A} \tag{1}$$

where K_p (m^3 μg^{-1}) is the G/P partitioning coefficient for a given compound, F and A are the particle and gas phase concentrations (ng m^{-3}) of the compound, respectively, and TSP (μg m^{-3}) is the total suspended particulate material concentration. When both *ad*sorptive and *ab*sorptive partitioning are operative, K_p is given by (*8*)

$$K_p = \frac{760RT}{p_L^\circ}\left[\frac{10^{-2} N_S a_{TSP}}{e^{-9.87\times10^{-3}(Q_1-Q_v)/RT}} + \frac{f_{om} / (10^6 M_{om})}{\zeta}\right] \tag{2}$$

where R is the ideal gas constant (8.206 x 10^{-5} m^3 atm mol^{-1} K^{-1}), T is temperature (K), p_L°

is the pure compound liquid vapor pressure (torr) (sub-cooled if necessary), N_S is the molar concentration of adsorption sites on the particle surface (mol cm^{-2}), a_{TSP} is the TSP specific surface area (m^2 g^{-1}), Q_1 is the enthalpy of desorption from the particle surface (kJ mol^{-1}), Q_v is the enthalpy of evaporation for the pure compound as a liquid (sub-cooled if necessary) (kJ mol^{-1}), f_{om} is the organic matter (om) phase mass fraction of TSP, M_{om} is the mean molecular weight of the om-phase (g mol^{-1}), and ζ is the mole-fraction-scale activity coefficient of the compound of interest in the om-phase. The expression outside the parentheses represents the inverse of the saturation concentration (in mol m^{-3}) of the compound of interest. The first and second terms inside the parentheses represent the adsorption and absorption terms, respectively.

Within a given compound class (*e.g.* polycyclic aromatic hydrocarbons (PAHs), *n*-alkanes, etc.), the expressions inside the parentheses of equation (2) are only weakly compound dependent, and log [(*F*/TSP) /*A*] will tend to be correlated with log p_L^o according to (*8*)

$$\log K_p = m_r \log p_L^o + b_r \qquad (3)$$

where m_r is usually near -1.

Based on a comparison of K_p values that were measured for PAHs partitioning to environmental tobacco smoke (ETS) and estimated for partitioning to UPM, Liang and Pankow (*9*) have suggested that absorption may frequently be the dominant G/P partitioning mechanism for SOCs in urban air. In addition, Odum *et al.* (*10*) recently showed, from smog chamber studies, that the partitioning of photooxidation products that

form secondary organic aerosol (SOA) is best described by an absorptive G/P partitioning model. In this paper we discuss smog chamber experiments that were performed to examine the partitioning of two classes of SOCs (PAHs and *n*-alkanes) to three different types of model aerosol: inorganic, solid ammonium sulfate; non-polar, liquid organic dioctyl-phthalate; and polar, amorphous SOA generated from the photooxidation of whole gasoline vapor. These data are then compared to ambient partitioning data, collected during two heavy smog episodes in Pasadena, CA, to obtain information about both the nature of UPM and the operative G/P sorption mechanism during summertime urban smog episodes.

EXPERIMENTAL SECTION

Smog Chamber Experiments. Five experiments were conducted in the Caltech 60 m^3 flexible outdoor Teflon smog chamber that has been described in detail elsewhere (*10-12*). Prior to each experiment, the chamber was flushed with four to five bag volumes of purified compressed air (rehumidified to 10% relative humidity) while being allowed to bake at 31-38 °C under sunlight for at least 12 h.

Solid, inorganic aerosol was generated by atomizing an aqueous solution of ammonium sulfate ($(NH_4)_2SO_4$) using a stainless steel, constant rate atomizer. Before entering the smog chamber, the aerosol was passed via heated copper tubing through a diffusion dryer, packed with indicating silica gel, and a ^{85}Kr charge neutralizer. The

initial particle number concentration in the chamber was ~7 × 10^4 cm^{-3}, with a number median diameter of 110 nm.

Liquid, dioctyl-phthalate (DOP) aerosol was generated by atomizing a 0.005 % (by weight) solution of DOP in pentane using a stainless steel, constant rate atomizer. Before entering the smog chamber, the DOP aerosol was passed through a diffusion dryer, packed with activated charcoal to remove pentane, and a ^{85}Kr charge neutralizer. The initial particle number concentration in the chamber was ~10^4 cm^{-3}, with a number median diameter of 500 nm.

Amorphous secondary organic aerosol (SOA) was generated by first injecting $(NH_4)_2SO_4$(s) seed particles into the chamber at a concentration of 10^4 cm^{-3} (total aerosol volume ~20 μm^3 cm^{-3}). This was followed by the injections of propene, NO, and NO_2 into the chamber (which was completely shrouded from sunlight with a black plastic tarpaulin) to obtain initial mixing ratios of 300 ppb, 640 ppb, and 340 ppb, respectively. Propene was used to generate hydroxyl radicals in sufficient concentration during the inception of the experiment. The SOA was generated using "Industry Average" gasoline obtained from the Auto/Oil Air Quality Research Improvement Program (*13*). A volume of 700 μL of "Industry Average" gasoline was completely volatilized in a glass dilution bulb that was gently heated while being purged with purified lab air that was directed into the chamber through Teflon lines. The initial total gas-phase concentration of the whole-gasoline vapor in the chamber was 9000 μg m^{-3}. After making initial particle, NO_x, and hydrocarbon measurements to ensure that the contents were well mixed, the tarpaulin was removed to initiate photooxidation. The photochemical reactions were extinguished 2 h

after the start of the experiment by covering the chamber with the black tarpaulin. Approximately 500-600 μg m^{-3} (total aerosol volume of 500-600 μm^3 cm^{-3}, as compared to the initial seed aerosol volume of ~20 μm^3 cm^{-3}) of SOA and more than 1 ppm of ozone were generated during this period. The ozone was titrated down to a mixing ratio of 150 ppb by slowly vaporizing 330 μL of liquid tetramethylethylene into the chamber. This precaution was taken in order to avoid excessive destruction of the SOC model compounds by ozone.

For all of the experiments, the SOCs were added to the chamber after the aerosol was generated. The chamber was covered with the black tarpaulin before the addition of the SOCs to ensure that no photochemical degradation took place. Most of the SOCs were added by injecting ~300 μL of a 250 ng μL^{-1} per component mixture of PAHs and *n*-alkanes in methylene chloride through a hot (300 °C) injector located at the base of the chamber. Two *n*-alkanes (C_{16} and C_{17}) were added to the chamber by injecting individual 50 μL aliquots of these compounds at ~10^4 ng μL^{-1} in methylene chloride.

Sampling of the SOCs commenced approximately one hour after their inection into the chamber in order to allow G/P partitioning equilibrium to be achieved. Chamber contents were sampled through a copper tube (i.d. = 0.5 in) that extended ~30 cm into the chamber. Sampling event durations and conditions are listed in Table 1. A 102-mm diameter glass fiber filter (GFF) (with an identical back-up filter) was used to collect particle phase organic compounds. The data obtained with the backup filter were used to correct for filter adsorption artifacts, as described for quartz filters by Hart and Pankow (*14*). Following the filters, two parallel trains were used to collect the gas phase SOCs.

One train employed two sequential adsorption/thermal desorption (ATD) cartridges containing ~1 g each of Tenax-GC to collect the more volatile compounds. The second train employed two sequential 198 cm^3 polyurethane foam (PUF) plugs to collect the less volatile compounds. During sampling, the flow rates (L min^{-1}) were: filters, 70.8; Tenax-GC train, 0.324; and PUF train, 70.8. The GFFs were pre-cleaned by baking at 370 °C overnight, then held at room temperature in a desiccator containing indicating silica gel prior to sampling. The PUF plugs were Soxhlet-extracted with methylene chloride for 24 h before use. Each ATD cartridge was cleaned by pumping one liter of 1:1 hexane:acetone through the cartridge at 2 mL min^{-1}, purged with ultra pure helium at 50 °C for 20 min to remove the solvents, then conditioned at 300 °C for 2h with a 1 mL min^{-1} flow of ultra-pure helium.

The total suspended particulate matter concentration was measured for each experiment by collecting particles with a 47-mm Teflon-coated glass fiber filter at a flow rate of 30 L min^{-1} for 20 min. Filters were cleaned prior to use by Soxhlet extraction in methylene chloride for 12 h and were weighed both before and after sampling. In each case, prior to weighing, the filters were conditioned for 1 hr at 23 °C and 40 % RH.

Complete aerosol number and size distribution measurements were recorded for each experiment with a 1-min sampling frequency using a TSI (St Paul, MN) Model 3071 cylindrical scanning electrical mobility spectrometer (SEMS) equipped with a TSI Model 3025 condensation nuclei counter (*10, 12*). This equipment was housed in an enclosed cart maintained at 25 °C and located directly adjacent to the chamber. The SEMS system was operated with sheath and excess flows of 2.5 L min^{-1}, and inlet and classified aerosol

flows of 0.25 L min^{-1} to allow for the measurement of aerosol size distributions in the range of 30-850 nm. The aerosol size distribution data were used as an independent measure of the TSP.

Ambient Aerosol Sampling. Low-volume sampling using the same equipment and filters (GFFs) employed to sample the smog chamber was performed on the roof of Keck Laboratory at Caltech in Pasadena during two separate smog episodes. The sampling period in both cases was 12 pm to 4 pm. The average RH for the two smog episodes was 42%. Other sampling information is given in Table 1. The GFFs were weighed both before and after sampling using the procedure described above for the Teflon-coated filters.

A single high-volume aerosol sample, used just for carbon analysis, was also taken at the same location from 12 pm to 4 pm during the second smog episode. An 8 × 10 inch quartz fiber filter (QFF) was used to collect particles at a flow rate of 1.4 m^3 min^{-1}. The QFF was pre-cleaned by baking overnight at 370 °C, then held at room temperature in a desiccator containing indicating silica gel until used. After sampling, a portion of the QFF was analyzed for inorganic carbon (IC), elemental carbon (EC), and organic carbon (OC) by Sunset Laboratory (Forest Grove, OR). Total carbon (TC) was taken to be the sum IC + EC + OC. Another portion of the QFF was sent to Micromeritics (Norcross, GA) for specific surface area measurements.

Analytical Procedures. After sampling, each ATD cartridge was capped, sealed in a screw cap culture tube, and kept at -25 °C until analyzed. Each ATD cartridge was analyzed by thermal desorption with capillary GC/MS as described elsewhere (*15*).

Immediately after sampling, each PUF plug and each GFF was spiked with surrogate standard compounds (acenaphthene-d_{10}, phenanthrene-d_{10}, and chrysene-d_{12}), then Soxhlet-extracted overnight with 400 and 250 mL, respectively, of methylene chloride. PUF and GFF blanks were also extracted for each experiment. The extracts were concentrated down to ~30 mL by rotary evaporation, then kept at -25 °C until analyzed. Prior to GC/MS analysis, each extract was blown down to ~100 μL with N_2, weighed, and then spiked with internal standard compounds (naphthalene-d_8, anthracene-d_{10}, and perylene-d_{12}). Each extract was analyzed using GC/MS with a splitless injection of 1 μL. A 30-m, 0.32-mm-i.d., 0.25-μm film thickness DB-5 (J&W Scientific, Folsom) was used. The GC temperature program used was: hold at 50 °C for 2 min, 50-100 °C at 25 °C/min, 100-300 °C at 10 °C/min, then hold at 300 °C for 2 min.

ADSORPTIVE PARTITIONING TO $(NH_4)_2SO_{4(S)}$ AEROSOL.

If adsorption is the dominant partitioning mechanism, then only the first term in equation (2) is operative and a surface-area-normalized constant $K_{p,s}$ (m^3 m^{-2}) can be defined as (*16*)

$$K_{p,s} = \frac{K_p}{a_{TSP}10^{-6}} = \frac{760 \times 10^4 RTN_S}{e^{-9.87x10^{-3}(Q_l - Q_v)/RT} p_L^o} \quad (4)$$

Under these conditions, equation (3) becomes

$$\log K_{p,s} = m_{r,s} \log p_L^o + b_{r,s} \quad (5)$$

where $m_{r,s} = m_r$ and $b_{r,s} = b_r - \log (a_{TSP}/10^6)$.

Smog chamber experiments of adsorptive partitioning of SOCs to solid ammonium sulfate aerosol ($(NH_4)_2SO_4$) were performed. Comparison of these data to ambient SOC/UPM partitioning data can allow assessment of the relative importance of this sorption mechanism in ambient atmospheres. Table 2 gives the log K_p values for the PAHs and *n*-alkanes partitioning to $(NH_4)_2SO_4$ aerosol. Table 3 provides the corresponding m_r and b_r values. Log $K_{p,s}$ values were obtained by normalizing the measured K_p values with a_{TSP} according to equation (4). Assuming that the $(NH_4)_2SO_4$ particles were spherical with a density of 1.77 g cm^{-3}, a_{TSP} was estimated to be 17.5 m^2 g^{-1} from the aerosol size distribution data.

It is well known that adsorptive partitioning of organic compounds to inorganic surfaces is dependent on relative humidity (RH) (*16*, *17*), and that sorption becomes stronger as RH decreases. Since the partitioning experiments performed in the chamber with $(NH_4)_2SO_4$ were conducted at RH = 10%, and since the ambient data were collected at RH = 42%, extrapolation of the $(NH_4)_2SO_4$ log $K_{p,s}$ values to RH = 42% was necessary to permit a comparison of the two data sets. Storey *et al.* (*16*) have provided a detailed examination of the RH-dependence of the adsorption of a range of PAHs and *n*-alkanes to a quartz surface. The needed compound-specific extrapolations were therefore based on the 30% to 70% RH data of Storey *et al.* (*16*). It was assumed that: 1) only $b_{r,s}$ is a function of RH; and 2) the change in $b_{r,s}$ with RH for $(NH_4)_2SO_4$ is similar to that for quartz. The extrapolated compound-dependent increases in log $K_{p,s}$ for quartz between

RH = 42% and RH = 10% were therefore subtracted from the values for $(NH_4)_2SO_4$ obtained in this study. The results are shown in Figure 1. The a_{TSP}-normalized ambient smog *n*-alkane data are also shown in Figure 1. Sheffield and Pankow (*18*) have reported that $a_{TSP} = 2.1\ m^2\ g^{-1}$ for UPM collected during the summer in Portland, OR. Corn *et al.* (*19*) reported that $a_{TSP} = 1.9\ m^2\ g^{-1}$ for UPM collected during the summer in Pittsburgh, PA. These values are consistent with the measurements made in this study. The value of a_{TSP} for the ambient smog sample in this study was $2.0\ m^2\ g^{-1}$.

Normalizing ambient smog aerosol log K_p values by an estimate of a_{TSP} allows one to test whether adsorption is an important partitioning mechanism for UPM. As seen in Figure 1, sorption of *n*-alkanes to the ambient smog aerosol is much stronger than adsorption to the $(NH_4)_2SO_4$ aerosol. (A similar comparison for the PAHs is not possible because the concentrations of these compounds in the ambient samples were too low to be quantified accurately.) Considering that the inorganic portion of the midday smog aerosol is probably well represented by $(NH_4)_2SO_4$, it seems that adsorption to inorganic surfaces cannot account for the sorption strength of the *n*-alkanes observed in the ambient samples. This suggests that adsorption is not the operative mechanism controlling the partitioning of SOCs to urban summertime aerosol and that the log $K_{p,s}$ values calculated for the *n*-alkanes sorbing to ambient smog aerosol are not physically meaningful quantities.

ABSORPTIVE PARTITIONING TO ORGANIC AEROSOLS.

When absorption into a liquid (or at least amorphous) organic matter (om) phase is the dominant sorption mechanism, then the second term in equation (2) becomes the operative term and an om-phase-normalized constant $K_{p,om}$ can be defined as (*10*, *20*)

$$K_{p,om} = \frac{K_p}{f_{om}} = \frac{760RT}{10^6 M_{om} \zeta p_L^\circ} \quad (6)$$

and equation (3) can be written as

$$\log K_{p,om} = m_{r,om} \log p_L^\circ + b_{r,om} \quad (7)$$

where $m_{r,om} = m_r$ and $b_{r,om} = b_r - \log f_{om}$.

To examine the importance of absorptive partitioning of SOCs to UPM, smog chamber experiments of SOCs partitioning to two different types of model organic aerosol were performed and compared to the ambient SOC/UPM partitioning data. The two model aerosol types were non-polar, liquid dioctyl-phthalate (DOP) and amorphous secondary organic aerosol (SOA) generated from the photooxidation of whole-gasoline vapor. The measured log K_p values are given in Table 2. The corresponding log K_p vs. log p_L° correlation parameters are given in Table 3. The log $K_{p,om}$ vs. log p_L° plots appear in Figures 2 and 3. Also given are the regression lines for the partitioning of PAHs and *n*-alkanes to environmental tobacco smoke (ETS) as determined by Liang and Pankow (*9*). For the DOP, SOA, and ETS aerosols, f_{om} was taken to be 1.0, yielding $K_p = K_{p,om}$. For the ambient smog samples, carbon analyses revealed that inorganic carbon (*i.e.*

carbonate) in those samples was essentially zero so that the total aerosol carbon (TC) was given as the sum of the organic (OC) and elemental (EC) aerosol carbon components (TC = OC + EC). On average, total carbon constituted 21% of the TSP, with 87% of the total carbon being organic (OC/EC = 6.7). Allowing for the presence of other elements (*e.g.* hydrogen and oxygen) in the organic matrix, the mass of organic matter in the ambient aerosol was taken to be 1.6 times the organic carbon mass alone (*21*). These considerations lead to the estimate $f_{om} = 0.26$ for the ambient aerosol. This value was used with equation (6) and the assumption that the partitioning to the ambient smog aerosol was absorptive in nature to calculate log $K_{p,om}$ values for these samples. The results are shown in Figure 3.

The slopes of the three regression lines in Figure 2 are all close to -1. This indicates that within each of the three organic aerosols, ζ remained approximately constant for the PAHs across the compound range of interest. The intercepts of the three regression lines in Figure 2 are, moreover, not significantly different (95% confidence level), indicating that the factor $M_{om}\zeta$ is approximately the same for PAHs in the three organic aerosols considered.

Absorptive partitioning of *n*-alkanes to the organic aerosols is considered in Figure 3. On average, partitioning of the *n*-alkanes to the organic aerosols was weaker than that of the PAHs. More significantly, notice that when the data are considered within the absorption model framework, partitioning of the *n*-alkanes to ambient smog aerosol and to chamber-generated SOA is nearly identical. For the chamber-generated SOA, ambient smog aerosol, and ETS aerosol, the slopes of log $K_{p,om}$ vs. log p_L° regression

lines are all close to -1 and the intercepts are not significantly different (95% confidence level). Sorption of the *n*-alkanes to the DOP aerosol, however, was much stronger than to the other three aerosols. Since it is very likely that M_{DOP} was larger than the M_{om} values for the other aerosols, the increase of partitioning is a result of significantly lower ζ values for the *n*-alkanes in the DOP aerosol as compared to the other aerosol phases.

Often during summertime smog episodes in the south coast air basin, a significant fraction of the ambient organic aerosol can be of secondary origin (*22-27*). Using data from Claremont, CA, Turpin and Huntzicker (*27*) have provided a method to estimate the secondary organic carbon content of urban aerosol (OC_{sec}) based on the total OC (= OC_{pri} + OC_{sec}), and a derived correlation between the organic aerosol carbon of primary emission origin (OC_{pri}) and EC. Assuming that the OC_{pri}/EC ratio for Pasadena is similar to that observed by Turpin and Huntzicker (*27*) in Claremont, we estimate that 53-58% of total OC in the ambient smog aerosol samples was secondary in origin. Considering that the anthropogenic volatile organic gas profile in the South Coast Air Basin is similar to that of whole gasoline vapor (*28*), SOA generated in the basin is likely to be similar to the SOA generated from whole gasoline vapor in the smog chamber, at least on an om-phase activity basis. Thus the similarity found in this study between the sorption properties of the ambient smog aerosol and that of SOA generated from gasoline photooxidation may not seem that surprising. This similarity in om-phase activity between ambient organic smog aerosol and chamber-generated SOA suggests that smog chamber SOA yield data may be used to predict ambient SOA formation.

O'Brien *et al.* (*29*) reported that mono- and dicarboxylic acids constitute an

appreciable portion (22% and 10%, respectively) of the organic content of summertime particulate matter found in the Los Angeles area. Schuetzle *et al.* (*30*) found high concentrations of organic alcohols and difunctional organic compounds in SOA. Dielectric constants give a measurement of compound polarity. Reported dielectric constants for *n*-hexadecane, DOP, 1,2-benzenediol, and 3-hydroxybutanoic acid are 2.05 (20 °C), 5.22 (20 °C), 17.57 (115 °C), and 31.5 (23 °C), respectively (*31*). Based on the significant secondary organic content of the ambient smog aerosol examined here, it is likely that the om-phases of the ambient smog aerosol and the SOA generated from gasoline are significantly more polar than the DOP. Moreover, because of the similarity between the dielectric constant for DOP and that for *n*-hexadecane, ζ values for the *n*-alkanes in DOP are expected to be closer to 1.0 as well as lower than in the other aerosol phases.

From comparison of the relative spread in the log K_p vs. log p_L° correlation lines in Figures 2 and 3, we conclude that absorptive uptake of *n*-alkanes is more sensitive to changes in the polarity of the om-phase than is the case for PAHs. It would be useful to know all of the M_{om} values for the organic aerosols studied here so that this hypothesis could be tested by calculating average ζ values for the PAHs and *n*-alkanes for these different aerosol types. Unfortunately, the only M_{om} value that is known with certainty at the present time is M_{DOP} (390 g mol^{-1}). When log p_L° = -3, the regression parameters in Table 3 for DOP give log $K_{p,om}$ = -3.75 and -4.21 for the PAHs and *n*-alkanes, respectively. Using these values with equation (6) to estimate the activity coefficients yields ζ = 0.28 and 0.8, respectively, for these two compound classes. These results are

consistent with literature values for ζ in DOP. In particular, ζ values for benzene and octane in DOP have been reported to be 0.57 (60 °C) and 1.4 (120 °C) (*32*).

While it is instructive as well as useful to have a detailed understanding of the individual values of ζ and M_{om} for a given compound or class of compounds sorbing to a given organic aerosol, there are many circumstances for which knowledge of the product of $M_{om}\zeta$ alone will be sufficient. In this context, we note the sorption properties of ETS and the SOA generated from gasoline photooxidation were very similar, both for the PAHs and *n*-alkanes. This suggests that ETS may be a useful surrogate phase for SOA. It may therefore be possible to use ETS and the methods of Liang and Pankow (*9*) to estimate the log $K_{p,om}$ values for other classes of compounds (*e.g.* organic alcohols and carboxylic acids) in SOA. Similarly, DOP aerosol may be a useful surrogate for ambient organic aerosol that consists primarily of moderately non-polar organic compounds of primary emission origin (*e.g.* diesel exhaust).

In summary, we conclude that the G/P partitioning of semi-volatile organic compounds to urban particulate matter containing a significant fraction of secondary organic carbon will be dominated by absorptive partitioning. This finding is consistent with that of Liang and Pankow for UPM in general (*9*). This not only suggests that G/P partitioning in urban environments can be accurately parameterized using equation (6), but also supports the absorptive model for SOA formation proposed by Odum *et al.* (*10*).

ACKNOWLEDGMENTS

This work was supported in part by a grant from the U.S. Environmental Protection Agency's Office of Exploratory Research (U.S. EPA/OER) under Grant R822312-01-0. This work was also supported in part by the U.S. Environmental Protection Agency Center on Airborne Organics under grant R-819714-01-0, National Science Foundation grant ATM-9307603, the Coordinating Research Council, and the Chevron Corporation. We gratefully acknowledge the technical assistance of Timothy P.W. Jungkamp, Robert J. Griffin, Lorne M. Isabelle, and Wentai Luo in the design, sampling preparation, and analysis phases of the experimental work. We also appreciate Martha J. Shearer and Paul G. Tratnyek for their helpful suggestions on the statistical analysis of the data. Finally, the authors would like to thank Donna Reed for assisting with many details associated with the shipment of the sampling equipment.

REFERENCES

(1) Junge, C.E. In *Fate of Pollutants in the Air and Water Environments*; Suffet, I.H. Ed.;Wiley: New York, **1977**, 7-26.

(2) Yamasaki, H.; Kuwata, K.; Miyamoto, H. *Environ. Sci. Technol.* **1982**, *16*, 189-194.

(3) Pankow, J.F. *Atmos. Environ.* **1987**, *21*, 2275-2283.

(4) Gray, H. A.; Cass, G. R.; Huntzicker, J. J.; Heyerdahl, E. K.; Rau, J. A. *Sci. Tot. Environ.* **1984**, *36*, 17-25.

(5) Shah, J. J.; Johnson, R. L.; Heyerdahl, E. K.; Huntzicker, J. J. *JAPCA*, **1986**, *36*, 254-257.

(6) Pankow, J.F. *Atmos. Environ.* **1991**, *25A*, 2229-2239.

(7) Pankow, J.F. *Atmos. Environ.* **1992**, *26A*, 2489-2497.

(8) Pankow, J.F. *Atmos. Environ.* **1994**, *28*, 185-188.

(9) Liang, C.K.; Pankow, J.F. *Environ. Sci. Technol.* **1996**, *30*, 2800-2805. (See also Errata *Environ. Sci. Technol.* **1996**, *30*, 3650).

(10) Odum, J.R.; Hoffmann, T.; Bowman, F.; Collins, D.; Flagan, R.C.; Seinfeld, J.H. *Environ. Sci. Technol.* **1996**, *30*, 2580-2585.

(11) Pandis, S.N.; Paulson, S.E.; Seinfeld, J.H.; Flagan, R.C. *Atmos. Environ.* **1991**, *25A*, 997-1008.

(12) Wang, S.C.; Paulson, S.E.; Grosjean, D.; Flagan, R.C.; Seinfeld, J.H. *Atmos. Environ.* **1992**, *26A*, 403-420.

(13) Hochhauser, A.M.; Benson, J.D.; Burns, V.R.; Gorse, R.A.; Koehl, W.J.; Painter, L.J.; Ribbon, B.H.; Reuter, R.M.; Rutherford, J.A. SAE technical paper no. 912322,

Society of Automotive Engineers, Warren PA (1991).

(14) Hart, K.M.; Pankow, J.F. *Environ. Sci. Technol.* 28, 655-661.

(15) Round, S.A.; Tiffany, B.A.; Pankow, J.F. *Environ. Sci. Technol.* **1993**, *27*, 366-377.

(16) Storey, J.M.; Luo, W.T.; Isabelle, L.M.; Pankow, J.F. *Environ. Sci. Technol.* **1995**, *29*, 2420-2428.

(17) Goss, K. U. *Environ. Sci. Technol.* **1992**, *26*, 2287-2294.

(18) Sheffield, A.E.; Pankow, J.F. *Environ. Sci. Technol.* **1994**, *28*, 1759-1766.

(19) Corn, M.; Montgomery, T.L.; Esmen, N.A. *Environ. Sci. Technol.* **1971**, *5*, 155-158.

(20) Pankow, J.F. In *Gas and Particle Partitioning Measurements of Atmospheric Organic Compounds*; Lane D.A., Ed,; Gordon and Breach; Newark, NJ, in press.

(21) Gray, H.A. *Ph.D Thesis*, California Institute of Technology, Pasadena, CA 1986.

(22) Gartrell, G.Jr.; Friedlander, S.K. *Atmos. Environ.* **1975**, 9, 279-299.

(23) Grosjean, D.; Friedlander, S.K. *J. Air Pollut. Control Ass.* **1975**, 25, 1038-1044.

(24) Larson, S.M.; Cass, G.R.; Gray, H.A. *Aersol Sci. Technol.* **1989**, 10, 118-130.

(25) Turpin, B.J.; Huntzicker, J.J. *Atmos. Environ.* **1991**, 25A, 207-215.

(26) Pandis, S.N.; Harley, R.A.; Cass, G.R.; Seinfeld, J.H. *Atmos. Environ.* **1992**, 26A, 2269-2282.

(27) Turpin, B,J.; Huntzicker, J. J. *Atmos. Environ.* **1995**, *29*, 3527-3544.

(28) Harley, R.A.; Hannigan, M.P.; Cass, G.R. *Environ. Sci. Technol.* **1992**, *26*, 2395-2408.

(29) O'Brien, R.J.; Crabtree, J.H.; Holmes, J.R.; Hoggan, M.C.; Bockian, A.H. *Environ. Sci. Technol.* **1975**, *9*, 577-582.

(30) Schuetzle, D.; Cronn, D.; Crittenden, A.L.; Charlson, R.J. *Environ. Sci. Technol.* **1975**, *9*, 838-845.

(31) *CRC Handbook of Chemistry and Physics.* Lide R. L. Ed, 75th edition, CRC Press: Boca, Raton, 1994.

(32) Tiges, D.; Gmehling, J.; Medina, A.; Soares, M.; Bastos, J.; Alessi, P.; Kikic, I. *Activity Coefficients at Infinite Dilution*, vol. IX, Part 1; DECHEMA: Germany, 1986.

Table 1. Sampling Conditions for Collection of Ambient and Smog Chamber Aerosols

Event	Date	Sampling period (min)	Temperature (°C)	TSP ($\mu g\ m^{-3}$)
Ambient, low-vol	08/01/96	235	37	114
Ambient, low-vol	08/14/96	240	37	106
Ambient, high-vol	08/12/96	240	37	104
Chamber, gasoline SOA	08/02/96	30	31	540
Chamber, gasoline SOA	08/07/96	65	31	394
Chamber, DOP	08/05/96	60	36	210
Chamber, DOP	08/14/96	60	36	460
Chamber, $(NH_4)_2SO_4$	08/09/96	90	32	109

Table 2. Measured Log K_p Values for Different Types of Aerosols

Aerosol Type/ Average Conditions	Compound	log p_L^o (torr)[a]	log K_p (m^3 μg^{-1})
$(NH_4)_2SO_4$ (32 °C and 10% RH)	Heptadecane C_{17}	-3.07	-4.48
	Octadecane C_{18}	-3.57	-4.06
	Nonadecane C_{19}	-4.06	-4.04
	Eicosane C_{20}	-4.55	-3.58
	Heneicosane C_{21}	-5.04	-2.76
	Docosane C_{22}	-5.53	-2.30
	Tetracosane C_{24}	-6.51	-1.23
	Fluorene	-1.91	-5.48
	Phenanthrene	-2.74	-4.46
	Anthracene	-2.76	-4.52
	Fluoranthene	-3.87	-3.31
	Pyrene	-4.05	-3.27
DOP[c] (36 °C and 10% RH)	Hexadecane C_{16}	-2.45	-4.81
	Heptadecane C_{17}	-2.93	-4.32
	Heneicosane C_{21}	-4.86	-2.34
	Docosane C_{22}	-5.34	-1.58
	Tetracosane C_{24}	-6.30	-1.24
	Fluorene	-1.80	-4.95
	Phenanthrene	-2.62	-4.23
	Anthracene	-2.65	-4.31
	Fluoranthene	-3.74	-2.82
	Pyrene	-3.92	-2.80
Gasoline SOA[d] (31 °C and 10% RH)	Hexadecane C_{16}	-2.63	-5.53
	Heptadecane C_{17}	-3.12	-4.79
	Octadecane C_{18}	-3.62	-4.36
	Nonadecane C_{19}	-4.11	-3.71
	Eicosane C_{20}	-4.61	-3.70
	Heneicosane C_{21}	-5.10	-2.59
	Docosane C_{22}	-5.60	-2.72
	Tetracosane C_{24}	-6.58	-1.06
	Pentacosane C_{25}	-7.08	-0.44
	Napthalene	-0.21	-6.28
	Acenapthene	-1.58	-6.10
	Fluorene	-1.95	-5.58
	Phenanthrene	-2.78	-4.57
	Anthracene	-2.80	-4.01

	Fluoranthene	-3.92	-3.30
	Pyrene	-4.10	-3.15
	Chrysene	-5.34	-1.07
Pasadena UPM[b] (37 °C and 42% RH)	Octadecane C_{18}	-3.31	-5.07
	Eicosane C_{20}	-4.23	-4.36
	Heneicosane C_{21}	-4.71	-4.01
	Docosane C_{22}	-5.18	-3.55
	Tetracosane C_{24}	-6.13	-2.11

[a] log p_L° values are temperature corrected.

[b] log K_p values are the averages for the 08/01/96 and 08/14/96 experiments.

[c] log K_p values are the averages for the 08/05/96 and 08/14/96 experiments.

[d] log K_p values are the averages for the 08/02/96 and 08/07/96 experiments.

Table 3. Summary of Slopes (m_r) and Intercepts (b_r) for log K_p vs. log p_L^o Correlation Lines.

Aerosol Type	m_r	b_r
	PAHs	
$(NH_4)_2SO_4$ (T = 32 °C and RH = 10%)	-1.04	-7.41
DOP (T = 36 °C and RH = 10%)	-1.09	-7.02
Gasoline SOA (T = 31 °C and RH = 10%)	-1.05	-7.24
ETS[a] (T = 20 °C and RH = 60%)	-1.02	-6.90
	***n*-alkanes**	
$(NH_4)_2SO_4$ (T = 32 °C and RH = 10%)	-0.96	-7.66
DOP (T = 36 °C and and RH = 10%)	-0.98	-7.15
Gasoline SOA (T = 31 °C and RH = 10%)	-1.09	-8.37
Ambient (T = 37 °C and RH = 42%)	-1.03	-8.68
ETS[a] (T = 20 °C and RH = 60%)	-0.89	-7.44

[a] data are from ref *12*.

LIST OF FIGURES

Figure 1. Adsorptive Partitioning of PAH and *n*-Alkanes

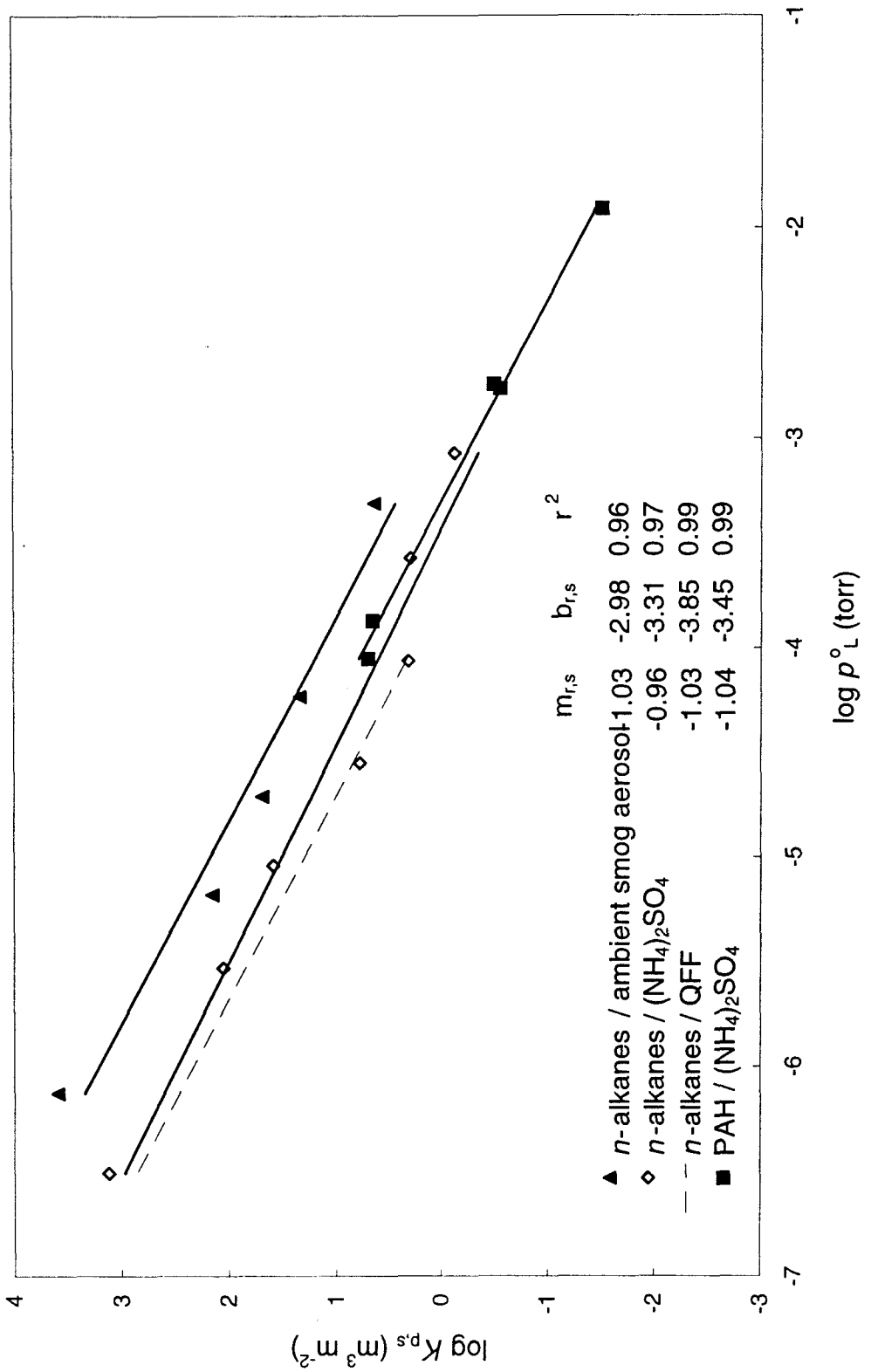

Figure 2. Absorptive Partitioning of PAH

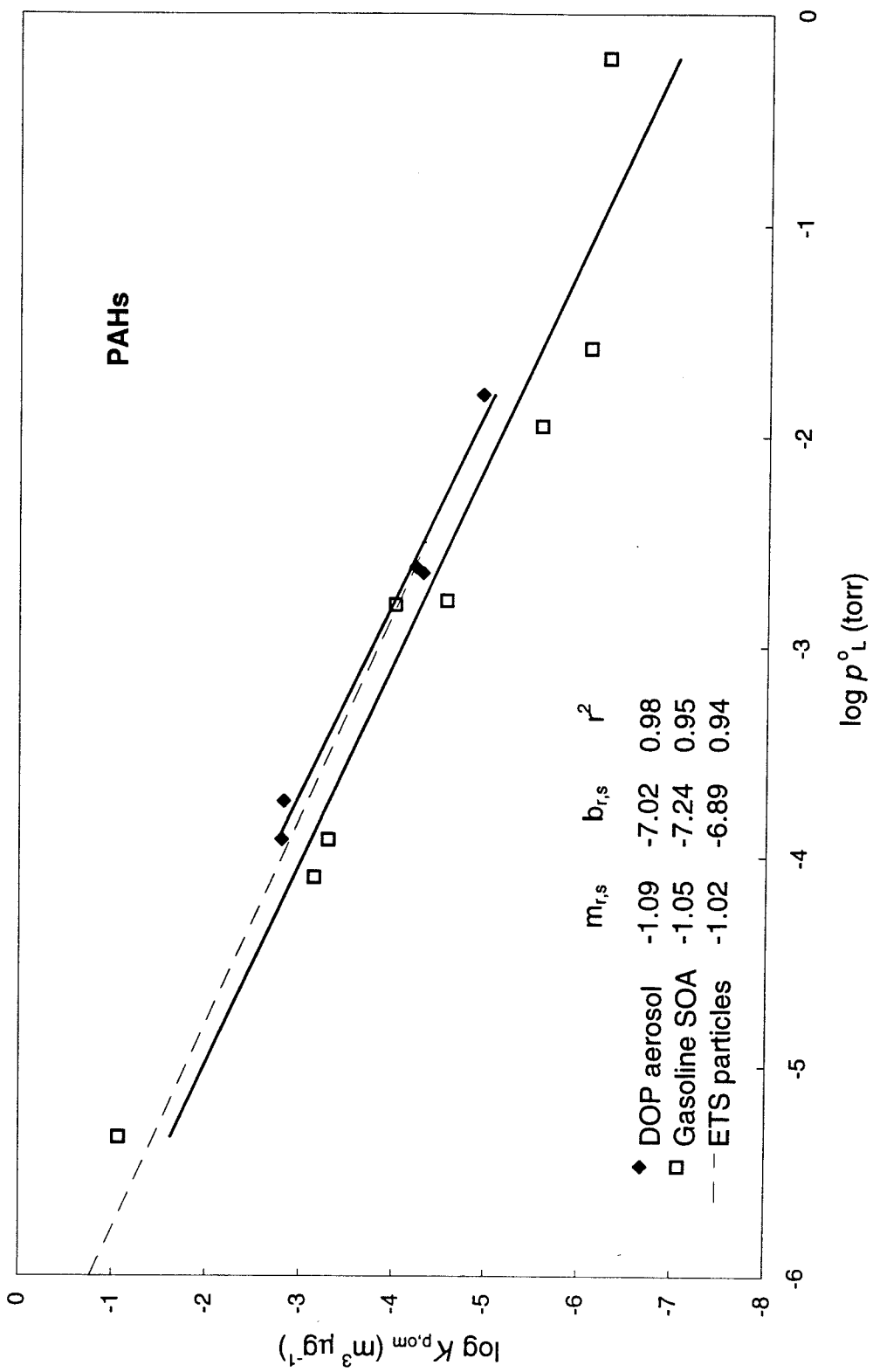

Figure 3. Absorptive Partitioning of n-Alkanes

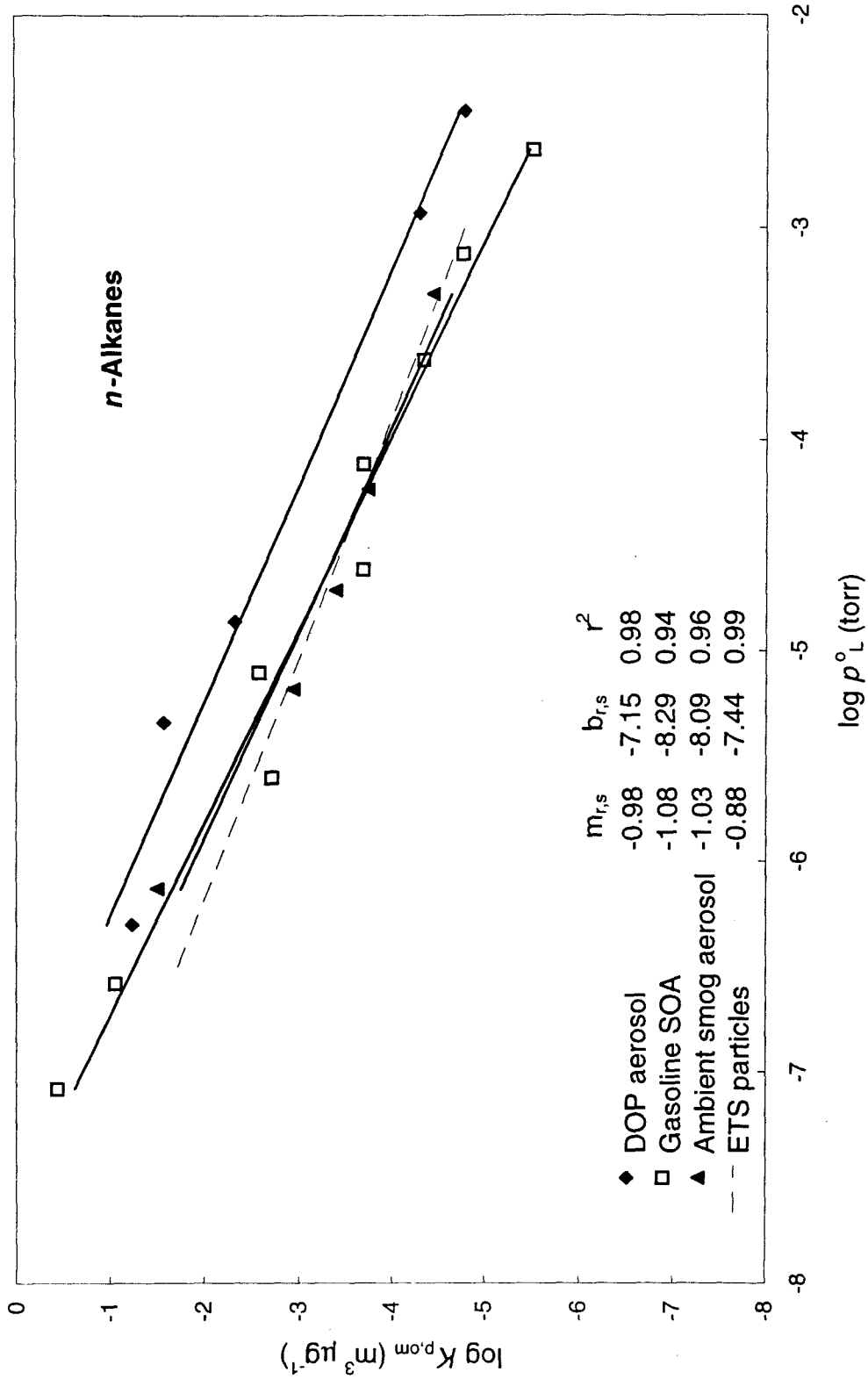

Chapter 5:

Observations on Modeling and Measuring Ambient Carbonaceous Aerosol

Submitted to *Environ. Sci. Technol*, 1998.

ABSTRACT

Predictions of atmospheric carbonaceous aerosol using a state-of-the-science, three-dimensional, size- and chemically-resolved, aerosol model are compared with ambient measurements made during the Southern California Air Quality Study (SCAQS). These comparisons reveal significant uncertainties associated with both model prediction and ambient measurement of carbonaceous aerosol. In particular, results strongly suggest that the spatial and diurnal variation of urban diesel emissions should be represented separately from those of regular light-duty vehicle emissions in the construction of emissions inventories. Also, appropriate emissions inventories and aerosol formation potentials need to be obtained for important, primary, gas-phase, semi-volatile organic compounds. Furthermore, method standards need to be established for appropriate sampling and analytical protocols for ambient organic and elemental aerosol carbon measurements.

INTRODUCTION

Atmospheric particulate matter (PM) has become a major regulatory focus because of recently discovered health impacts and new regulations drafted by the United States Environmental Protection Agency (*1- 3*). Historically, ozone has been the primary focus of air pollution control efforts. While these efforts have yielded significant reductions of this recalcitrant oxidant in many areas, the complexity and non-linearity of ozone formation make further progress even more costly. As with ozone, achieving atmospheric PM reductions should prove to be a formidable task (*4*).

Atmospheric aerosol results from the complex combination of direct emission (primary PM) and in-situ atmospheric photochemical production (secondary PM). Emitted primary PM includes combustion produced organic and elemental carbon, mechanically generated carbon and mineral dust, and combustion- and mechanically derived metals. Secondary PM results from the atmospheric reactions of both inorganic (e.g. oxides of sulfur and nitrogen) and organic (e.g. anthropogenic aromatics and biogenic terpenes) compounds. As a result of the well-defined number of inorganic species and an earlier understanding of their gas/aerosol thermodynamics, accurate algorithms for predicting secondary inorganic aerosol formation are included in several atmospheric aerosol models (*4-11*). Secondary organic aerosol (SOA) formation, on the other hand, occurs via the atmospheric reactions of potentially hundreds of organic compounds. In addition, the gas/aerosol thermodynamics of the oxidation products were

poorly understood until recently (*12-15*). As a result, previous modeling of ambient SOA formation has been limited and provisional (*16, 17*).

Pandis *et al.* (*16, 17*) produced the first version of a size-resolved secondary organic aerosol module, assuming that SOA formation occurs via the condensation of saturated non-volatile reaction products. The one-dimensional trajectory model, into which the module was implemented, predicted that diurnal concentrations of SOA at Claremont, CA closely follow the accumulated reaction rate of the parent primary species. Most photochemically produced gas phase species (e.g. ozone, peroxyacetylnitrate) exhibit such behavior. Predictions of the diurnal profile and concentration of total SOA in Claremont on August 28, 1987 matched data reasonably well (*16-19*).

As with atmospheric modeling, reliable techniques for measuring/estimating ambient concentrations of secondary organic aerosol have lagged behind those for inorganic aerosol. One common technique involves delineating ambient organic carbon (OC) and elemental carbon (EC) aerosol concentrations under conditions when photochemical production of secondary OC should be low. These measurements are then used to develop correlations between EC and this "primary" OC. Deviations from these primary OC/EC correlations, during days of high photochemical activity, are then used to estimate SOA contributions (*18, 19*). Whereas this has been the most widely used technique, there still exist a number of uncertainties regarding its reliability for accurately measuring/estimating levels of secondary, as well as primary, organic aerosol. One of the major reasons for this uncertainty is a result of the fact that ambient concentrations of

semi-volatile organics substantially exceed those of non-volatile organics (*12-15, 20, 21*). This semi-volatile carbon, which includes hundreds of both primary and secondary species, absorptively partitions to ambient organic aerosol in a manner that depends upon temperature as well as concentration and composition of the aerosol (*12-15, 22-24*). As a result, the very act of measurement disturbs the system, making accurate determination of the fraction of ambient organic mass that is actually in the aerosol phase inherently difficult. In addition, semi-volatile species adsorb to filter sampling media, often resulting in an overestimation of ambient organic aerosol concentrations (*18, 25*). Furthermore, the actual allocation of total carbon into categories of organic and elemental carbon depends strongly upon the analytical technique used to quantify the components. As such, organic and elemental carbon are not absolute quantities, but rather are operationally defined. Therefore, SOA concentrations estimated using the EC/OC ratio technique described above depend upon the EC/OC analytical technique employed.

In this paper, we present comparisons between model predictions and ambient measurements of carbonaceous aerosol in the California South Coast Air Basin during the 1987 Southern California Air Quality Study (SCAQS) and discuss some of the problems associated with both measurement and model, that must be addressed before atmospheric models can be confidently used to predict EC, OC, and SOA.

MODEL DESCRIPTION

The three-dimensional, size- and chemically resolved, aerosol model is comprised of interacting modules that describe the emission, transport, transformation (both chemical and physical), and deposition of the majority of species relevant to urban and regional atmospheric chemistry (*4, 10*). In this model, the aerosol size distribution is assumed to be internally mixed (i.e. equivalent sized particles have identical chemical compositions).

Gas-Phase Chemistry and Aerosol Thermodynamics

Gas-phase chemistry is based on the condensed version of the LCC chemical mechanism (*26*) with extensions by Harley *et al.* (*27*). The species in the chemical mechanism are given by Meng *et al.* (*10*). The original mechanism includes 35 chemical species to which hydrochloric acid (HCl) and five biogenic monoterpene species have been added (α-pinene, β-pinene, Δ^3-carene, limonene, myrcene). Semi-volatile reaction products of toluene, higher aromatics, and the five biogenic monoterpene species, which participate in SOA formation, have been added and are listed, along with their stoichiometric and gas/aerosol-partitioning coefficients, in Table 1.

To predict *a priori* the amount of SOA formed from the atmospheric oxidation of a hydrocarbon would require complete knowledge of all the oxidation products, their stoichiometric reaction coefficients, their vapor pressures, and their associated activity coefficients in the aerosol phase. Whereas this would be the most fundamental approach,

it is impractical given the current state of knowledge. Complete product information is not available for most of the relevant parent species; and even if it were, estimating all the associated parameters would be extremely challenging. As a result, the concept of aerosol yield was introduced to parameterize the aerosol forming potential of parent hydrocarbon species. The aerosol yield (Y) is defined as, $Y = \Delta M_o/\Delta HC$, where ΔM_o is the mass concentration of organic aerosol formed for a given reacted concentration of parent hydrocarbon (ΔHC). Aerosol yields are determined experimentally by placing specified concentrations of hydrocarbon(s) and nitrogen oxides in an irradiated smog chamber, allowing the mixture to react photochemically, and measuring ΔHC and ΔM_o to compute Y. Odum *et al.* (*12-15*) have shown that while the aerosol yield is an intrinsic property of a given hydrocarbon, it is also dependent upon the mass concentration of organic aerosol (M_o) into which the oxidation products can absorptively partition, in a manner described by the following equilibrium expression,

$$Y = M_o \sum_i \left[\frac{\alpha_i K_{om,i}}{1 + K_{om,i} M_o} \right] \quad (1)$$

where α_i and $K_{om,i}$ are the stoichiometric-reaction and gas/aerosol-partitioning coefficients for product i, respectively. Odum *et al.* (*12-15*) have shown that oxidation products that form SOA are often semi-volatile in nature and partition between gas- and aerosol phases in a manner that can be described by Raoult's Law. This process is parameterized using a partitioning coefficient ($K_{om,i}$) (*12, 22*),

$$K_{om,i} = \frac{A_i / M_o}{G_i} = \frac{760RT}{10^6 MW_{om} \zeta_i p^o_{L,i}} \quad (2)$$

where A_i and G_i are the aerosol- and gas phase concentrations of the species, R is the ideal gas constant, T is temperature, ζ_i is the activity coefficient of the semi-volatile species in the absorbing organic aerosol phase, MW_{om} is the mean molecular weight of the absorbing organic aerosol, and $p^{\circ}_{L,i}$ is the pure-liquid (sub-cooled, if necessary) saturation vapor pressure of the partitioning species. As Equation (2) suggests, the mass fraction of a species in the aerosol phase at equilibrium depends upon the mass concentration of absorbing organic aerosol available for partitioning (M_o). As a result, aerosol yields depend strongly upon M_o as Equation (1) indicates.

It has been shown (*12-15*) that aerosol yield data, as a function of M_o, for a given SOA producing parent species can be parameterized with Equation (1) by assuming that each parent species produces two hypothetical, semi-volatile products that form the SOA. A stoichiometric and partitioning coefficient are determined for each hypothetical product by fitting smog chamber yield data (*12-15*). The optimized coefficients for the SOA producing parent species, chosen by fitting data from more than 100 smog chamber experiments for 17 different aromatic species and 8 different biogenic terpenes, are listed in Table 1.

Thermodynamics for aerosol phase inorganics are computed using the thermodynamic module, Simulating Composition of Atmospheric Particles at Equilibrium 2 (SCAPE2) described by Kim and Seinfeld (*28*) and Meng *et al.* (*29*). In particular, SCAPE2 includes the thermodynamics of sodium, sulfate, ammonium, nitrate, chloride, potassium, calcium, magnesium and carbonates.

Results presented here are obtained using SCAPE2, along with the KM algorithm for the computation of activity coefficients. The calculation of water activity is based on the ZSR algorithm (*30*).

Dynamic Aerosol Equation

The general dynamic equation that describes the evolution of the size and composition of an internally mixed aerosol is (*10, 31*),

$$\frac{\partial p_i(\mu,\boldsymbol{x},t)}{\partial t} = -\left(\overline{\boldsymbol{V}}(\boldsymbol{x},t) - V_s(\mu)\boldsymbol{k}\right)\bullet\nabla\bullet\boldsymbol{K}(\boldsymbol{x},t)\nabla p_i + H_i(\mu,\boldsymbol{x},t)p(\mu,\boldsymbol{x},t) - \frac{1}{3}\frac{\partial}{\partial\mu}\left(Hp_i\right) + S_i(\mu,\boldsymbol{x},t) + L_i(\mu,\boldsymbol{x},t)p \tag{3}$$

where $\boldsymbol{x}$ is the spatial coordinate vector, t is time, $p_i(\mu,\boldsymbol{x},t) = (dm/d\mu)q_i$, μ is normalized particle diameter $\mu=\ln(D_p/D_0)$, m is the particle mass, q_i is the mass concentration distribution of species i, $\overline{\boldsymbol{V}}(\mathbf{x},t)$ is the mean advective flow, V_s is the settling velocity of the particle, $\boldsymbol{k}$ is the unit vector in the z-direction, $\boldsymbol{K}$ is the eddy diffusivity tensor, H_i is the rate of condensation/evaporation, S_i is the rate of sources such as emissions and nucleation, and L_i is the rate of removal processes.

The rates of condensation/evaporation for sulfate, ammonia, nitric acid, hydrochloric acid, and semi-volatile organic aerosols are computed using (*31*),

$$H_i = \frac{1}{m}\frac{dm_i}{dt} = \frac{2\pi D_p D_i}{m}\frac{C_{\infty,i} - C_{s,i}}{\frac{2\lambda}{\gamma_i D_p} + 1} \tag{4}$$

where D_i is the molecular diffusivity of species i in air, $C_{\infty,i}$ is the concentration of species i in the bulk gas, $C_{s,i}$ is the concentration at the particle surface, λ is the mean free path of air, and γ_i the accommodation coefficient of species i on the aerosol. One of the main features of the model is that $C_{s,i}$ is computed *dynamically* for each condensing species using the thermodynamic model SCAPE2 for the inorganics and using equation (2) for the secondary organic species.

Emissions

Emissions data for gaseous compounds are described by Harley *et al.* (*27*). Day-specific emission inventories for the August 1987 episode were obtained from the California Air Resources Board (CARB) (*32*). Discussion of gaseous emissions for this episode appears in Meng *et al.* (*10*). VOC, CO, and NO_x emissions have been scaled according to recent suggestions by Harley (*33*).

SO_2 and chemically- and size-resolved primary particle emissions used are those presented by Lurmann *et al.* (*34*). Particle emissions are allocated among six chemical species: sulfate, elemental carbon (EC), non-volatile organic material (OO), sodium, chloride, and "other" species. Emissions of OO have been updated to include emissions from commercial meat char-broiling, for which a daily mass emission inventory was obtained from CARB. A diurnal profile and size-distribution appropriate for commercial meat char-broiling particulate emissions was obtained from the literature (*35*).

Initial and Boundary Conditions

The simulations discussed herein are of a 3-day smog episode that occurred in the SoCAB on August 27-29, 1987. High ozone (>240 ppb) and PM_{10} levels were measured during this episode. Boundary and initial conditions for the episode are specified using routine surface-level air quality and aircraft-based measurements acquired during the Southern California Air Quality Study (SCAQS) (*27*). The initial size- and composition-resolved aerosol concentrations are provided by Lurmann *et al.* (*34*), which were estimated based on the annual averages in South Coast Air Basin (SoCAB) (*36*). A more complete discussion of the conditions is given by Meng *et al.* (*10*).

RESULTS AND DISCUSSION

Evaluation of the performance of an atmospheric model frequently begins with a detailed comparison between model predictions and ambient measurements for conserved tracer species. Figures 1 and 2 compare prediction and observations for two conserved particulate tracers, elemental carbon (EC) and primary aerosol organic carbon (PAOC), respectively. Figure 1 shows that predictions for EC match the ambient measurements of Turpin and Huntzicker (*18*) fairly well during the early morning and late afternoon on August 27 and 28. However during the middle of the day, predictions tend to follow the measurements of McMurry *et al.* (*37*). During the night, model predictions severely overestimate the observations of both groups. The main emission source for EC is

medium- and heavy-duty diesel vehicles (*38*). In the construction of the CARB motor-vehicle emission inventory, the spatial and temporal traffic profiles of diesel-powered vehicles were assumed to be identical to those of regular gasoline-powered vehicles. As a result, diesel PM emissions are keyed to follow those of regular passenger-car traffic patterns, with the largest emissions occurring in the morning rush-hour period, followed by a steady lower emission rate during the middle of the day and a final increase during the evening traffic commuting period. However in the Los Angeles Basin, the main heavy/medium-duty diesel trafficking does not begin until after the morning rush-hours, with the heaviest period occurring during the middle of the day and rapidly subsiding by the evening traffic commuting period (*39*). The fact that diesel PM emissions do not have the correct temporal and spatial profiles might provide sufficient explanation as to why predicted EC concentrations greatly exceed measured values during the night, and underestimate them during the middle of the day, in Claremont. While there may be significant passenger vehicle activity during the night in Claremont, it is unlikely that there is much medium- and heavy-duty diesel traffic occurring.

As with EC, Figure 2 shows that predicted and measured primary aerosol organic carbon (PAOC) concentrations match reasonably well during the early morning/evening, while the predictions from 9:00 to 17:00 and from 20:00 to 2:00 for both days show poor agreement with the measurements of Turpin and Huntzicker. There are several possible explanations for this. Figure 3 shows a comparison of measured and predicted carbon monoxide (CO) concentrations for Claremont during the two-day period. While the overall match between prediction and measurement is quite good, and is much better than

that for EC and PAOC, there is a tendency for predictions to be overestimated during the middle of the night and underestimated during the middle of the day. This suggests that either the spatial and temporal profiles of motor vehicle emissions (i.e. the major emission source for CO) are not quite correct or that the model simulation of atmospheric mixing is too vigorous in the middle of the day and too quiescent at night. Figure 4 shows percent biases between model predictions and the ambient observations of Turpin and Huntzicker (*18*) for EC, PAOC, and CO. From around 2:00 to 9:00, PAOC and CO are over/underpredicted by similar amounts. As such it is not possible to distinguish whether the biases during these times are a result of inaccurate model mixing/transport or inaccurate emissions inventories or a combination of both. During the afternoon period and at night, the biases for PAOC are larger than those for CO. This suggests that either the emission inventories for PAOC are incorrect during these times or that there are problems with the PAOC measurements, as will be discussed below. The biases for EC are always greater than those for CO, especially at night. This observation strongly suggests that the spatial/temporal profiles for EC emissions (i.e. diesel-powered vehicle emissions) are incorrect, and that diesel emissions should be given their own spatial/temporal emissions profiles in the construction of future emissions inventories.

While it seems evident that there are problems with the current primary PM emissions inventory, discrepancies between predicted and measured concentrations of EC and PAOC, almost certainly, are not entirely a result of this cause. As Figure 1 clearly indicates, there is significant disagreement between the two measurement methods employed in the SCAQS study for EC alone. Turpin and Huntzicker (*18*) sampled with a

traditional quartz fiber filter sampler and McMurry *et al.* (*37*) used an eight-stage impactor; furthermore, the two groups used different analytical techniques to determine EC and OC concentrations. The discrepancy in these two data sets points out that there are still significant problems associated with determining ambient EC/OC levels. One major problem is that EC and OC are not well defined species, like CO or O_3. They are operationally defined quantities that depend upon the applied sampling method and analytical technique. Hering *et al.* (*40*) present an analysis of 8 different sampling methods and analytical techniques for EC/OC and show that significant variability exists among the various methods. Most of the variability in EC measurements was a result of differences in analytical techniques, whereas most of the OC variability was attributed to differences in sampling methods and their associated adsorption artifacts (*40*). Such measurement uncertainty increases the difficulty of evaluating model predictions, since there is no absolute basis of comparison between measurement and prediction. This suggests that a standard method for EC/OC measurements needs to be established and should be used in both the characterization of primary sources, for the construction of PM emissions inventories, and in ambient measurements

Another problem associated with measurement of OC is that of adsorptive sampling artifacts. As mentioned previously, ambient concentrations of semi-volatile OC are much larger than those of non-volatile OC (*12-15, 20, 21*), making accurate determination of the fraction of organic mass that is actually in the aerosol phase inherently difficult. The concentration of total (i.e. gas phase + aerosol phase) secondary organic material (TSOM) contributing to SOA formation is highest in the middle of the

day (see Figure 5) because of the photochemical nature of its origin. However, most of this highly-polar, semi-volatile mass is in the gas phase in the atmosphere (*12-15,* and Figure 5), but can be seemingly distributed to the aerosol phase during sampling, making the middle of the day the most difficult time to accurately measure organic aerosol concentrations. Thus, the likelihood of overestimating the ambient concentration of organic aerosol, as a result of sampling artifacts, is highest during times of high photochemical activity, which is precisely the time of day when measurements suggests that total organic aerosol (i.e. primary + secondary organic aerosol; TOA) concentrations peak (see Figure 6). Turpin and Huntzicker (*15*) have attempted to correct the TOA measurements for artifacts, but it is uncertain as to how well such corrections actually work (*40*). As a result, it is difficult to determine whether the discrepancy between predicted and measured PAOC and TOA concentrations, shown in Figures 3 and 6, is attributable to inaccuracies in the model, or to uncertainties in the measurements, or both. The fact that such uncertainty exists suggests that more robust and accurate sampling methods for OC must continue to be developed.

Predicted and measured estimates of secondary organic aerosol (SOA) concentrations are shown in Figure 5. While measured and predicted concentrations do peak at the same time of day on both August 27 and 28, the predicted SOA formation curves do not peak as sharply as measurements suggest they should, and predicted concentrations fall well below measured estimates during the day. Measured estimates of SOA concentrations are those of Turpin and Huntzicker (*15*) and are determined using the OC/EC ratio technique described in the Introduction. Unfortunately, it is difficult to

determine the accuracy of this technique for measuring actual SOA concentrations. In addition to the sampling problems discussed above, this technique assumes that ambient OC/EC ratios are independent of time of day or season, which seems unlikely considering the different time profiles of the various OC/EC emission sources (*39*). For example, Figure 7 shows a comparison of the ratio of ambient levels of EC and primary aerosol OC (PAOC) at Claremont over the two-day period for both model prediction (assuming a constant conversion of 1.2 between OC and organic mass , OM) and measurement. While the two show good agreement, a few measured data points (represented in Figure 7 as open circles) do not correspond well with the bulk of the measurements. These data points correspond to measurements taken during the early morning rush hour and show that the EC/OC ratio is much higher during this period. So EC/OC ratios are not constant at a given receptor site and depend upon time of day as well as season of the year. This observation reveals the difficulty in trying to use average EC/OC ratios to estimate ambient SOA concentrations. Thus determining why model predicted SOA concentrations fall below those of measured estimates during the daytime is difficult.

Measurement difficulties, however, are most likely not the only reason for the discrepancy between prediction and measured estimates. One major reason why model predictions are lower than measured estimates during the day is because the model predicts that ambient primary organic aerosol (PAOC) concentrations are lowest in the middle of the day. As discussed previously, SOA concentrations are highly coupled to PAOC concentrations. If the model predicted PAOC to peak in the middle of the afternoon, as the measurements suggest, then the formation curves for SOA shown in

Figure 5 would peak more sharply and SOA levels would be higher by at least 50% during the daylight hours. This is because there is a significant amount of secondary organic material in the gas phase that is available for absorption by PAOC (i.e. see TSOM in Figure 5). Thus until model predictions and measurements of PAOC agree more closely, it will be difficult to obtain agreement between SOA model predictions and measured estimates.

Another possible reason why model predictions underestimate measured SOA estimates during the middle of the day is that the current emission inventories used in the model do not contain emissions of primary, semi-volatile organics. Whereas this class of compounds may not be important in terms of its ozone formation potential, it most likely plays a significant role in secondary aerosol formation. The vapor pressures of these compounds (e.g. long chain and highly branched alkanes/alkenes/aldehydes, polycyclic aromatic hydrocarbons) are already sufficiently low, such that they partition a portion of their mass, as primary species, into the aerosol phase. The secondary products formed from the atmospheric reactions of these species include nitrated and oxygenated counterparts of the primary parent species, and as such, will have even lower vapor pressures than the parent compounds, resulting in large aerosol formation potentials. For example, the C_{15} biogenic sesquiterpenes have SOA yields of essentially 100% (*15*); and semi-volatile polycyclic aromatic hydrocarbons, such as fluoranthene and pyrene, which exist primarily in the gas phase as primary species, produce nitrated reaction products that reside completely in the aerosol phase (*41*). Considering that the ambient concentrations of semi-volatile primary species are much larger than those of non-volatile primary

aerosol phase organics (*20, 21*), it seems highly likely that they play an important role in ambient SOA formation. This, coupled with the increasing concern over the health impacts of ambient particulate matter and the resulting new regulations, suggest that significant effort should be applied to obtaining speciated emission inventories and to determining aerosol formation potentials for this important class of SOA-forming compounds.

The discussions outlined above reveal that there are still significant uncertainties associated both with modeling and measuring ambient carbonaceous aerosol. Emphasis in the future should be applied to obtaining more accurate and complete primary PM and primary semi-volatile organic emissions inventories and to ensuring that mixing/transport modules produce accurate predictions. Furthermore, serious effort should be applied to the development of ambient organic aerosol sampling methods that overcome problems associated with adsorption artifacts. Since ambient SOA concentrations depend so intimately on PAOC concentrations, it will be difficult to obtain accurate predictions of ambient SOA formation until such issues are resolved.

ACKNOWLEDGMENT

We would like to acknowledge support by the Electric Power Research Institute, the Coordinating Research Council, and General Motors Corporation.

REFERENCES

1. Schwartz, J; Dockery, D. W.; Neas, L. M. *J. Air Waste Manage. Assoc.*, **1996**, 46, 927.
2. Pope, C. A. III; Bates, D. V.; Raizenne, M. E. *Environ. Health Perspect.*, **1995**, 103, 472.
3. *Fed. Reg.* **61** (no. 241), 65763 (13 December 1996).
4. Meng, Z.; Dabdub, D.; Seinfeld, J.H. *Science*, **1997**, 277, 116.
5. Pilinis, C.; Seinfeld, J. H. *Atmos. Environ.*, **1988**, 22, 1985.
6. Russell, A. G.; McCue, K. F., Cass, G. R. *Environ. Sci. Technol.*, **1988**, 22, 263.
7. Chang, J. S.; Middleton, P. B.; Stockwell, W. R.; Walcek, C. J.; Pleim, J. E.; Lanford, H. H.; Madronich, S.; Binkowski, F. S.; Seaman, N. L.; Stauffer, D. R.; Byun, D., McHenry, J. N.; Hass, H.; Samson, P. J. *National Acid Precipitation Assessment Program*, **1991**, Washington, D. C.
8. Wexler, A. S.; Lurmann, F. W.; Seinfeld, J. H. *Atmos Environ.*, **1994**, 28, 531.
9. Binkowski, F. S.; Shankar, U. *J. Geophys. Res.*, **1995**, 100, 26191.
10. Meng, Z.; Dabdub, D.; Seinfeld, J. H. *J. Geophys. Res.*, **1998**, 103, 3419.
11. Jacobson, M. Z. *Atmos. Environ.*, **1997**, 31A, 587.
12. Odum, J. R.; Hoffmann, T.; Bowman, F.; Collins, D.; Flagan, R. C.; Seinfeld, J. H. *Environ. Sci. Technol.*, **1996**, 30, 2580.
13. Odum, J. R.; Jungkamp, T. P. W.; Griffin, R. J.; Flagan, R. C.; Seinfeld, J. H. *Science*, 1997, 276, 96.

14. Odum, J. R.; Jungkamp, T. P. W.; Griffin, R. J.; Forstner, H. J. L.; Flagan, R. C.; Seinfeld, J. H. *Environ. Sci. Technol.*, **1997**, 31, 1890.

15. Hoffmann, T.; Odum, J. R.; Bowman, F.; Collins, D.; Klockow, D.; Flagan, R. C.; Seinfeld, J. H. *J. Atmos. Chem.*, **1997**, 26, 189.

16. Pandis, S. N.; Harley, R. A.; Cass, G. R.; Seinfeld, J. H. *Atmos. Environ.*, **1992**, 26A, 2269.

17. Pandis, S. N.; Wexler, A. S.; Seinfeld, J. H. *Atmos. Environ.*, 1993, 27A, 2403.

18. Turpin, B. J.; Huntzicker, J. J. *Atmos. Environ.*, **1995**, 29B, 3527.

19. Turpin, B. J.; Huntzicker, J. J. *Atmos. Environ.*, **1991**, 25A, 207.

20. Fraser, M. P.; Cass, G. R.; Simoneit, B. R. T.; Rasmussen, R. A. *Environ. Sci. Technol.*, **1997**, 31, 2356.

21. Fraser, M.; Cass, G. R.; Simoneit, B. R. T.; Rasmussen, R. A. *Environ. Sci. Technol.*, in press.

22. Pankow, J. F. *Atmos. Environ.*, **1994**, 28A, 185.

23. Liang, C. K.; Pankow, J. F. *Environ. Sci. Technol.*, **1996**, 30, 2800.

24. Liang, C. K.; Pankow, J. F.; and Odum, J. R.; Seinfeld, J. H. *Environ. Sci. Technol.*, **1997**, 31, 3086.

25. McDow, S. R.; Huntzicker, J. J. *Atmos. Environ.*, **1990**, 24A, 2563.

26. Lurmann, F. W.; Carter, W. P. L.; Coyner, L. A. Report to the U. S. Environmental Protection Agency under contract 68-02-4104, **1987**.

27. Harley, R. A.; Russell, A. F.; McRae, G. J.; Cass, G. R.; Seinfeld, J. H. *Environ. Sci. Technol.*, **1993**, 27, 378.

28. Kim, Y. P.; Seinfeld, J. H. *Aerosol Sci. Technol.*, **1995**, 22, 93.

29. Meng, Z.; Seinfeld, J. H.; Saxena, P.; Kim, Y. P. *Aerosol Sci. Technol.*, **1995**, 23, 131.

30. Robinson, R. A.; Stokes, R. J. *Electrolyte Solutions*, *2nd ed.*, **1965**, Butterworth, London.

31. Wexler, A. S.; Lurmann, F. W.; Seinfeld, J. H. *Atmos. Environ.*, **1994**, 28, 531.

32. Wagner, K. K.; Allen, P. D. *SCAQS Emission Inventory for August 27-29, 1987*, (Tape ARA714), Technical Support Division, California Air Resources Board, Sacremento, CA, **1990**.

33. Harley, R. A.; Sawyer, R. F.; Milford, J. B. *Environ. Sci. Technol.*, **1997**, 31, 2829.

34. Lurmann, F. W.; Wexler, A. S.; Pandis, S. N.; Musarra, S.; Kumar, N.; Seinfeld, J. H. *Atmos. Environ.*, **1997**, 31, 2695.

35. Gray, H.A. Ph.D. Theis, 1986, California Institute of Technology, Pasadena, CA.

36. Solomon, P. A.; Fall, T.; Larson, S. M.; Lin, P.; Vasquez, F.; Cass, G. R. Report to the California Air Resources Board under contract A4-144-32, **1988**.

37. McMurry, P. H. Final Report to the California Air Resources Board under contract A732-075, **1989**.

38. Schauer, J. J.; Rogge, W. F.; Hildemann, L. M.; Mazurek, M. A.; Cass, G. R. *Atmos. Environ.*, **1996**, 30, 3837.

39. Dreher, D. B.; Harley, R. A. *J. Air Waste Manage. Assoc.*, **1998**, in press.

40. Hering, S. V.; Appel, B. R.; Cheng, W.; Salaymeh, F.; Cadle, S. H.; Mulawa, P. A.; Cahill, T. A.; Eldred, R. A.; Surovik, M.; Fitz, D.; Howes, J. E.; Knapp, K. T.;

Stockburger, L.; Turpin, B. J.; Huntzicker, J. J.; Zhang, X.; McMurry, P.H. *Aerosol Sci. Technol.*, **1990**, 12, 200.

41. Fan, Z. H.; Chen, R. H.; Birla, P.; Kamens, R. M. *Atmos. Environ.*, **1995**, 29, 1171.

Table 1. Stoichiometric and Partitioning Coefficients for SOA Species

Parent Compound	Secondary Product	Stoichiometric Coefficient	Partitioning Coefficient ($\mu g\ m^{-3}$)
Toluene	ATO1	0.071	0.0530
Toluene	ATO2	0.138	0.0019
Higher Aromatics	AAR1	0.038	0.042
Higher Aromatics	AAR2	0.167	0.0014
Monoterpenes	AAP1	0.038	0.1710
Monoterpenes	AAP2	0.326	0.0040

LIST OF FIGURES

Figure 1. Predicted and Measured EC at Claremont, CA

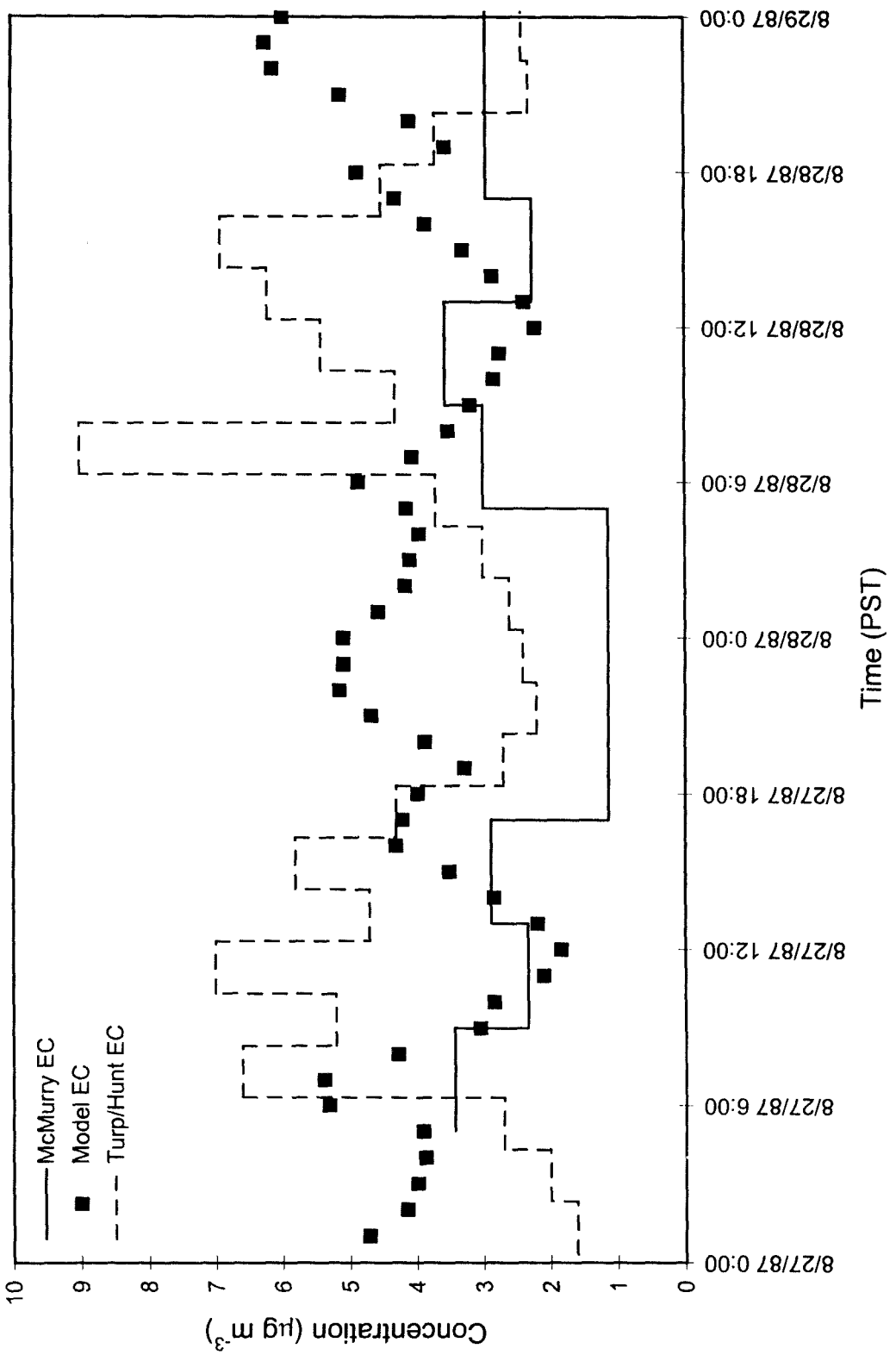

Figure 2. Predicted and Measured POA at Claremont, CA

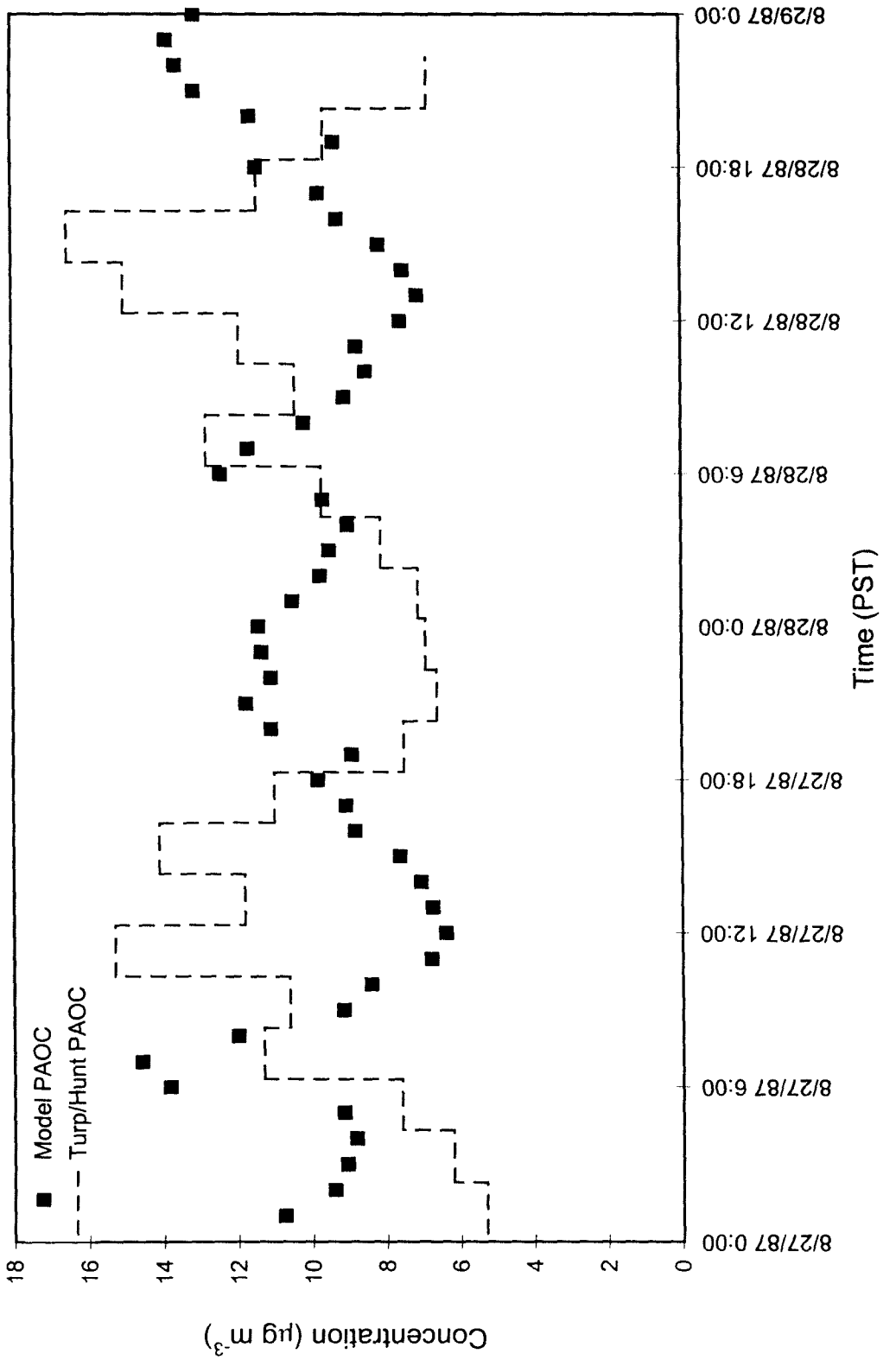

Figure 3. Predicted and Measured CO at Claremont, CA

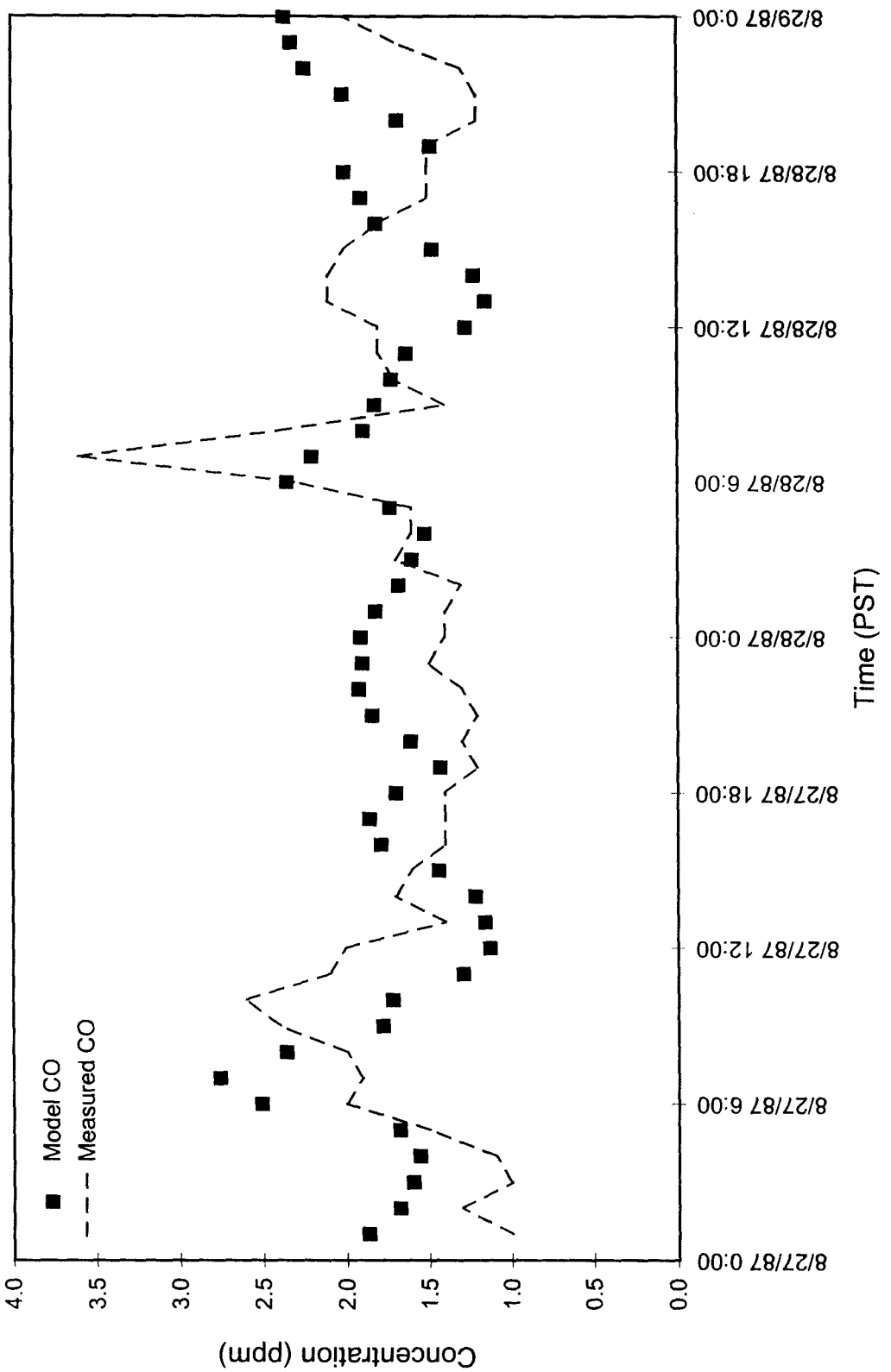

Figure 4. Biases in EC, PAOC, and CO at Claremont, CA

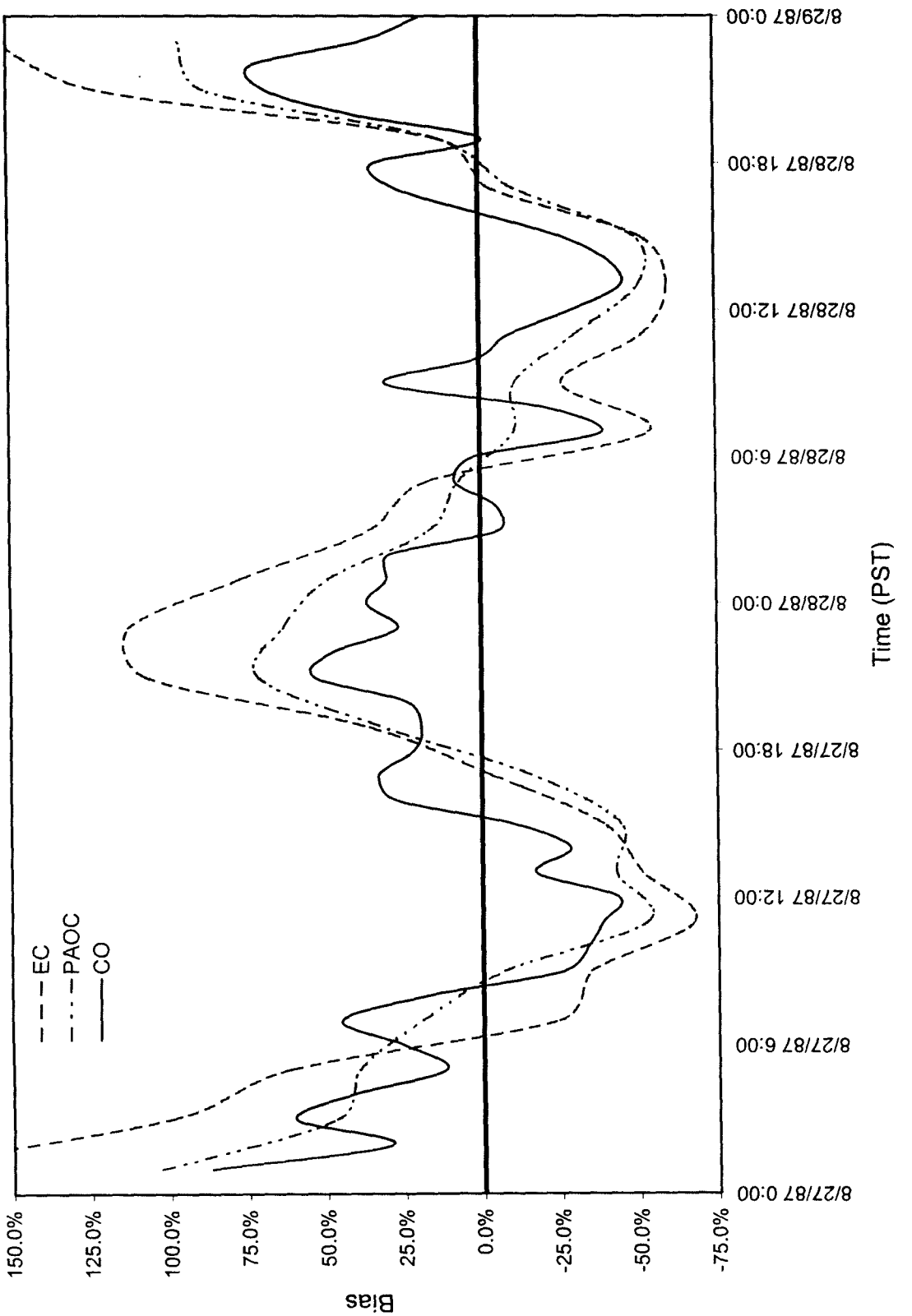

Figure 5. Predicted and Estimated SOA/TSOM at Claremont, CA

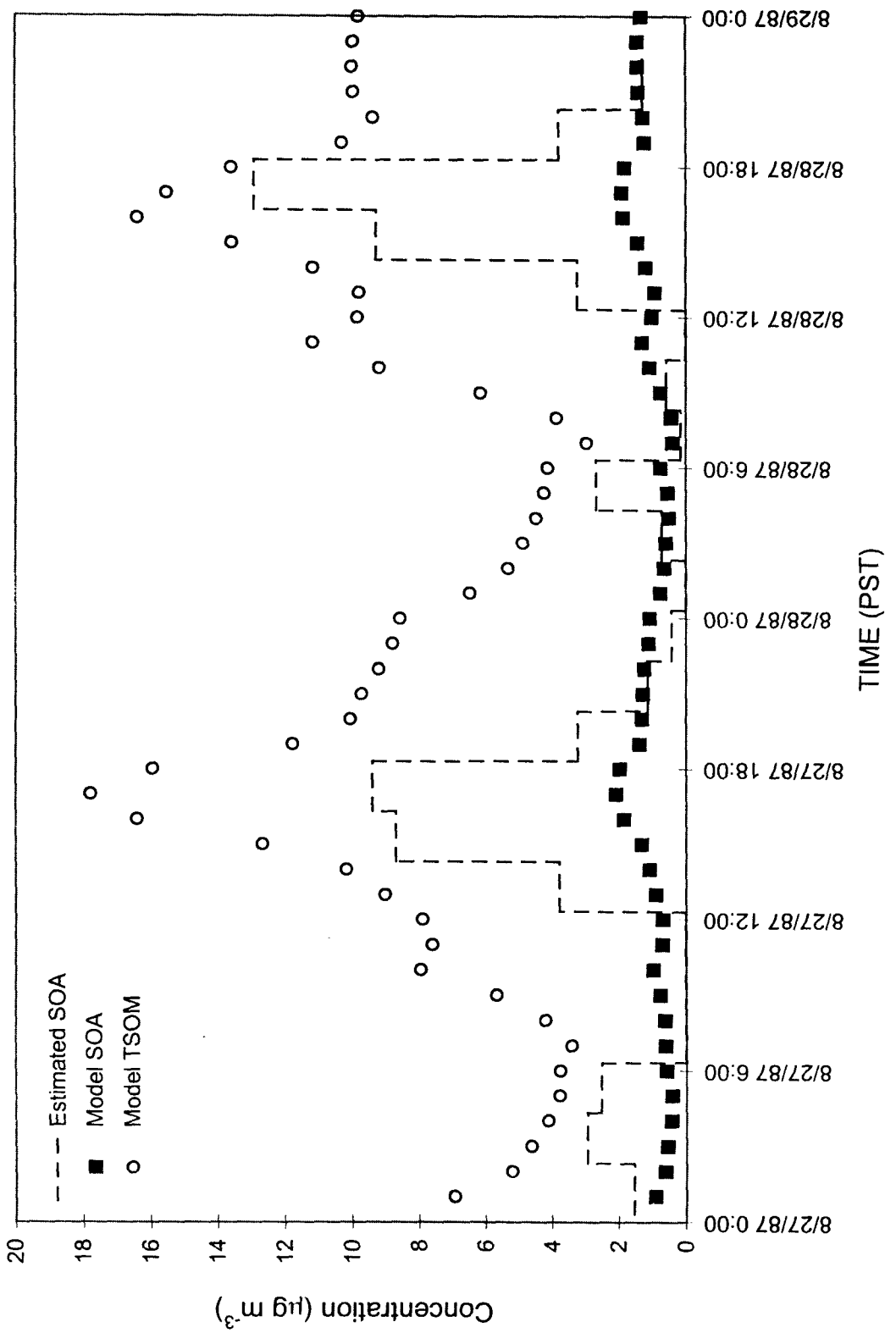

Figure 6. Predicted and Measured TOA at Claremont, CA

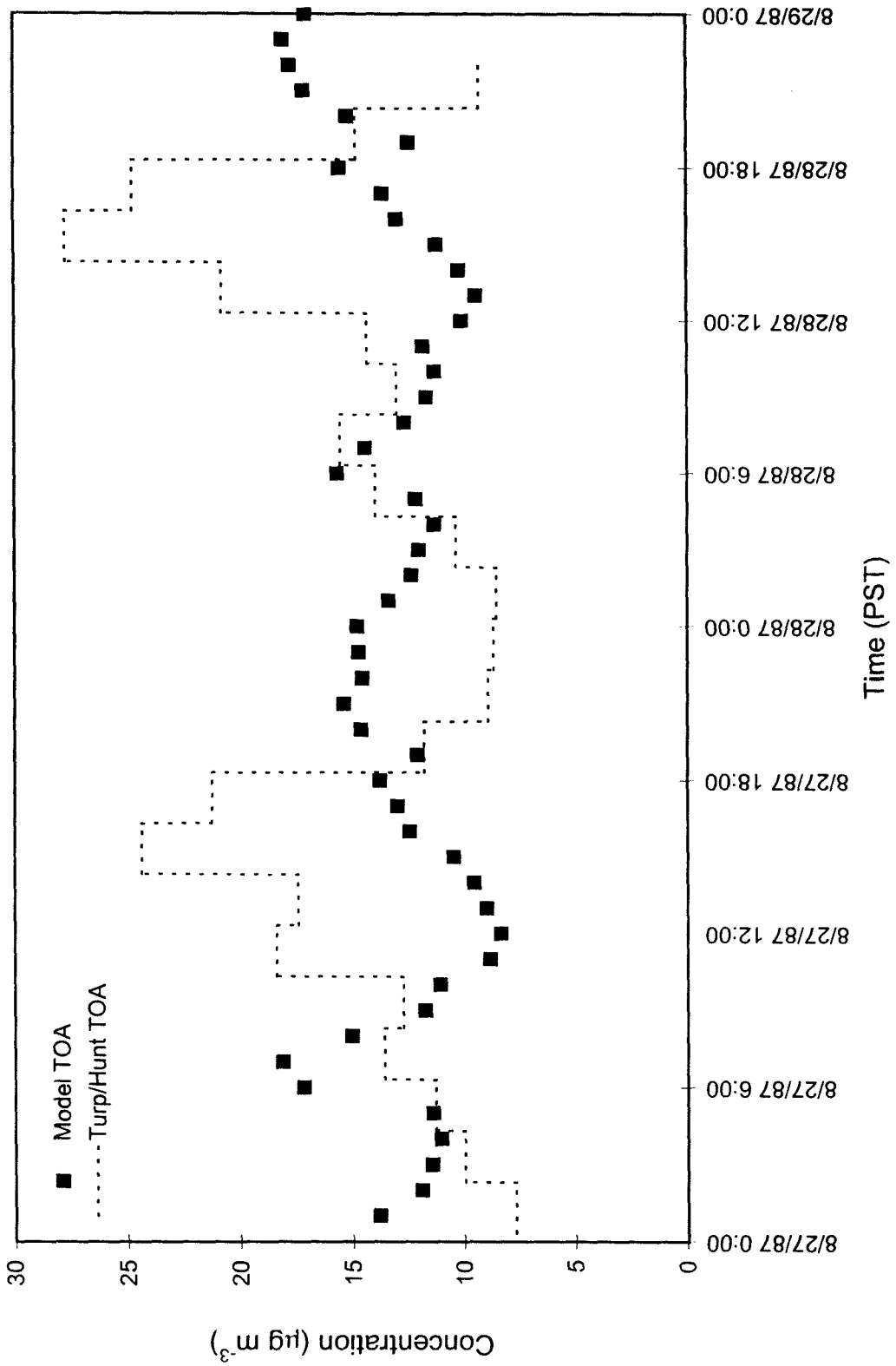

Figure 7. Predicted and Estimated Primary EC/OC at Claremont, CA